Antibiotics in Water Treatment:

The Role of Water Quality Conditions on their Fate and Removal during Chlorination and Nanofiltration

A Dissertation
Presented to
The Academic Faculty

by

Amisha D. Shah

In Partial Fulfilliment
of the Requirements for the Degree
Doctor of Philosophy in the School of Civil and Environmental Engineering

Georgia Institute of Technology
December 2008

Antibiotics in Water Treatment:

The Role of Water Quality Conditions on their Fate and Removal during Chlorination and Nanofiltration

Approved by:

Dr. Jae-Hong Kim
School of Civil and Environmental Engineering
Georgia Institute of Technology

Dr. Ching-Hua Huang
School of Civil and Environmental Engineering
Georgia Institute of Technology

Dr. Qilin Li
Department of Civil and Environmental Engineering
Rice University

Dr. James Mulholland
School of Civil and Environmental Engineering
Georgia Institute of Technology

Dr. Paul Wine
School of Chemistry and Biochemistry
School of Earth and Atmospheric Sciences
Georgia Institute of Technology

Dr. Sotira Yiacoumi
School of Civil and Environmental Engineering
Georgia Institute of Technology

Date Approved: July 25th, 2008

Acknowledgements

First of all, I would like to thank my advisors, Dr. Jae-Hong Kim and Dr. Ching-Hua Huang, for providing knowledge, guidance, and support throughout my graduate studies. I hope that they will not only remain my advisors but my friends for life. I would also like to thank Dr. Paul Wine, Dr. Sotira Yiacoumi, and Dr. Qilin Li for serving in my committee, as well as Dr. James Mulholland for not only serving on my committee but for also willing to write recommendation letters for me, for which I'm sure he had to get quite creative. I would like to thank Dr. Zhu teaching me a great deal about analytical chemistry and for truly serving as a life-saver during stressful research moments.

I would also like to thank numerous funding sources which include Saehan Industries Inc., Georgia Water Resources Institute, as well as the NSF IGERT Fellowship. I would also like to thank Sarper Sarp and Dr. Jaeweon Cho's lab (GIST/Korea) for providing ζ-potential measurements, Dr. Paul Winget at the U.S. EPA National Exposure Research Laboratory, Athens, GA, for performing atomic charge calculations, and Saehan Industries, Inc. and Dow Chemical Company for providing NF membrane samples for testing.

I would like to thank my lab mates, Wan-Ru, Sang-Hyuck, Lokesh, Hoon, Doo-Il, Yong-yun, Min, Seung-jin, Yoori, Varun, Yu, Piti, Saurabh, Eddie, and Richard for spending countless hours with me in the office and for helping me in the lab. I would especially like to thank my grad school friends, Emily, Sara, Gayle, Dave, John, Ben, Kelly, Natalie, Farhan, Jorge, Gretchen, and Dawn for being the best of friends and understanding the challenges of grad school. I would also like to thank my college friends for continuing to love me.

I would most of all though like to thank my family, my mom, my dad, and my brother, Ankoor, who love me unconditionally regardless of my mood, who always tell me to be a better person, and most importantly, give me money when I need it (smile).

Table of Contents

List of Tables

List of Figures

Abstract

Antibiotics are a group of compounds used in large quantities for both human therapy and animal food production. In recent years, antibiotics have been detected at low concentrations (up to μg/L) in wastewater effluents and surface waters in the U.S., Canada, and parts of Europe. The presence of such contaminants in the environment is of concern due to their potential to promote bacterial resistance as well as to trigger long-term adverse human health effects. Chemical disinfection, one of the essential water treatment processes, may aid in their removal but may also form byproducts that can remain biologically active. Nanofiltration is another water treatment process that may provide an effective physical barrier for these contaminants.

The goal of this study was to understand the effect chlorination and nanofiltration processes have on the fate of select antibiotics during water treatment, especially under varying water quality conditions. Changes in pH were found to significantly influence the reaction rate of one veterinary antibiotic, carbadox (CDX), with aqueous chlorine where apparent second-order rate constants, k_{app}, ranged from 51.8 to 3.15×10^4 $M^{-1}s^{-1}$ at pH 4-11. Byproduct formation was also influenced by pH as initial chlorine attack on CDX's hydrazone N-H moiety led to further attack by different nucleophiles whose strengths were pH dependent, thus yielding various non-chlorinated, hydroxylated, and larger molecular weight byproducts.

The pH was also found to significantly alter steady-state rejection of several antibiotics by different nanofiltration (NF) membranes of varying pore size. In particular, the greatest influence was observed for the Saehan NE 70 membrane in which case rejection was highly dependent on antibiotic speciation and membrane charge. For the

antibiotic, trimethoprim (TMP), a characteristic trend was found from pH 3-10 where the lowest rejection (50.1%) was observed near circumneutral pH conditions but increased above and below this pH to reach close to 91%. On the other hand, removal of the antibiotic, sulfamethoxazole (SMX) was as low as 37.4% at pH 4.8 but increased dramatically to > 97% at pH ≥ 8.0 due to repulsion effects observed between the negatively charged SMX species (SMX^-) and the negatively charged membrane. Further understanding of such pH effects was then mechanistically investigated using transport models such as the steric-hindrance pore model and the extended Nernst-Planck equation that incorporated parameters related to solute size (r_s) and charge (z), membrane pore size (r_p), membrane thickness to porosity ($\Delta x/A_k$), and membrane charge density (X).

In addition, the presence of tertiary amines such as trimethylamine (TMA) and 4-morpholineethanesulfonic acid (MES) significantly enhanced the transformation of antibiotics, TMP and flumequine (FLU), as well as the organic contaminant, salicylic acid (SA) during chlorination. Addition of MES exhibited dose-dependent effects where the pseudo-first order (observed) rate constants, k_{obs}^{amine} (s^{-1}), for TMP, FLU, and SA degradation increased linearly from 1×10^{-3} to 2.6×10^{-2} s^{-1}, 1.3×10^{-5} to 1.7×10^{-2} s^{-1}, and 3.9×10^{-6} to 8.7×10^{-3} s^{-1}, respectively, when MES dosages up to 5× the initial antibiotic/organic contaminant concentration were added. In contrast, addition of varying TMA dosages led FLU and SA to decay rapidly up to ~45 min but then decay at a slower rate up to 360 min, a trend strongly deviating from pseudo-first order kinetics, and most likely due to TMA auto-decomposition over time after its initial reaction with aqueous chlorine.

Overall, this study improves the fundamental understanding of the fate of antibiotics during chlorination and nanofiltration of water treatment processes, and the results will help industries to better develop strategies for effectively controlling this emerging group of contaminants in the future.

CHAPTER 1

Literature Review

1. Introduction

1.1 Occurrence of Antibiotics in the Environment

Antibiotics are a group of compounds used annually in large quantities to treat bacterial diseases in humans as well as to promote growth and prevent disease in animals such as cattle, swine, poultry, and fish during animal food production. Often, these compounds are only partially metabolized by the user and can subsequently be excreted into wastewater, manure, or directly into water systems during fish farming [1]. In such cases, antibiotics may further be exposed to soils and sediments as well as to surface water and groundwater due to agricultural runoff and wastewater effluent contamination.

In recent years, numerous investigations have been made to assess the prevalence of antibiotics as well as other pharmaceutical and personal care products (PPCPs) in wastewater effluents, surface waters, and groundwater, especially at low concentrations where they may still remain biologically potent. As analytical techniques once restricted the detection of these compounds at trace levels, recent advances in this area have allowed a more in depth analysis of the presence and fate of these low level contaminants in various types of water matrices.

In the US, one of the most comprehensive and well-known studies was conducted by the U.S. Geological Survey from 1999-2000 where the occurrence of 95 organic wastewater contaminants including various PPCPs were assessed at 139 stream sites throughout the country [3]. Antibiotics were found in ~ 48% of these stream sites at individual concentrations up to ~ 2 μg/L. In addition, other PPCPs (e.g., reproductive

hormones and prescription and nonprescription drugs) were found at ~ 32-82% of these stream sites at individual concentrations up to ~ 10 μg/L [3]. Similar studies were also conducted in Canada [4] and several European countries [5-7] to measure antibiotics alone in final effluents of wastewater treatment plants and surface waters. Several antibiotics that were commonly detected include an erythromycin metabolite, erythromycin-H_2O ($\leq$ 6 μg/L), sulfamethoxazole (SMX) ($\leq$ 2 μg/L), clarithromycin ($\leq$ 0.536 μg/L), and tetracycline ($\leq$ 0.977 μg/L) [4-7].

1.2 Promoting Antibiotic-Resistant Bacteria

The presence of antibiotics in such water systems is of concern primarily due to the potential to trigger antibiotic-resistant bacteria in the environment. Recently, significant unease has been raised regarding their prevalence especially in the medical community where diseases and disease agents that were once thought to be controlled by antibiotics are beginning to resist such therapies [8]. Antibiotic-resistant bacteria are found to be commonplace in hospitals and hospital effluents where antibiotics are regularly administered. A study in 1988 found that the fecal samples of hospitalized patients currently using antibiotics were most resistant to ampicillin where ~ 54 % of 53 patients exhibited low resistance ($\geq$ 10% plated bacteria are resistant) while ~ 15% exhibited high resistance ($\geq$ 50% plated bacteria are resistant) [9]. Interestingly enough, the fecal samples of hospitalized patients not currently using antibiotics also exhibited significant levels of resistance where 67.2% of 189 patients presented low resistance to any of the seven antibiotics tested (ampicillin, streptomycin, tetracycline, kanamycin, chloramphenicol, gentamicin, and nalidixic acid) while 45.0% presented high resistance [9]. Antibiotic-resistant bacteria were also found in raw wastewater, wastewater effluents,

and surface waters in Europe [2] and Australia [10]. As seen in Table 1, a number of resistance phenotypes for various enterococci bacteria (commensal members of the intestinal microbiota of humans and animals) were quantified from raw and treated wastewater collected from a wastewater plant in northern Portugal receiving domestic sewage and industrial effluent [2]. In this case, resistance was 1) negligible for vancomycin, 2) low for amoxicillin and sulfamethoxazole/trimethoprim, 3) prevalent for erythromycin, ciprofloxacin, and tetracycline which ranged from 23-57% for *E. faecalis* and *E. faecium* species, and 4) high for gentamicin which ranged from 39-100% for all three species. Resistance was also found to remain close to constant before and after wastewater treatment for all antibiotics except ciprofloxacin where it was found to increase [2].

Table 1. Prevalence (%) of enterococci with resistance (or intermediary) phenotype for the antibiotics tested * (taken from [2])

	No. of isolates[†]	AML	GEN	ERY	CIP	SXT	TET	$R > 1$[‡]
Enterococcus faecalis	30	0	100	35 (35)	23 (60)	0	57	30
Enterococcus faecium	43	2 (2)	39 (61)	40 (40)	33 (26)	0	38	30
Enterococcus hirae	52	0	41 (46)	7 (2)	2	0	13	4
Other[§]	8	13	0 (100)	71	25	14	29	25
Raw water	56	0	50 (41)	33 (7)	9 (20)	0	31	18
Treated wastewater	77	3 (1)	50 (46)	23 (30)	25 (23)	1	33	21
Total	133	2 (1)	50 (44)	27 (21)	18 (22)	1	32	20

*None of the 65 isolates tested was resistant to vancomycin.
[†]Twelve isolates of *Enterococcus hirae*, one of *Enterococcus faecalis* and one of *Enterococcus faecium* were not able to grow on Mueller Hinton agar and were not tested for antibiotic resistance phenotype.
[‡]$R > 1$. Resistant to more than one antibiotic; as all *Enterococcus faecalis* strains were resistant to GEN, this antibiotic was not considered for this analysis.
[§]Other refers to *Enterococcus avium* and *Enterococcus durans* isolates.
AML, amoxicillin; GEN, gentamicin; ERY, erythromycin; CIP, ciprofloxacin; SXT, sulfamethoxazole/trimethoprim; TET, tetracycline.

A similar study was conducted off the central east coast of Australia where resistance among *Escherichia coli* isolates were determined from a variety of sources, including wastewater treatment plants and surface waters at non-point and point sources [10]. The quantity of resistant isolates to at least one of the antibiotics tested (ampicillin,

cephalothin, nalidixic acid, sulfafurazole, gentamicin, and tetracycline) ranged from 31-87% [10].

Fundamentally speaking, antibiotics become resistant through varying mechanisms in which the mode of action is dependent on both the antibiotic and the genetic resistance determinant chosen by the target microorganism [11,12]. First, the bacterium must acquire the drug resistance genes. This can occur initially through sequential chromosomal mutations within the bacterium but later these resistant genes can be transferred from one bacterium to another through transport of naked DNA (transformation process), plasmids, transposons, or bacteriophages [8,13]. Such a step-by-step process has led to high-level resistance of bacteria towards penicillin and tetracycline [8] as well as vancomycin [14,15], for example. Plasmid transfer can also be promoted in wastewater treatment leading to mean transfer frequencies, representing the number of resistant recipient bacteria per resistant donor, for in-situ mating of 4.9×10^{-5} and 7.5×10^{-5} in primary and secondary settling tanks, respectively [16]. Second, these genes can then carry out differing mechanisms within the cell to inactivate the antibiotic compound. In many cases, such mechanisms are specific to the type of antibiotic present, although it is possible for multiple types of mechanisms to provide resistance to the same antibiotic [8]. Some mechanisms include enzyme modification leading to chemical alteration of the antibiotic through hydrolysis or derivatization, active efflux of the antibiotic from the cell, and modification of the target in order to eliminate or reduce antibiotic binding [17].

Furthermore, it is important to note that, albeit at low concentrations, antibiotics found in the natural environment can continually replenished from contamination sources

and significantly promote the presence of antibiotic-resistant bacteria. Notably, low levels of tetracycline have actually been found to promote transfer of its own resistant genes (through self-transfer of conjugative transposons and mobilization of coresident plasmids) from one bacterium to another by tenfold or at least 100-fold for *E. faecalis* [18] and *Bacteriodes* species [19], respectively.

1.3 Effect of Water Treatment Processes on Antibiotics

The presence of antibiotics in the environment has led to numerous studies investigating the role specific environmental and water treatment processes may have on the fate and transformation of these compounds. Environmental processes related to adsorption and/or oxidation within soils and sediments [20-26] , photolysis [27-29], and biodegradation [30,31] have all been previously investigated in depth. How water treatment processes affect the fate of antibiotics and other organic contaminants is highly dependent on compound properties and water quality characteristics. This study particularly addresses the effects of two water treatment processes, chlorination and membrane filtration. In the following sections, background information will be presented regarding the potential for these and other water treatment processes to remove various PPCPs, especially under varying water quality and operating conditions.

1.3.1 Removal of PPCPs during Wastewater Treatment

In general, water is treated in two different process trains depending on influent water quality. The first process train is related to wastewater treatment which is applied to domestic and industrial wastewaters with high oxygen-demand materials. Typical biological wastewater treatment is designed to remove organic matter, occasionally

oxidize ammonia nitrogen to nitrate nitrogen, and in recent years due to eutrophication, remove phosphorus and nitrogen as well [32]. The treatment process can be broken down into a primary, secondary, and possibly an advanced treatment stage where different biological, chemical, or physical processes take place [33]. The primary stage is related to the physical operation of sedimentation where insoluble organic matter is removed. The effluent from the first stage then undergoes second stage treatment which typically relies on microorganisms to biodegrade the remaining soluble organic material. Different bioreactors can be designed to utilize aerobic, anaerobic, or anoxic microbial environments [32]. In some wastewater treatment facilities, additional processes can then be included such as disinfection by chlorination or ultraviolet (UV) radiation, microbial degradation of phosphorus and nitrogen, and other treatments for pollutant and particle removal [32,33].

The removal of antibiotics as well as other PPCPs during wastewater treatment has widely been assessed in literature by either investigating their removal on-site before and after treatment and/or after a particular treatment step [34-40] or through various scaled-down treatment systems that have been conducted in the laboratory [41,42]. In wastewater treatment, removal of such compounds is primarily driven by sorption and biodegradation. Disinfection processes may also play a significant role, but since wastewaters are not consistently disinfected, their role will be outlined in later sections when drinking water treatment is discussed.

1.3.1.1 Sorption and Biodegradation

As previously mentioned, sorption onto suspended solids is one of the main removal mechanisms of antibiotics and other PPCPs as the suspended solids can then be

removed during sedimentation as primary and secondary sludge [43]. Sorption is primarily driven by either absorption which occurs when aliphatic and aromatic compound moieties interact with the microbial cell wall and fat fractions of the sludge, or adsorption which is dominated by electrostatic interactions between positively charged compound moieties and the microorganism's negatively charged surface [43]. In this environment, sorption can be quantified through an equilibrium relationship between the compound concentrations in the sludge and water phase, as expressed by the Freundlich isotherm (eq 1) below:

$$C_{sorbed} = K_d \cdot C_{dissolved}^{\ n} \qquad (1)$$

where K_d (mL/g or L/kg) is the sorption constant representing the level of partition between the sludge and water phase. $C_{dissolved}$ (mg/mL) and C_{sorbed} (mg/g) are the dissolved and sorbed compound mass quantities per liter of wastewater, respectively. n is a constant and typically close to 1.0 [32]. The K_d values for a number of antibiotics and PPCPs in activated sludge are listed in Table 2.

Table 2. Summary of estimated sorption constants (K_d) in activated sludge for select antibiotics and PPCPs from literature.

Compound	K_d (mL/g or L/kg)
Tetracycline	8400 ± 500 [44]
Oxytetracycline	3020 [45]
Ciprofloxacin	416.9 [45]
Sulfamethoxazole	256± 169 [34]
Trimethoprim	208± 49 [34]
Azithromycin	376± 86 [34]
Clarithromycin	262± 93 [34]
Estrone	402± 126 [46]
17β-estradiol	476± 192 [46]
17α-ethinylestradiol	584± 136 [46]

Among these compounds, tetracycline and oxytetracycline appear to exhibit the largest K_d values and thus the greatest sorption capacity. Their strong desire to partition into the sludge phase is contradictory to their high water solubility and low *n*-octanol/water partitioning coefficients. However, it is found that tetracyclines exhibit strong ionic interactions and metal-complexing properties that most likely drive their sorption potential [44]. Such behavior is thus hypothesized to lead to substantial removal of these compounds during the secondary treatment stage and wastewater treatment in general, as witnessed by 78.4-86.4% removal of tetracycline during the activated sludge process when two lab-scale batch reactors were operated [44]. On the other hand, the remaining antibiotics and PPCPs listed in Table 2 exhibited significantly lower K_d values and are predicted to not be removed well during this process. This is further supported by the

low overall removal observed for compounds such as sulfamethoxazole and clarithromycin which were found at median concentrations of 430 and 380 ng/L in the raw influent and 290 and 240 ng/L in the final effluent, respectively, at two municipal wastewater treatment facilities in Switzerland from 2002-2003 [34].

Biodegradation has also been suggested as a viable option for antibiotic and PPCP removal. A couple of factors should be considered for their possible overall effect in limiting the activated sludge treatment. First, PPCPs are typically at significantly low concentrations in comparison to the large quantity of other organic material in the wastewater matrix, and their ability to induce microbial enzymes could be insufficient [47] . Second, antibiotics as well as a number of PPCPs are bioactive by nature in which case microorganisms may not favor them to be used as energy or carbon sources [33]. With the above limits in mind, however, various studies have determined that certain PPCPs are quite susceptible towards biodegradation and have assessed their reaction rates. One study in particular by Joss et *al.* assessed various groups of PPCPs such as antibiotics, antidepressants, anti-epileptics, hormones, analgesics/anti-inflammatory drugs, iodinated contrast media agents, lipid regulators, neurological drugs, and fragrances. It was found that among them, only four of the 35 compounds tested had degraded by more than 90% over 48 hrs. The four compounds included 17β-estradiol, estrone, paracetamol, and ibuprofen [42]. In addition, 17 of these compounds had degraded by less than 50%, including various sulfonamide antibiotics [42] which were found to be resistant to biodegradation in an additional study as well [48].

Furthermore, limited understanding still remains regarding the various byproducts that can be formed during biodegradation process, especially in regards to their potential

to remain biologically potent. For example, in one study [49], the antibiotic, trimethoprim, was oxidized to form two major byproducts within five days in the presence of nitrifying activated sludge, as seen in Figure 1. In this case, while it appears that the byproducts have only been slightly modified in structure, any changes in their antibacterial activity has yet to be determined [33].

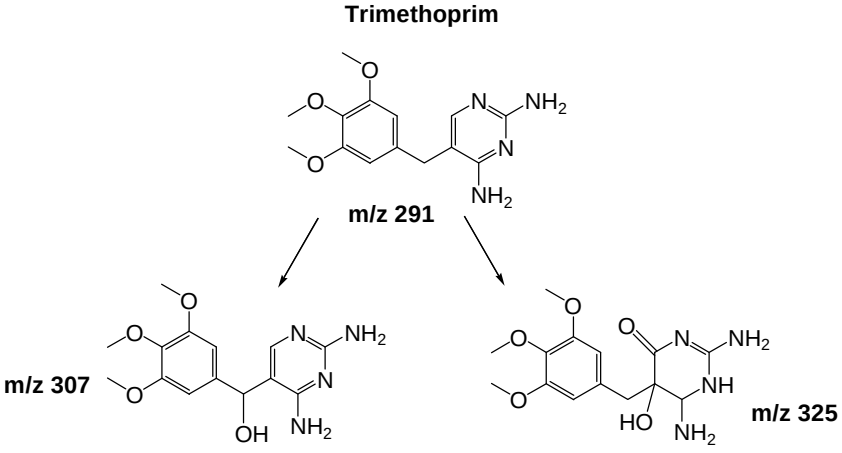

Figure 1. Trimethoprim and its biodegradation byproducts (taken from [49]).

1.3.1.2 Influence of Operating Conditions

It is considered that both changes in influent water quality and plant operating conditions can significantly alter the removal efficiency of PPCPs. Influent water quality though is hard to predict where PPCP loading, flow rate, and the overall concentrations present in wastewater influents can be strongly time dependent [33]. On the other hand, operating conditions can be controlled and monitored up to a certain degree. Parameters such as solids retention time (SRT) or hydraulic retention time (HRT) can be increased to allow for greater PPCP removal [33,44,50]. Solids and hydraulic retention times both refer to the mean residence times of a solid particle and fluid elements within the reactor, respectively. Increasing the SRT or HRT is considered useful practice for a number of

reasons. First, longer residence times allow for longer reaction times of various removal processes (e.g., sorption and biodegradation) to take place and eventually reach equilibrium [33]. Second, longer SRTs can alter the physicochemical properties of microbial flocs which have been shown to become more hydrophobic and less negatively charged on the surface as verified through contact angle and surface charge measurements taken over time [51,52]. Properties which may in turn increase sorption which is a particular process dependent on hydrophobic interactions.

Additional literature has also found that when specific bacteria are used to degrade other contaminants in wastewater such as ammonia (i.e., ammonia oxidizing bacteria) during an additional nitrification step, they can enhance the degradation of various micropollutants, including PPCPs, as well [53-55]. In particular, the antibiotic, trimethoprim, was found to be highly susceptible towards biodegradation in the presence of such bacteria, as seen in Figure 2 [54]. In this study, two separate batch experiments were conducted (Batch-1 and Batch-2), both spiked with mixed liquor suspended solids, ammonia, and trimethoprim, but Batch-2 was additionally spiked with allylthiourea to prevent nitrification of the ammonia oxidizing bacteria [54]. Over 96 hrs, when these ammonia oxidizing bacteria were inhibited, trimethoprim loss decreased from 70 to 25% (Figure 2) [54].

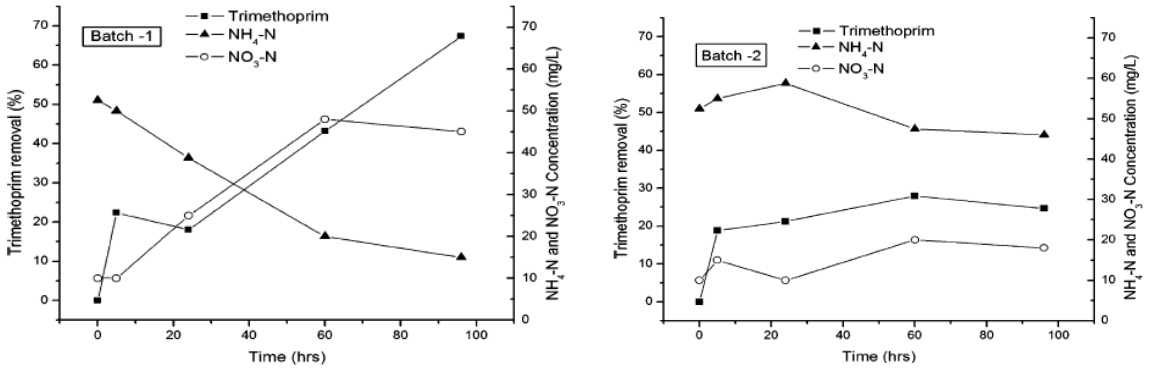

Figure 2. Trimethoprim removal in nitrifying activated sludge. Batch 1 is without allylthiourea addition, and Batch 2 is with allylthiourea addition (taken from [54]).

1.3.2 Removal during Drinking Water Treatment

The second process train considered is drinking water treatment which is applied to surface waters and groundwater to obtain proper water quality for direct human use and consumption. The primary objectives for this treatment are to remove waterborne pathogenic organisms (e.g., bacteria, viruses, protozoa, and algae) and to remove various inorganic and organic constituents. Inorganic constituents may include compounds derived directly from natural waters, contaminated waters, or may result from leached piping and plumbing materials such as lead, copper, and zinc. In addition, compounds such as arsenic, lead, and cadmium may present a health concern since they are known or are suspected to be carcinogens [56]. Organic constituents are prevalent in part due to naturally occurring sources from plants, algae, and microorganisms [56]. A large portion of these compounds is categorized as natural organic matter (NOM) which is a complex mixture of fulvic and humic acids, hydrophilic acids, and carbohydrates [57]. Additional organic constituents may be synthetic compounds such as pesticides, herbicides, organic

solvents, metal degreasers, and polychlorinated byiphenyls (PCBs) which have originated from wastewater effluent and agricultural/urban runoff due to domestic and commercial activities [56].

A conventional drinking water treatment plant is designed to remove the above mentioned constituents in water through a sequence of processes including chemical feed, coagulation/flocculation, sedimentation, filtration, and disinfection. This treatment process can be adapted depending on each facility's specific influent water quality conditions where certain steps may be eliminated (e.g., filtration) while alternative steps may be included (e.g., membrane filtration) [58]. As previously discussed, antibiotics and other PPCPs are organic constituents of concern as they are found in surface waters and groundwater and may make their way into the influents of drinking water treatment facilities. In these following sections, specific treatment processes will be addressed, especially in regard to their ability to remove PPCPs under varying water quality characteristics. In particular, the removal of PPCPs during chlorination and membrane filtration will be outlined in greater depth as they are the focus in this study described in later chapters.

1.3.2.1 Chemical Precipitation Processes

The chemical precipitation processes considered here refers both to coagulation/flocculation as well as to chemical lime softening. Coagulation/flocculation is a process where particles are destabilized, flocs are formed, and NOM is removed upon addition of aluminum- or iron- based salts which then precipitate as metal hydroxides [59,60]. Chemical lime softening removes dissolved calcium and magnesium cations when lime and soda ash are added and pH is increased [60]. Due to particle precipitation,

it is considered that soption which is dependent on hydrophobic and/or electrostatic interactions (similar to that described for sorption in wastewater) could be the main driving mechanism for eliminating antibiotics and other PPCPs. However, it is found that removal of PPCPs by chemical precipitation is generally poor ($\leq$ 33% removal [59,61,62]), as evidenced by several studies where PPCPs were either spiked into surface waters in the laboratory [59,61] or evaluated in the field given existing influent PPCP concentrations [62].

1.3.2.2 Adsorption by Granular and Powdered Activated Carbon

Granular activated carbon (GAC) and powdered activated carbon (PAC) play an important role in water treatment due to their ability to adsorb various organic compounds that cause taste and order problems, pose health risks, and are related to NOM which can form disinfection by-products down the treatment line. The performance of both systems can be significantly affected by various factors related to the activated carbon sorbent (e.g., surface area, pore size distribution, surface charge, and oxygen content) and to the organic compound (e.g., size, charge, shape, and hydrophobicity) [63]. Over the years, most water utilities in the U.S. have primarily used GAC over PAC (25% of 645 utilities and 29% of 600 utilities used PAC in 1977 and 1986, respectively) due to greater adsorption capacity and easier process control [57].

Different antibiotics and PPCPs have been removed by the activated carbon processes at varying degrees depending on the applied GAC/PAC dose [59,61,64]. Given that these processes are sorption controlled, one study by Westerhoff *et al.* aimed to correlate their removals to specific solute properties such as the *n*-octanol/water partitioning coefficient, K_{ow} [59]. In this case, a large number of PPCPs and endocrine-

disrupting compounds were spiked into three different surface water samples (pH = 7.5-8.2, [DOC] = 3-4 mg/L C), and treated with two different powdered activated brands (AC800 (Acticarb) and WPM (Calgon Carbon Corp.)) at dosages ranging from 1-20 mg/L for a contact time of 4 hrs [59]. The removal results using 5 mg/L WPM specifically were then plotted against the predicted log K_{ow} values for each compound, as shown in Figure 3 [59]. Compounds were grouped based on whether LC/MS/MS or GC/MS/MS analytical techniques were used to measure them. For GC/MS/MS compounds, observed percentage removals and log K_{ow} values correlated poorly, while a reasonable linear trend was observed for LC/MS/MS compounds (R^2 = 0.88 after excluding seven outlier compounds) [59]. According to the authors, deviations from this LC/MS/MS linear trend were due to possible inaccuracies in K_{ow} estimation [59]. K_{ow} values were predicted for compounds in their neutral form without considering compound charge for protonated bases and deprotonated acids and in the past have been considered difficult to predict for some heterocyclic or aromatic nitrogen-containing compounds [59].

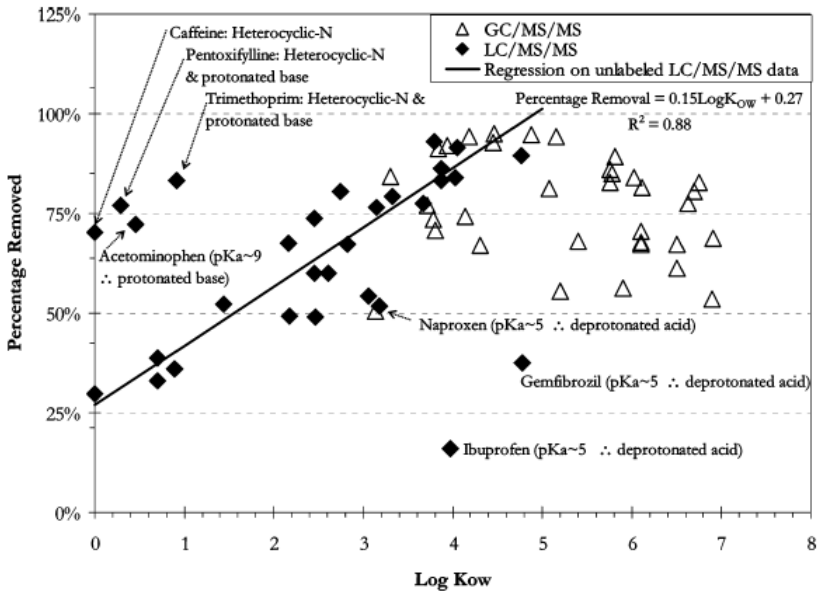

Figure 3. Percent removal of PPCPs and endocrine-disrupting compounds as a function of predicted log K_{ow} (taken from [59]).

It should be further noted that for the removal by GAC/PAC, antibiotics and other PPCPs can be significantly affected by water quality conditions, especially in waters with high dissolved organic carbon (DOC) content where competitive adsorption may begin to play a role. Competitive adsorption in natural waters occurs when dissolved organic matter adsorbs to sites on activated carbon, leading to less adsorption sites for PPCPs either due to direct competition or pore blockage [57,65]. Previous experiments have been conducted where several antibiotics (trimethoprim, carbadox, and various sulfonamides) and 17β-estradiol were spiked in either distilled (DI) or natural waters before different PAC dosages were added [59,61]. Antibiotic removal after a 4 hr contact time in DI water ranged from 57 to 97% and 81% to 98% while in Missouri River water (pH = 7.7 and [DOC]= 10.7 mg/L C) removal typically decreased to range from 49 to 73% and 65 to 100% for PAC dosages of 10 and 20 mg/L, respectively [61]. For 17β-estradiol experiments, a similar trend was found where the average removal after a 4 hr

contact time in DI water (buffered to pH 8.2) was 80% while in Colorado River water (pH 8.2, [DOC] = 3.0 mg/L–C) the average removal decreased to 45% for a 1.0 mg/L PAC dosage [59].

1.3.2.3 Chemical Oxidation with Aqueous Chlorine

Aqueous chlorine ($HOCl$ / OCl^-) is an important drinking water disinfectant and is used in both drinking water and wastewater treatment to achieve chemical oxidation of undesirable taste-, odor-, and color-causing compounds and reduced inorganic species [66,67]. Aqueous chlorine is typically present either as hypochlorous acid ($HOCl$) or its dissociated form, hypochlorite ion (OCl^-), at pH > 5 (eq 2), and may form molecular $Cl_{2(aq)}$ at very low pH or high Cl^- concentrations (eq 3) .

$$HOCl \rightarrow OCl^- + H^+ \quad pK_a = 7.4 \text{ (at 25°C) [68]} \qquad (2)$$

$$Cl_2 + H_2O \rightarrow HOCl + Cl^- + H^+ \quad K = 5.1\times 10^{-4}\ M^2 \text{ (at 25°C) [69]} \qquad (3)$$

In recent decades, the electrophilic character of aqueous chlorine has drawn substantial attention due to reactions with NOM leading to the formation of harmful chlorinated disinfection byproducts (DBPs) (e.g., trihalomethanes (THMs) and haloacetic acids (HAAs)). Substrates such as NOM are readily oxidized since they consist of organic molecules with electron-rich sites that are susceptible towards electrophilic attack. The reaction mechanisms of aqueous chlorine with NOM are complex and may involve oxidation with oxygen transfer and substitutions or additions that lead to chlorinated byproducts [67,70]. The above reactions may then be followed by a number of non-oxidation processes, such as elimination, hydrolysis, and rearrangement reactions [67], further complicating the range of byproducts formed.

Organic compounds such as antibiotics and PPCPs can be considered targets for transformation by aqueous chlorine. Since many antibiotics and PPCPs possess structural moieties and functional groups that are electron-rich, such as activated aromatic rings and amines, chemical transformation of these compounds during chlorine treatment is likely. The rate and extent of such reactions, as well as the byproducts formed, will be highly dependent on the compound's chemical properties, the applied chlorine dose, and water conditions such as pH, temperature, and concentrations and types of dissolved organic or inorganic species present.

Prior studies indicate that a number of PPCPs are highly susceptible towards chlorine oxidation and are readily transformed under various drinking water and wastewater conditions. Thus far, studies have either assessed particular groups of PPCPs that exhibit biological activity (e.g., endocrine disruptors [71,72], β-blockers [73], analgesics [73], and antibiotics [61,74]), or have focused on the detailed reactivity of individual compounds (e.g., 17β-estradiol [75], acetaminophen [76], naproxen [77], caffeine [78], and triclosan [79]). In many of these studies, laboratory-scale experiments were conducted by assessing the removal of spiked PPCPs by aqueous chlorine in synthetic water and/or waters taken from water treatment plants or natural rivers. One particular study examined a large number of PPCPs in which degradation varied greatly (<10% to >90%) after an initial chlorine dose of 2.8-6.75 mg/L as Cl_2, a 24-h contact time, and a solution pH of 5.5 [59]. Concentrations of PPCPs in full-scale treatment plants before and after chlorination were also monitored in order to evaluate the removal of these compounds by chlorine [80]. In many of these studies, reaction kinetics were examined in synthetic waters to determine whether the selected compounds were likely to

be completely depleted during contact times typical of drinking water and wastewater treatment. In limited cases, byproduct analyses were conducted to assist in determining whether reaction products could potentially retain the biological activity of the corresponding parent compounds [75].

Compared to the broad range of PPCPs detected in surface waters, drinking water supplies and wastewaters, the number of PPCP compounds that have been investigated in depth regarding the mechanisms and products of their transformation by chlorine is still quite limited. A fundamental understanding of the reactions of PPCPs with chlorine is critical because it enables identification of reactive functional groups/structural moieties and creates the basis for predicting the fate of other emerging contaminants on the structural basis. For example, many of the target PPCP compounds contain aromatic functional groups with electron-donating substituents (e.g., substituted phenols and aromatic ethers [71,73,75,76,79]) that are known to react readily with chlorine [81]. In a study addressing chlorination of natural hormones (17β-estradiol, estrone, estriol, and progesterone) and one synthetic hormone (17α-ethinylestradiol), all molecules with a phenolic group were rapidly oxidized ($t_{1/2}$= 6-8 min at pH 7, $[chlorine]_0$ = 1 mg/L as Cl_2), whereas progesterone which lacks a phenolic group remained unchanged over 30 min in the presence of excess chlorine [72]. Another study addressing chlorination of analgesics, found that all such compounds containing aromatic ether substituents were reactive towards excess chlorine, whereas those lacking such substituents (e.g., ibuprofen and ketoprofen) did not show any significant losses over 5 days [73]. Amine-containing compounds such as several β-blockers have also been shown to be reactive towards chlorine [73].

1.3.2.4 Rejection by Membrane Filtration

Membrane filtration includes a group of pressure-driven processes such as microfiltration (MF), ultrafiltration (UF), nanofiltration (NF), and reverse osmosis (RO) that are capable of removing a wide variety of contaminants including salts, turbidity, synthetic organic compounds, and pathogens in both wastewater and drinking water treatment [82]. These technologies serve as barriers that vary in effective pore size, and thus each filtration technique is optimized to remove a target group of contaminants in the most cost-effective manner based on solute size. MF membranes, the loosest of all four membranes, typically range in pore size/radius from 0.05-5 μm and are primarily designed to remove microorganisms and particles [83]. Removal is dependent on steric-hindrance effects relative to the size of the membrane pore but can be further aided by cake layer formation on the membrane surface from feedwater materials that can constrict these pores and lead to greater removal potential [83]. UF membranes are slightly tighter in comparison where its pore size/radius ranges from ~1-13 nm [84]. They can be used to further remove humic acids and viruses as well as to achieve greater than 6-log removal for all currently known drinking water pathogens [82,84]. In addition, MF or UF processes can be commonly used in water treatment as a pretreatment step before applying RO or NF membrane filtration.

RO and NF membranes are the most commonly used membrane processes in the U.S. for potable water treatment [85]. In particular, RO membranes, the tightest of all four membranes, are used in a filtration process considered to be diffusion-controlled while operating at a high driving force and pressure. RO membrane filtration has been commonly used to convert seawater (desalination) or brackish water into drinking water

through removal of dissolved salts, primarily in regard to sodium chloride (NaCl) [85]. NF membranes have originally served as an attractive economic alternative to RO membranes due to the lower operating pressures involved and higher water permeability. NF membranes do not retain monovalent salts well and therefore can not be effectively used for desalination, but they retain multivalent ions, making them useful for softening purposes where 60 to 80% hardness can be removed [85]. NF membranes also have a unique porosity, lying between the highly porous MF/UF membranes and RO, and thus low-molecular weight organic contaminants such as pesticides [86-88], endocrine-disrupting compounds [89-91], and various antibiotics and PPCPs [89,92,93] have been shown in numerous studies to be effectively removed.

For antibiotics and PPCPs in particular, NF membrane removal is highly dependent on solute properties, membrane properties, operating conditions, and various water quality characteristics. To date, no known studies have assessed the effect of NF membranes in pilot- or full-scale treatment plants. Instead, studies have been assessed primarily in lab-scale experiments using small-scale cross-flow filtration systems [89,91,92,94] or stirred cells [90,95] where feed water is spiked with antibiotics or PPCPs in either synthetic [89,91,92,94] or natural waters [96]. In addition, compounds of varying molecular weights, shapes, and dipole moments are evaluated using a number of different membranes of varying pore sizes where feed conditions such as pH and ionic strength are altered to assess changes in rejection. Removal is typically dominated by several key mechanisms such as 1) adsorption which is usually greatest at the initial stages of operation, 2) steric hindrance, and/or 3) electrostatic repulsion. Attempts to model the effects of such mechanisms have also been conducted in several studies for

uncharged compounds [91,92,97,98] but has been more limited for charged compounds [98,99].

1.4 Research Objectives

The purpose of this study is to evaluate the impact water quality conditions may have on the fate of select human and veterinary antibiotics during chlorination and nanofiltration in water treatment. The following chapters are meant to present a detailed assessment of how water quality conditions such as pH can affect key mechanisms related to chemical oxidation with aqueous chlorine as well as rejection during nanofiltration. Reaction kinetics and reaction mechanisms and pathways will be assessed along with evaluating the byproducts formed which may or may not retain their biological properties. In addition, rejection due to nanofiltration will be assessed with compounds of varying solute size and membranes with varying pore size. As pH changes, effects of membrane surface charge and antibiotic speciation will be examined. Both a steric-hindrance pore model and the extended Nernst-Planck equation will be applied to the experimental data in order to further elucidate antibiotic-membrane interactions.

The antibiotics investigated in this study were chosen due to their prevalence in wastewaters and surface waters at low concentrations along with their characteristic physicochemical properties. The details regarding their physicochemical properties are as follows. First, carbadox (CDX) is a veterinary antibiotic selected for investigation during chlorination in Chapter 2 primarily due to the presence of electron-rich sites that make this compound readily susceptible towards oxidation under applicable water treatment conditions. As discussed in Chapter 3, the further effect of additional constituents such as tertiary amines during chlorination includes two antibiotics,

flumequine (FLU) and trimethoprim (TMP) and the pharmaceutical compound, salicylic acid (SA). FLU and SA have previously been found to react slowly or negligibly with free chlorine alone and were hypothesized to exhibit enhanced transformation when tertiary amines are added. TMP was investigated due to previous literature suggesting that the pyrimidine moiety which is a functional group belonging to TMP is susceptible towards this enhancement effect as well [100]. Chapters 4 and 5 are related to the removal of the selected antibiotics, sulfamethoxazole (SMX), CDX, and TMP during nanofiltration. These antibiotics were chosen due to their low molecular weight (250-300 amu) and their range of charge properties that are hypothesized to effect rejection under varying water quality conditions such as pH.

1.5 References

1) T. Kümpel, R. Alexy, K. Kümmerer, What Do We Know About Antibiotics in the Environment?, in: K. Kümmerer (Ed.). Pharmaceuticals in the Environment, Springer-Verlag, Berlin, 2001, pp. 67-76.

2) M.F. da Silva, I. Tiago, A. Verissimo, R.A.R. Boaventura, O.C. Nunes, C.M. Manaia, Antibiotic Resistance of Enterococci and Related Bacteria in an Urban Wastewater Treatment Plant, Fems Microbiology Ecology 55 (2006) 322-329.

3) D.W. Kolpin, E.T. Furlong, M.T. Meyer, E.M. Thurman, S.D. Zaugg, L.B. Barber, H.T. Buxton, Pharmaceuticals, Hormones, and Other Organic Wastewater Contaminants in Us Streams, 1999-2000: A National Reconnaissance, Environmental Science & Technology 36 (2002) 1202-1211.

4) X.S. Miao, F. Bishay, M. Chen, C.D. Metcalfe, Occurrence of Antimicrobials in the Final Effluents of Wastewater Treatment Plants in Canada, Environmental Science & Technology 38 (2004) 3533-3541.

5) C.S. McArdell, E. Molnar, M.J.F. Suter, W. Giger, Occurrence and Fate of Macrolide Antibiotics in Wastewater Treatment Plants and in the Glatt Valley Watershed, Switzerland, Environmental Science & Technology 37 (2003) 5479-5486.

6) R. Hirsch, T. Ternes, K. Haberer, K.L. Kratz, Occurrence of Antibiotics in the Aquatic Environment, Science of the Total Environment 225 (1999) 109-118.

7) F. Tamtam, F. Mercier, B. Le Bot, J. Eurin, Q. Tuc Dinh, M. Clément, M. Chevreuil, Occurrence and Fate of Antibiotics in the Seine River in Various Hydrological Conditions, Science of The Total Environment 393 (2008) 84-95.

8) S.B. Levy, B. Marshall, Antibacterial Resistance Worldwide: Causes, Challenges and Responses, Nature Medicine 10 (2004) S122-S129.

9) S.B. Levy, B. Marshall, S. Schluederberg, D. Rowse, J. Davis, High Frequency of Antimicrobial Resistance in Human Fecal Flora, Antimicrob. Agents Chemother. 32 (1988) 1801-1806.

10) A.J. Watkinson, G.B. Micalizzi, G.M. Graham, J.B. Bates, S.D. Costanzo, Antibiotic-Resistant Escherichia Coli in Wastewaters, Surface Waters, and Oysters from an Urban Riverine System, Appl. Environ. Microbiol. 73 (2007) 5667-5670.

11) S.B. Levy, Balancing the Drug-Resistance Equation, Trends in Microbiology 2 (1994) 341-342.

12) S.B. Levy, Factors Impacting on the Problem of Antibiotic Resistance, Journal of Antimicrobial Chemotherapy 49 (2002) 25-30.

13) J. Jensen, Veterinary Medicines and Soil Quality: The Danish Situation as an Example, in: C. G. Daughton,T. L. Jones-Lepp (Ed.). Pharmaceuticals and Personal Care Products in the Environment, Scientific and Regulatory Issues, Oxford University Press, Washington, D.C., 2001, pp. 282-302.

14) K. Hiramatsu, Vancomycin Resistance in Staphylococci, Drug Resistance Updates 1 (1998) 135-150.

15) L.M. Weigel, D.B. Clewell, S.R. Gill, N.C. Clark, L.K. McDougal, S.E. Flannagan, J.F. Kolonay, J. Shetty, G.E. Killgore, F.C. Tenover, Genetic Analysis of a High-Level Vancomycin-Resistant Isolate of Staphylococcus Aureus, Science 302 (2003) 1569-1571.

16) P.A. Mach, D.J. Grimes, R-Plasmid Transfer in a Wastewater Treatment-Plant, Applied and Environmental Microbiology 44 (1982) 1395-1403.

17) J. Davies, Inactivation of Antibiotics and the Dissemination of Resistance Genes, Science 264 (1994) 375-382.

18) O.R. Torres, R.Z. Korman, S.A. Zahler, G.M. Dunny, The Conjugative Transposon Tn925 - Enhancement of Conjugal Transfer by Tetracycline in Enterococcus-Faecalis and Mobilization of Chromosomal Genes in Bacillus-Subtilis and E-Faecalis, Molecular & General Genetics 225 (1991) 395-400.

19) A.M. Stevens, N.B. Shoemaker, L.Y. Li, A.A. Salyers, Tetracycline Regulation of Genes on Bacteroides Conjugative Transposons, J. Bacteriol. 175 (1993) 6134-6141.

20) J. Tolls, Sorption of Veterinary Pharmaceuticals in Soils: A Review, Environmental Science & Technology 35 (2001) 3397-3406.

21) H.C. Zhang, C.H. Huang, Reactivity and Transformation of Antibacterial N-Oxides in the Presence of Manganese Oxide, Environmental Science & Technology 39 (2005) 593-601.

22) H.C. Zhang, C.H. Huang, Oxidative Transformation of Triclosan and Chlorophene by Manganese Oxides, Environmental Science & Technology 37 (2003) 2421-2430.

23) H.C. Zhang, C.H. Huang, Oxidative Transformation of Fluoroquinolone Antibacterial Agents and Structurally Related Amines by Manganese Oxide, Environmental Science & Technology 39 (2005) 4474-4483.

24) H. Zhang, C.-H. Huang, Adsorption and Oxidation of Fluoroquinolone Antibacterial Agents and Structurally Related Amines with Goethite, Chemosphere 66 (2007) 1502-1512.

25) S.A. Sassman, A.K. Sarmah, L.S. Lee, Sorption of Tylosin a, D, and a-Aldol and Degradation of Tylosin a in Soils, Environmental Toxicology and Chemistry 26 (2007) 1629-1635.

26) T.J. Strock, S.A. Sassman, L.S. Lee, Sorption and Related Properties of the Swine Antibiotic Carbadox and Associated N-Oxide Reduced Metabolites, Environmental Science & Technology 39 (2005) 3134-3142.

27) E. Fasani, M. Rampi, A. Albini, Photochemistry of Some Fluoroquinolones: Effect of Ph and Chloride Ion, Journal of the Chemical Society-Perkin Transactions 2 (1999) 1901-1907.

28) C.W. Knapp, L.A. Cardoza, J.N. Hawes, E.M.H. Wellington, C.K. Larive, D.W. Graham, Fate and Effects of Enrofloxacin in Aquatic Systems under Different Light Conditions, Environmental Science & Technology 39 (2005) 9140-9146.

29) A. Lindstrom, I.J. Buerge, T. Poiger, P.A. Bergqvist, M.D. Muller, H.R. Buser, Occurrence and Environmental Behavior of the Bactericide Triclosan and Its Methyl Derivative in Surface Waters and in Wastewater, Environmental Science & Technology 36 (2002) 2322-2329.

30) I.A. Parshikov, J.P. Freeman, J.O. Lay, R.D. Beger, A.J. Williams, J.B. Sutherland, Regioselective Transformation of Ciprofloxacin to N-Acetylciprofloxacin by the Fungus Mucor Ramannianus, Fems Microbiology Letters 177 (1999) 131-135.

31) H.G. Wetzstein, M. Stadler, H.V. Tichy, A. Dalhoff, W. Karl, Degradation of Ciprofloxacin by Basidiomycetes and Identification of Metabolites Generated by the Brown Rot Fungus Gloeophyllum Striatum, Applied and Environmental Microbiology 65 (1999) 1556-1563.

32) C.P.L. Grady, Jr., G.T. Daigger, H.C. Lim, Biological Wastewater Treatment, 2nd Ed., Marcel Dekker, Inc., New York, 1999.

33) S. Kim, A.S. Weber, A. Batt, D.S. Aga, Removal of Pharmaceuticals in Biological Wastewater Treatment, in: D. S. Aga (Ed.). Fate of Pharmaceuticals in the Environment and in Water Treatment Systems, CRC Press, Boca Raton, 2008, pp. 349-361.

34) A. Gobel, A. Thomsen, C.S. McArdell, A. Joss, W. Giger, Occurrence and Sorption Behavior of Sulfonamides, Macrolides, and Trimethoprim in Activated Sludge Treatment, Environmental Science & Technology 39 (2005) 3981-3989.

35) T.A. Ternes, M. Stumpf, J. Mueller, K. Haberer, R.D. Wilken, M. Servos, Behaviour and Occurrence of Estrogens in Municipal Sewage Treatment Plants - I. Investigations in Germany, Canada and Brazil, Science of the Total Environment 228 (1999) 87.

36) R.H. Lindberg, P. Wennberg, M.I. Johansson, M. Tysklind, B.A.V. Andersson, Screening of Human Antibiotic Substances and Determination of Weekly Mass Flows in Five Sewage Treatment Plants in Sweden, Environmental Science & Technology 39 (2005) 3421-3429.

37) P.M. Thomas, G.D. Foster, Tracking Acidic Pharmaceuticals, Caffeine, and Triclosan through the Wastewater Treatment Process, Environmental Toxicology and Chemistry 24 (2005) 25-30.

38) M.J. Gomez, M.J.M. Bueno, S. Lacorte, A.R. Fernandez-Alba, A. Aguera, Pilot Survey Monitoring Pharmaceuticals and Related Compounds in a Sewage Treatment Plant Located on the Mediterranean Coast, Chemosphere 66 (2007) 993-1002.

39) O.A.H. Jones, N. Voulvoulis, J.N. Lester, The Occurrence and Removal of Selected Pharmaceutical Compounds in a Sewage Treatment Works Utilising Activated Sludge Treatment, Environmental Pollution 145 (2007) 738-744.

40) L. Lishman, S.A. Smyth, K. Sarafin, S. Kleywegt, J. Toito, T. Peart, B. Lee, M. Servos, M. Beland, P. Seto, Occurrence and Reductions of Pharmaceuticals and Personal Care Products and Estrogens by Municipal Wastewater Treatment Plants in Ontario, Canada, Science of the Total Environment 367 (2006) 544-558.

41) T.A. Ternes, P. Kreckel, J. Mueller, Behaviour and Occurrence of Estrogens in Municipal Sewage Treatment Plants - Ii. Aerobic Batch Experiments with Activated Sludge, Science of the Total Environment 225 (1999) 91-99.

42) A. Joss, S. Zabczynski, A. Gobel, B. Hoffmann, D. Loffler, C.S. McArdell, T.A. Ternes, A. Thomsen, H. Siegrist, Biological Degradation of Pharmaceuticals in Municipal Wastewater Treatment: Proposing a Classification Scheme, Water Research 40 (2006) 1686-1696.

43) T.A. Ternes, A. Joss, H. Siegrist, Scrutinizing Pharmaceuticals and Personal Care Products in Wastewater Treatment, Environmental Science & Technology 38 (2004) 392A-399A.

44) S. Kim, P. Eichhorn, J.N. Jensen, A.S. Weber, D.S. Aga, Removal of Antibiotics in Wastewater: Effect of Hydraulic and Solid Retention Times on the Fate of Tetracycline in the Activated Sludge Process, Environmental Science & Technology 39 (2005) 5816-5823.

45) F. Stuer-Lauridsen, M. Birkved, L.P. Hansen, H.C.H. Lutzhoft, B. Halling-Sorensen, Environmental Risk Assessment of Human Pharmaceuticals in Denmark after Normal Therapeutic Use, Chemosphere 40 (2000) 783-793.

46) H.R. Andersen, M. Hansen, J. Kjolholt, F. Stuer-Lauridsen, T. Ternes, B. Halling-Sorensen, Assessment of the Importance of Sorption for Steroid Estrogens Removal During Activated Sludge Treatment, Chemosphere 61 (2005) 139-146.

47) D.L. Sedlak, J.L. Gray, K.E. Pinkston, Contaminants in Recycled Water, Environmental Science & Technology 34 (2000) 509A-515A.

48) F. Ingerslev, B. Halling-Sorensen, Biodegradability Properties of Sulfonamides in Activated Sludge, Environmental Toxicology and Chemistry 19 (2000) 2467-2473.

49) P. Eichhorn, P.L. Ferguson, S. Perez, D.S. Aga, Application of Ion Trap-Ms with Qqtof-Ms in the Identification H/D Exchange and of Microbial Degradates of Trimethoprim in Nitrifying Activated Sludge, Analytical Chemistry 77 (2005) 4176-4184.

50) J.E. Drewes, T. Heberer, K. Reddersen, Fate of Pharmaceuticals During Indirect Potable Reuse, Water Science and Technology 46 (2002) 73-80.

51) W. Lee, S. Kang, H. Shin, Sludge Characteristics and Their Contribution to Microfiltration in Submerged Membrane Bioreactors, Journal of Membrane Science 216 (2003) 217-227.

52) B.Q. Liao, D.G. Allen, I.G. Droppo, G.G. Leppard, S.N. Liss, Surface Properties of Sludge and Their Role in Bioflocculation and Settleability, Water Research 35 (2001) 339-350.

53) S. Perez, P. Eichhorn, D.S. Aga, Evaluating the Biodegradability of Sulfamethazine, Sulfamethoxazole, Sulfathiazole, and Trimethoprim at Different Stages of Sewage Treatment, Environmental Toxicology and Chemistry 24 (2005) 1361-1367.

54) A.L. Batt, S. Kim, D.S. Aga, Enhanced Biodegradation of Iopromide and Trimethoprim in Nitrifying Activated Sludge, Environmental Science & Technology 40 (2006) 7367-7373.

55) W.K. Keener, D.J. Arp, Transformations of Aromatic Compounds by Nitrosomonas Europaea, Appl. Environ. Microbiol. 60 (1994) 1914-1920.

56) P.D. Cohn, M. Cox, P.S. Berger, Health and Aesthetic Aspects of Water Quality, in: R. D. Letterman (Ed.). Water Quality and Treatment: A Handbook of

Community Water Supplies (Awwa), McGraw-Hill, New York, 1999, pp. 2.1-2.86.

57) V.L. Snoeyink, R.S. Summers, Adsorption of Organic Compounds, in: R. D. Letterman (Ed.). Water Quality and Treatment: A Handbook of Community Water Supplies (Awwa), McGraw-Hill, New York, 1999, pp. 13.11-13.83.

58) G. Logsdon, A. Hess, M. Horsley, Guide to Selection of Water Treatment Processes, in: R. D. Letterman (Ed.). Water Quality and Treatment: A Handbook of Community Water Supplies (Awwa), McGraw-Hill, New York, 1999, pp. 3.1-3.26.

59) P. Westerhoff, Y. Yoon, S. Snyder, E. Wert, Fate of Endocrine-Disruptor, Pharmaceutical, and Personal Care Product Chemicals During Simulated Drinking Water Treatment Processes, Environmental Science & Technology 39 (2005) 6649-6663.

60) R.D. Letterman, A. Amirtharajah, C.R. O'Melia, Coagulation and Flocculation, in: R. D. Letterman (Ed.). Water Quality and Treatment: A Handbook of Community Water Supplies (Awwa), McGraw-Hill, New York, 1999, pp. 6.1-6.66.

61) C. Adams, Y. Wang, K. Loftin, M. Meyer, Removal of Antibiotics from Surface and Distilled Water in Conventional Water Treatment Processes, Journal of Environmental Engineering-Asce 128 (2002) 253-260.

62) N.M. Vieno, H. Harkki, T. Tuhkanen, L. Kronberg, Occurrence of Pharmaceuticals in River Water and Their Elimination a Pilot-Scale Drinking Water Treatment Plant, Environmental Science & Technology 41 (2007) 5077-5084.

63) S.A. Snyder, P. Westerhoff, Y. Yoon, D.L. Sedlak, Pharmaceuticals, Personal Care Products, and Endocrine Disruptors in Water: Implications for the Water Industry, Environmental Engineering Science 20 (2003) 449-469.

64) M. Fuerhacker, A. Dürauer, A. Jungbauer, Adsorption Isotherms of 17[Beta]-Estradiol on Granular Activated Carbon (Gac), Chemosphere 44 (2001) 1573-1579.

65) C. Pelekani, V.L. Snoeyink, Competitive Adsorption in Natural Water: Role of Activated Carbon Pore Size, Water Research 33 (1999) 1209-1219.

66) G. Tchobanoglous, F.L. Burton, Wastewater Engineering: Treatment, Disposal, and Reuse, 3rd Ed., McGraw-Hill, New York, 1991.

67) P.C. Singer, D.A. Reckhow, Chemical Oxidation, in: R. D. Letterman (Ed.). Water Quality and Treatment: A Handbook of Community Water Supplies (Awwa), McGraw-Hill, New York, 1999, pp. 12.11-12.51.

68) Crc Handbook of Chemistry and Physics, 87th Ed., D. R. Lide, CRC Press, Boca Raton, 2006.

69) T.X. Wang, D.W. Margerum, Kinetics of Reversible Chlorine Hydrolysis - Temperature-Dependence and General Acid Base-Assisted Mechanisms, Inorganic Chemistry 33 (1994) 1050-1055.

70) R.A. Larson, E.J. Weber, Reaction Mechanisms in Environmental Organic Chemistry, Lewis Publishers, Boca Raton, 1994.

71) A. Alum, Y. Yoon, P. Westerhoff, M. Abbaszadegan, Oxidation of Bisphenol a, 17 Beta-Estradiol, and 17 Alpha-Ethynyl Estradiol and Byproduct Estrogenicity, Environmental Toxicology 19 (2004) 257-264.

72) M. Deborde, S. Rabouan, H. Gallard, B. Legube, Aqueous Chlorination Kinetics of Some Endocrine Disruptors, Environmental Science & Technology 38 (2004) 5577-5583.

73) K.E. Pinkston, D.L. Sedlak, Transformation of Aromatic Ether-and Amine-Containing Pharmaceuticals During Chlorine Disinfection, Environmental Science & Technology 38 (2004) 4019-4025.

74) E. Chamberlain, C. Adams, Oxidation of Sulfonamides, Macrolides, and Carbadox with Free Chlorine and Monochloramine, Water Research 40 (2006) 2517-2526.

75) J.Y. Hu, S.J. Cheng, T. Aizawa, Y. Terao, S. Kunikane, Products of Aqueous Chlorination of 17 Beta-Estradiol and Their Estrogenic Activities, Environmental Science & Technology 37 (2003) 5665-5670.

76) M. Bedner, W.A. Maccrehan, Transformation of Acetaminophen by Chlorination Produces the Toxicants 1,4-Benzoquinone and N-Acetyl-P-Benzoquinone Imine, Environmental Science & Technology 40 (2006) 516-522.

77) G.R. Boyd, S.Y. Zhang, D.A. Grimm, Naproxen Removal from Water by Chlorination and Biofilm Processes, Water Research 39 (2005) 668-676.

78) J.P. Gould, J.T. Richards, The Kinetics and Products of the Chlorination of Caffeine in Aqueous-Solution, Water Research 18 (1984) 1001-1009.

79) K.L. Rule, V.R. Ebbett, P.J. Vikesland, Formation of Chloroform and Chlorinated Organics by Free-Chlorine-Mediated Oxidation of Triclosan, Environmental Science & Technology 39 (2005) 3176-3185.

80) J.E. Renew, C.H. Huang, Simultaneous Determination of Fluoroquinolone, Sulfonamide, and Trimethoprim Antibiotics in Wastewater Using Tandem Solid Phase Extraction and Liquid Chromatography-Electrospray Mass Spectrometry, Journal of Chromatography A 1042 (2004) 113-121.

81) H. Gallard, U. Von Gunten, Chlorination of Phenols: Kinetics and Formation of Chloroform, Environmental Science & Technology 36 (2002) 884-890.

82) J.S. Taylor, M. Wiesner, Membranes, in: R. D. Letterman (Ed.). Water Quality and Treatment: A Handbook of Community Water Supplies (Awwa), McGraw-Hill, New York, 1999, pp. 11.11-11.71.

83) J.G. Jacangelo, C.A. Buckley, Microfiltration, in: J. Mallevialle, P. E. Odendaal,M. R. Wiesner (Ed.). Water Treatment: Membrane Processes, McGraw-Hill, New York, 1996, pp. 11.11-11.39.

84) C. Anselme, E.P. Jacobs, Ultrafiltration, in: J. Mallevialle, P. E. Odendaal,M. R. Wiesner (Ed.). Water Treatment: Membrane Processes, McGraw-Hill, New York, 1996, pp. 10.11-10.88.

85) J.S. Taylor, E.P. Jacobs, Reverse Osmosis and Nanofiltration, in: J. Mallevialle, P. E. Odendaal,M. R. Wiesner (Ed.). Water Treatment: Membrane Processes, McGraw-Hill, New York, 1996, pp. 9.1-9.70.

86) Y. Kiso, Y. Nishimura, T. Kitao, K. Nishimura, Rejection Properties of Non-Phenylic Pesticides with Nanofiltration Membranes, Journal of Membrane Science 171 (2000) 229-237.

87) B. Van der Bruggen, K. Everaert, D. Wilms, C. Vandecasteele, The Use of Nanofiltration for the Removal of Pesticides from Groundwater: An Evaluation, Water Science and Technology: Water Supply 1 (2001) 99-106.

88) S.-S. Chen, J.S. Taylor, L.A. Mulford, C.D. Norris, Influences of Molecular Weight, Molecular Size, Flux, and Recovery for Aromatic Pesticide Removal by Nanofiltration Membranes, Desalination 160 (2004) 103-111.

89) K. Kimura, G. Amy, J.E. Drewes, T. Heberer, T.-U. Kim, Y. Watanabe, Rejection of Organic Micropollutants (Disinfection by-Products, Endocrine Disrupting Compounds, and Pharmaceutically Active Compounds) by Nf/Ro Membranes, Journal of Membrane Science 227 (2003) 113-121.

90) A.I. Schafer, L.D. Nghiem, T.D. Waite, Removal of the Natural Hormone Estrone from Aqueous Solutions Using Nanofiltration and Reverse Osmosis, Environmental Science and Technology 37 (2003) 182-188.

91) L.D. Nghiem, A.I. Schafer, M. Elimelech, Removal of Natural Hormones by Nanofiltration Membranes: Measurement, Modeling, and Mechanisms, Environmental Science & Technology 38 (2004) 1888-1896.

92) L.D. Nghiem, A.I. Schafer, M. Elimelech, Pharmaceutical Retention Mechanisms by Nanofiltration Membranes, Environmental Science & Technology 39 (2005) 7698-7705.

93) L.D. Nghiem, A.I. Schafer, M. Elimelech, Role of Electrostatic Interactions in the Retention of Pharmaceutically Active Contaminants by a Loose Nanofiltration Membrane, Journal of Membrane Science 286 (2006) 52-59.

94) C. Bellona, J.E. Drewes, The Role of Membrane Surface Charge and Solute Physico-Chemical Properties in the Rejection of Organic Acids by Nf Membranes, Journal of Membrane Science 249 (2005) 227-234.

95) L.D. Nghiem, A.I. Schafer, T.D. Waite, Adsorption of Estrone on Nanofiltration and Reverse Osmosis Membranes in Water and Wastewater Treatment, Water Science and Technology 46 (2002) 265-272.

96) A.M. Comerton, R.C. Andrews, D.M. Bagley, C.Y. Hao, The Rejection of Endocrine Disrupting and Pharmaceutically Active Compounds by Nf and Ro Membranes as a Function of Compound a Water Matrix Properties, Journal of Membrane Science 313 (2008) 323-335.

97) B. Van der Bruggen, C. Vandecasteele, Modelling of the Retention of Uncharged Molecules with Nanofiltration, Water Research 36 (2002) 1360-1368.

98) T.U. Kim, J.E. Drewes, R.S. Summers, G.L. Amy, Solute Transport Model for Trace Organic Neutral and Charged Compounds through Nanofiltration and Reverse Osmosis Membranes, Water Research 41 (2007) 3977-3988.

99) S. Lee, R.M. Lueptow, Membrane Rejection of Nitrogen Compounds, Environmental Science & Technology 35 (2001) 3008-3018.

100) W.A. Prutz, Reactions of Hypochlorous Acid with Biological Substrates Are Activated Catalytically by Tertiary Amines, Archives of Biochemistry and Biophysics 357 (1998) 265-273.

CHAPTER 2

Reaction Kinetics and Transformation of Carbadox and Structurally Related Compounds with Aqueous Chlorine

Abstract

The potential release of carbadox (CDX), a commonly used antibacterial agent in swine husbandry, into water systems is of concerns due to its carcinogenic and genotoxic effects. Until this study, the reactivity of carbadox towards aqueous chlorine is poorly understood. Chemical reactivity, reaction kinetics, and transformation pathways of carbadox and structurally-related compounds with free and combined chlorine under typical water treatment conditions were determined. Free chlorine reacts rapidly with CDX and desoxycarbadox (DCDX), a main metabolite of CDX with no ring *N*-oxide groups. Competition kinetics and batch experiments were used to evaluate highly pH dependent kinetics where k_{app} for CDX ranged from 51.8 to 3.15×10^4 $M^{-1}s^{-1}$ at pH 4-11. DCDX typically reacted 3.3-7.3 times slower, except at pH $\geq$ 9.83. Structurally related compounds including olaquindox, quindoxin, quinoxaline *N*-oxide, quinoxaline, and quinoline *N*-oxide did not react with free chlorine. Unique reactivity of CDX and DCDX involves deprotonation of their hydrazone N-H moieties where initial chlorine attack results in a chlorinated intermediate. Further nucleophilic attack forms non-chlorinated, hydroxylated, and larger molecular weight by-products. All CDX by-products retain their biologically active *N*-oxide groups, suggesting that they may remain potent as antibacterial agents.

2.1 Introduction

Carbadox (methyl-3-(2-quinoxalinylmethylene) carbazate *N,N'*-dioxide) (CDX) (Figure 1) is a veterinary antibacterial agent commonly used in swine husbandry to promote growth and prevent dysentery and bacterial enteritis. In recent years, CDX and one of its major metabolites desoxycarbadox (DCDX) (Figure 1) have been shown to harbor carcinogenic and genotoxic effects (*1-3*). Such concerns have led the European Union to ban the use of CDX in its animal feeds since 1999 (*4*), and the Health Canada to issue a ban on CDX sales since 2001 after reports of misuse and accidental contamination (*3*).

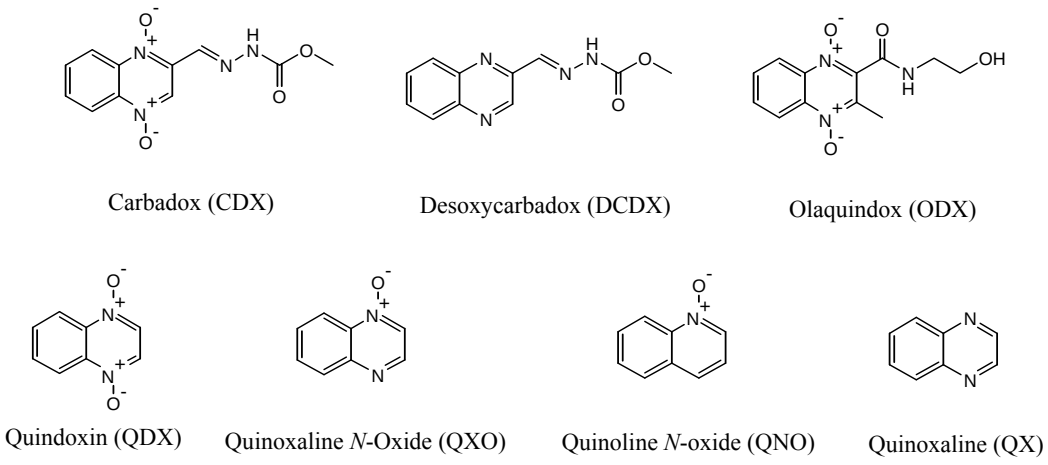

Figure 1. Structures of CDX and related compounds investigated in this study.

Only now, however, have studies begun to investigate the far reaching effects that CDX may have on the surrounding environment, by way of potential exposure of this compound from animal feeds into soil-water matrices. CDX and DCDX have been shown to significantly sorb to soils, in which case sorption was well-correlated to organic carbon, enhanced by the presence of K^+, and found to have a large sorption capacity in

clay minerals (*5*). Exposure to soils and sediments also increases the interaction of these compounds with naturally occurring oxidants such as manganese oxides which have been reported to readily oxidize CDX and to a much slower extent DCDX (*6*). Other transformation pathways such as photolysis of various quinoxaline *N*,*N*'-dioxides (QNOs) has been well documented in past literature and indicates that multiple products can be formed when irradiated under acidic to neutral aqueous conditions (*7,8*) or in methanol (*9,10*). Due to this photoreactivity, further evidence suggests that compounds that contain the QNO moiety such as CDX, quindoxin (QDX) and olaquindox (2-methyl-3-(*N*-(2-hydroxyethyl)carbamoyl)-quinoxaline *N,N'*-dioxide) (ODX) (Figure 1) can undergo photolysis, bind to endogenous proteins, and potentially lead to a photoallergic response (*11-13*). An additional study in 1990 concluded that CDX was more reactive upon irradiation towards human serum albumin (a model protein), compared to QDX and ODX, and should be regarded as a potential photoallergen (*12*).

The persistence of CDX in wastewaters and surface waters has been recently assessed by two occurrence studies, one testing 104 streams in the United States (US) (*13*), and the other testing eight wastewater effluents from five urban centers in Canada (*14*). Both the US and Canadian studies failed to detect concentrations of CDX above their method detection limits (MDL) of 0.1 μg/L and 5 ng/L, respectively. Given the extensive use of this product in animal farming practices, this suggests that while recalcitrance of CDX may be poor, reactivity of these compounds in the environment is likely. To this date, no known studies have assessed the occurrence of DCDX in wastewaters or surface waters.

A limited understanding, however, still remains in regard to the possible effects that water treatment processes have on the fate of CDX and DCDX that originate from

agricultural runoff and wastewater intakes. Chlorination and chloramination are likely processes that may affect the fate of these compounds due to common use in water and wastewater treatment for disinfection purposes. Prior studies indicate that a variety of antibiotics are highly susceptible towards chlorine oxidation and are readily transformed both in laboratory controlled systems (*15-17*) and in full-scale treatment plants (*18*). Complete mineralization is seldom achieved but rather a range of higher- or lower-molecular weight and chlorinated by-products can be formed (*16,17*). Chlorination of antibiotics under water disinfection conditions have been conducted for only a limited number of structural classes, and currently, no studies have addressed the potential reactivity of CDX and DCDX.

In this study, we have evaluated the chemical reactivity, reaction kinetics, and transformation pathways of CDX, DCDX, and various structurally related compounds including ODX, QDX, quinoxaline *N*-oxide (QXO), quinoline *N*-oxide (QNO) and quinoxaline (QX) (Figure 1) with free chlorine and combined chlorine (CC). We determined reaction kinetics over varying pH conditions using both competition kinetics and batch experiments and modeled the rates observed to known speciation and reaction effects. By-product identification and reactivity of structurally related compounds were used to facilitate identification of reactive functional groups and reaction mechanisms and pathways. Additional experiments were conducted in surface waters to confirm that reaction rates and by-products observed could be applied to real water matrices.

2.2 Experimental Section.

2.2.1 Chemicals and Reagent Preparation. Details for chemical reagents, preparation of stock solutions, and collection and handling of surface water samples are described in Sup. Info. Text S1.

2.2.2 Batch Experiments. To assess slow kinetic rates and reaction by-products, batch reactions were conducted in 25-mL amber glass vials at pH 4-11 under continuous stirring at 25°C. Reactions were buffered using 50 mM acetate (pH 4-5.5), 50 mM phosphate (pH 6-8) or 10 mM borate (pH 9-11). Initial concentration of test compounds (Figure 1) was 10 μM (slow reaction kinetics) or 50 μM (by-product analysis). Reactions were initiated by adding either *excess* (10x) or *equal* molar amounts of free chlorine or combined chlorine compared to the target compound. Sample aliquots were periodically taken and instantaneously quenched with $Na_2S_2O_3$ at twice the initial oxidant dose. Batch experiments were also conducted for CDX reaction with free chlorine in $H_2{}^{18}O$ at pH 9 whose detailed experimental setup is available in Sup. Info. Text S2.

2.2.3 Competition Kinetics Experiments. Competition kinetics were employed for CDX and DCDX reactions with free chlorine from pH 6-11. For CDX, DCR was used as a competitor whose reaction with free chlorine is comparatively fast over a similar pH range (*19*). CDX and DCR were added at equimolar concentrations (10 μM) to seven batch reactors at various pHs. Varying substoichiometric amounts of free chlorine (1.5-6.25 μM) were then added. The pH control, mixing conditions and temperature were identical to batch experiments. Sample aliquots were taken after each reaction was completed and analyzed using HPLC/UV/MS. DCDX competition kinetics experiments

were similarly conducted, although CDX was used as a competitor instead of DCR due to DCDX product interference with the DCR peak during HPLC analysis. Initial DCDX and CDX concentrations were added at equimolar amounts of 7.5 μM.

2.2.4 Compound Analysis. *Batch Experiments:* Loss of the target compound over time was monitored using two Agilent 1100 HPLC systems: (I) with a Zorbax SB-C18 column (2.1 × 150 mm, 5 μm) at a flow rate of 0.2 mL/min, and (II) with a Zorbax RX-C18 column (4.6 × 250 mm, 5 μm) at a flow rate of 0.8 mL/min. All compounds (except for DCDX) were detected using a diode-array UV/vis detector (DAD). Due to product interference, DCDX was measured using MS selected ion monitoring (SIM Ion *m/z* 231.1-232.1, fragmentation voltage 25 eV). *Competition Kinetics Experiments:* Simultaneous detection of CDX and DCR and simultaneous detection of DCDX and CDX were conducted using the HPLC system I with DAD detection. *Reaction By-Products***:** Products were analyzed by an Agilent 1100 HPLC/DAD/MSD system with a Zorbax SB-C18 column (2.1 × 150 mm, 5 μm) at a flow rate of 0.2 mL/min. MS analysis was conducted by electrospray ionization in positive mode at both low and high fragmentation voltages (80 and 220 eV). The employed detection wavelengths, HPLC mobile phase conditions and MS parameters are described in Sup. Info. Text S3.

2.3 Results and Discussion

2.3.1 CDX and DCDX Reaction Kinetics with Chlorine. While previous evidence suggests that both the carbazate and imine moieties are susceptible towards acid- and base-catalyzed hydrolysis (*20-22*), CDX degradation over time at an even wider pH range

(2.5-11) without the presence of oxidants was confirmed to be insignificant, especially when considered in oxidant-involved reaction times. Related results are outlined in Sup. Info. Text S4.

For experiments with free or combined chlorine, no measurable loss was observed when an equivalent amount of quenching agent, $Na_2S_2O_3$, was added to the compound alone. $Na_2S_2O_3$ was also verified to have negligible effect on the CDX concentration observed over time, contrary to a previous finding for the antibiotic, sulfamethoxazole (SMX), which suggested that back-reaction of SMX intermediates occurred upon addition of $Na_2S_2O_3$, compromising parent compound peak area (*16*). Experiments conducted to verify the negligible effect of $Na_2S_2O_3$ are outlined in Sup. Info. Text S5.

At pH 3.9-5.4, reaction rates of CDX or DCDX with free chlorine were slow enough to be monitored by parent compound decay over time in batch experiments. The overall CDX (or DCDX) decay can be characterized by a second-order rate expression (eq. 1),

$$\frac{d[CDX]}{dt} = -k_{app}{}^{CDX}[CDX]_T[free\ chlorine]_T = -k_{obs}{}^{CDX}[CDX]_T \qquad (1)$$

Subscript T represents the total concentration of all species for each compound. Under excess chlorine conditions, the loss of CDX or DCDX on a log scale was well correlated with time ($r^2 > 0.99$ for all replicates), verifying first order kinetics with respect to the parent antibacterial agent. In these experiments, residual free chlorine was 28-36% of the initial chlorine dose after reaction completion. Bulking $[\text{free chlorine}]_T$ and k_{app} together yields the pseudo-first order rate constant k_{obs} (s^{-1}). First order kinetics with respect to free chlorine was confirmed with CDX by adding varying doses of excess free chlorine

(100-300 μM), where a well-correlated linear trend ($r^2 > 0.99$) was found between the free chlorine concentration and k_{obs}.

Preliminary experiments found that for pH ≥ 6.3, CDX and DCDX completely reacted in < 10 s in the presence of excess free chlorine. Competition kinetics have been used extensively to assess fast reaction kinetics of various organic contaminants with ozone and hydroxyl radicals (·OH) formed during advanced oxidation processes (AOPs) (*23-27*) and have been modified to apply to this study. A competitor is introduced into the reaction matrix at an equimolar ratio with the target compound, in which both compounds and free chlorine should follow first-order kinetics, as seen by eq. 1 and 2.

$$\frac{d[competitor]}{dt} = -k_{app}^{\ competitor}[competitor]_T[free\ chlorine]_T \qquad (2)$$

Upon dividing the second-order rate expressions with each other, the free chlorine terms can be eliminated, resulting in eq. 3:

$$\frac{d[CDX]}{d[competitor]} = \frac{k_{app}^{\ CDX}[CDX]_T}{k_{app}^{\ competitor}[competitor]_T} \qquad (3)$$

and upon integration, leading to eq. 4:

$$\ln\left(\frac{[CDX]_{T,0}}{[CDX]_{T,t}}\right) = \frac{k_{app}^{\ CDX}}{k_{app}^{\ competitor}}\ln\left(\frac{[competitor]_{T,0}}{[competitor]_{T,t}}\right) \qquad (4)$$

Both $[CDX]_{T,0}$ and $[competitor]_{T,0}$ represent the reactant concentrations before addition of free chlorine, whereas $[CDX]_{T,t}$ and $[competitor]_{T,t}$ represent the remaining reactant concentrations after a specific substoichiometric dose of free chlorine has been added. Plotting this equation leads to a linear correlation, in which the ratio $k_{app}^{CDX} / k_{app}^{competitor}$ can be determined. Previous knowledge of $k_{app}^{competitor}$ can then lead to determination of

$k_{app}^{CDX \text{ or } DCDX}$. Using DCR as the competitor for CDX and CDX as the competitor for DCDX, the relationships between the relative loss of CDX or DCDX in comparison to its competitor (i.e., eq. 4) from pH 6.2-10.7 were obtained (Sup. Info. Figures S1 (CDX) and S2 (DCDX)). All experiments obtained linear trends with $r^2 \geq 0.97$, except for CDX/DCR experiments at pH 10.70 with $r^2 > 0.94$. Based on the k_{app}^{DCR} values (1.0×10^3 - 9.50×10^4 $M^{-1}s^{-1}$) that were previously determined at pH 6-11 (*19*), the k_{app}^{CDX} values were calculated.

Plotting the determined k_{app}^{CDX} values (by batch and competition kinetics) versus correspoding pH yields Figure 2a. Results show that k_{app}^{CDX} is highly dependent upon pH with a maximum reaction rate at pH ~8.32, where k_{app}^{CDX} is 3.15×10^4 $M^{-1}s^{-1}$. k_{app}^{CDX} decreased up to three orders of magnitude as pH was lowered (e.g., $k_{app}^{CDX} = 51.8$ $M^{-1}s^{-1}$ at pH 3.95), and decreased approximately one order of magnitude as pH was raised (e.g., $k_{app}^{CDX} = 2.13 \times 10^3$ $M^{-1}s^{-1}$ at pH 10.7).

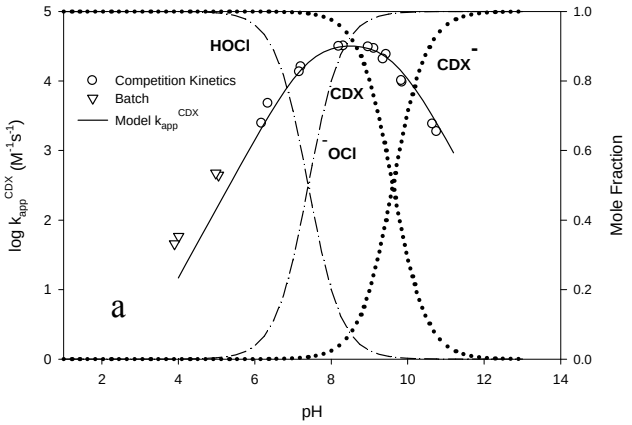

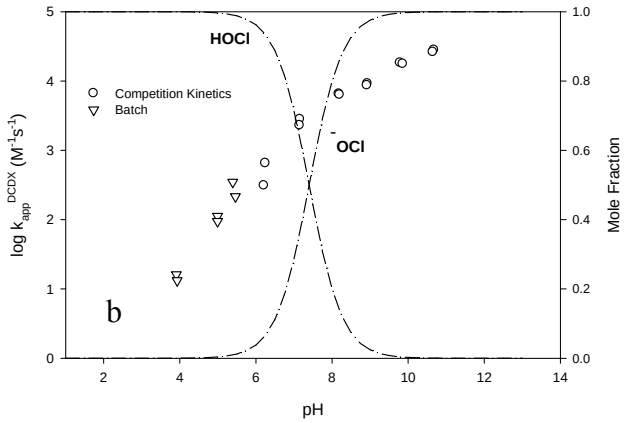

Figure 2. Effect of pH on the apparent second-order rate constants (k_{app}^{CDX} and k_{app}^{DCDX}) for (a) CDX and (b) DCDX reaction with free chlorine using batch and competition kinetic experiments (pH 3.91-10.7, 25°C).

After determining k_{app}^{CDX} at various pHs through model fitting of Figure 2a (see more discussion below), this data was integrated into DCDX/CDX competition kinetics results to calculate the k_{app}^{DCDX} values. As shown in Figure 2b, k_{app}^{DCDX} increased steadily from pH 3.91 (14.6 $M^{-1}s^{-1}$) to pH 10.67 (2.62×10^4 $M^{-1}s^{-1}$). In comparison to CDX, DCDX reacts 3.3-7.3 times slower than CDX from pH 3.91-9.05; however DCDX reacts 1.9-12.4 times faster at pH ≥ 9.83.

At water treatment facilities, water quality conditions are typically near neutral pH. In this situation, CDX and DCDX will degrade rapidly in the presence of free chlorine ($k_{app}^{CDX} = 1.47 \times 10^4$ $M^{-1}s^{-1}$ and $k_{app}^{DCDX} = 2.57 \times 10^3$ $M^{-1}s^{-1}$ at pH 7.2), suggesting that while target compounds may not be present, the by-products formed can be of significance. However, any slight deviations of pH from neutral conditions can have a strong impact on the reaction rate and transformation of CDX and DCDX in real world applications. Furthermore, both CDX and DCDX were found to react at about four

orders of magnitude slower rates with CC than with free chlorine at pH 7.2. Even so, their half-lives are still within the typical residence times in wastewater (5-30 min) and drinking water clearwells (1-24 hr) (more detailed CC results are available in Sup. Info. Text S6).

To further verify similar reactivity in real water matrices, CDX and DCDX reaction rates were assessed in surface water samples under excess free chlorine conditions (Sup. Info. Text S1). Both CDX and DCDX in surface waters (pH = 7.2, DOC = 2.8 mg/L-C) without adding buffer were found to undergo complete transformation in < 30 s at final pH 8.3 and 8.5, respectively, confirming that these compounds are still prone towards rapid decay. Direct comparison of apparent rate constants for CDX and DCDX between surface waters and synthetic waters could not be done using competition kinetics since the competitors' rate constants under these particular water conditions were unknown.

2.3.2 Reactive Moiety Identification by Structurally Related Compounds. ODX did not react at pH 7.39 for up to two hours, and QX, QDX, QXO, and QNO (Figure 1) did not react at pH 7.06-7.13 for up to one hour under excess free chlorine conditions. These results clearly indicate that the quinoxaline *N,N'*-dioxide and quinoxaline moiety on CDX and DCDX, respectively, are not reactive to initial chlorine attack. Instead, the hydrazone side chain of CDX and DCDX is involved. Since CDX and DCDX share the same side chain, it seems quite reasonable that they exhibit fairly comparable reaction rates with chlorine as observed.

2.3.3 Kinetic Model for CDX Reaction with Chlorine. CDX and DCDX's side-chain hydrazone N-H may deprotonate, forming an anion species (can be seen in Scheme 1),

where the estimated pK_a was 9.61 for CDX (by Strock *et al.* (*5*) using Chemaxon). Free chlorine (HOCl and OCl^-) also exhibits pH speciation with pK_a of 7.4 (*28*). CDX and HOCl speciation likely affect the apparent rate constant (k_{app}^{CDX}) trend seen from pH 3.9 to 10.7 (Figure 2a) and therefore are incorporated into eq. 1 in order to derive species-specific rate constants (eq. 5). Previous studies have shown that OCl^- is a much weaker oxidant than HOCl (*16,17,19,29*). Our experimental results concurred with these findings and found that reaction with OCl^- had negligible effect on the overall observed reaction rate and thus the reactions with OCl^- were neglected.

$$\frac{d[CDX]}{dt} = -(k_1[CDX][HOCl] + k_2[CDX^-][HOCl]) \quad (5)$$

Each species concentration can be expressed as a distribution coefficient α (defined by pK_a and $[H^+]$) multiplied by the total of each species concentration (eq. 6):

$$\frac{d[CDX]}{dt} = -(k_1\alpha_{CDX}\alpha_{HOCl} + k_2\alpha_{CDX^-}\alpha_{HOCl}) \times [CDX]_T[free\ chlorine]_T \quad (6)$$

Combining eqs. 1 and 6 yields the following:

$$k_{app}^{CDX} = k_1\alpha_{CDX}\alpha_{HOCl} + k_2\alpha_{CDX^-}\alpha_{HOCl} \quad (7)$$

The data in Figure 3a were fitted to eq. 7 to solve for k_1 and k_2 using the Marquardt-Levenberg nonlinear least-squares regression algorithm from SigmaPlot 2004 software (SYSTAT Software, Inc.). The model compared well to the experimental results from pH 10.7 to 6.27 but highly deviated from experimental results at pH < 6.27. However, by eliminating the first term, $k_1\alpha_{CDX}\alpha_{HOCl}$, from eq. 7, which resulted in eq. 8, the kinetic model correlated well ($r^2 = 0.980$) with experimental results (Figure 2a) where k_2 was $6.02 \pm 0.14 \times 10^6\ M^{-1}s^{-1}$.

$$k_{app}^{CDX} = k_2 \alpha_{CDX^-} \alpha_{HOCl} \quad (8)$$

This model (eq. 8) was applied since CDX reaction rate constants exhibit a well-defined bell-shaped pH profile (Figure 2a). As pH increases, the stronger oxidant HOCl becomes increasingly less abundant while the more reactive CDX^- species in regard to oxidation becomes increasingly more abundant. Such opposite trends for pH often results in a maximum rate at $pH_{max} = (pK_{a,HOCl} + pK_{a,substrate})/2$ (*30*). Indeed, the maximum rate of CDX is near the average of the pK_as of HOCl and CDX ($pH_{max} = 8.5$). This phenomenon suggests that the reaction is completely dominated by HOCl and CDX^- species, and the influence of HOCl and CDX species on the observed reaction rate is negligible (eq. 8).

The pH profile of DCDX's rate constants (Figure 2b), however, differs significantly from that of CDX, an unexpected outcome since the same hydrazone moiety is involved in the reaction. An estimated pK_a of 9.77 (by Chemaxon) for DCDX's hydrazone N-H was reported (*5*). Clearly the experimental data cannot be fitted by either eq. 7 or eq. 8 model based on such pK_a value, although the specific mechanisms leading to this observed phenomenon are not currently understood.

2.3.4 Identification of Chlorination Byproducts. Product generation over time was analyzed for reactions under excess free chlorine conditions at acidic, neutral, and alkaline conditions, respectively. The reaction solutions were quenched with $Na_2S_2O_3$ prior to LC/MS analyses. Separate experiments have confirmed that quenching does not alter the products. Overall, product structure identification was based on spectral

fragmentation patterns, product evolution at different pHs, and other confirmatory experiments (see discussion later).

Five major products (m/z 205, 261, 279, 293, and 321) of CDX (*m/z* 263) were identified (spectra shown in Sup. Info. Figure S3 and structures shown in Scheme 1). The latter four products can be short-written as M-2, M+16, M+30, and M+58 products, indicating the net mass loss or gain of the product from the parent CDX. Similarly, six major products (*m/z* 175, 189, 229, 247, 261, and 289) of DCDX (*m/z* 231) were identified (spectra shown in Sup. Info. Figure S4 and structures shown in Scheme 1). Note that DCDX differs from CDX by -32 amu in mass. The latter four products of DCDX also differ from those in the case of CDX by exactly -32 amu in mass and exhibit quite similar fragmentation patterns, suggesting that these are very comparable products. Fragmentation peaks show clear presence of the quinoxaline fragment (*m/z* 129-131 (slight mass variation due to varying protonation patterns)) for all products, indicating that this heterocyclic aromatic ring was not compromised during reaction with chlorine.

The different products formed at various pHs also give clues to their identities (Figure 3 (CDX) and Sup. Info. Figure S5 (DCDX)). The *m/z* 321 from CDX and *m/z* 289 from DCDX (i.e., M+58 products) were formed only at pH 4.3 and 5.4 where acetate buffer was used to maintained the pH but absent at other higher pHs where acetate buffer was not used, indicating that these products could be acetate (59 amu)-parent compound adducts. In the mass spectra, primary fragmentation indicates loss of 42 amu, which supports cleavage of CH_3CO (Figures S3a and S4a). The *m/z* 321 product also was found to be more dominant at pH 5.4 than pH 4.3 (Figure 3), suggesting that the stronger CH_3COO^- nucleophile (pK_a of acetate is 4.7 (*31*)), instead of CH_3COOH, drove product

formation. To confirm this, two parallel experiments at equimolar CDX and free chlorine were conducted with (pH 5.04) and without acetate buffer (adjusted using HCl, pH 4.98). Without acetate buffer, *m/z* 321 did not form (Sup. Info. Figure S6). The formation of acetate-parent adduct points to the involvement of nucleophilic attack, most likely at the side-chain imine C. Although acetate is a fairly weak nucleophile (*32*), its high concentration in the reaction matrix (50mM) likely rendered it a competitive reactant.

The involvement of nucleophilic attack was further confirmed by experiments with excess chloride ions, also a weak nucleophile (*32*). Reactions of CDX with excess free chlorine were conducted with the presence of 50 mM NaCl at pH 4.06, 4.92 (adjusted by HCl and NaOH) and 7.41 (phosphate buffer). Note that the pH conditions were not acidic enough to generate aqueous chlorine (Cl_2) from the reaction of Cl^- with HOCl (*31*). At pH 7.41, no chlorinated products were found but instead, a hydroxylated product was formed (*m/z* 279). In contrast, at pH 4.06 and 4.92 where hydroxide ion (a much stronger nucleophile (*32*)) concentration is limited, a chlorinated product was observed (*m/z* 297), supporting nucleophilic attack by Cl^- similarly to CH_3COO^- (Sup. Info. Figure S7).

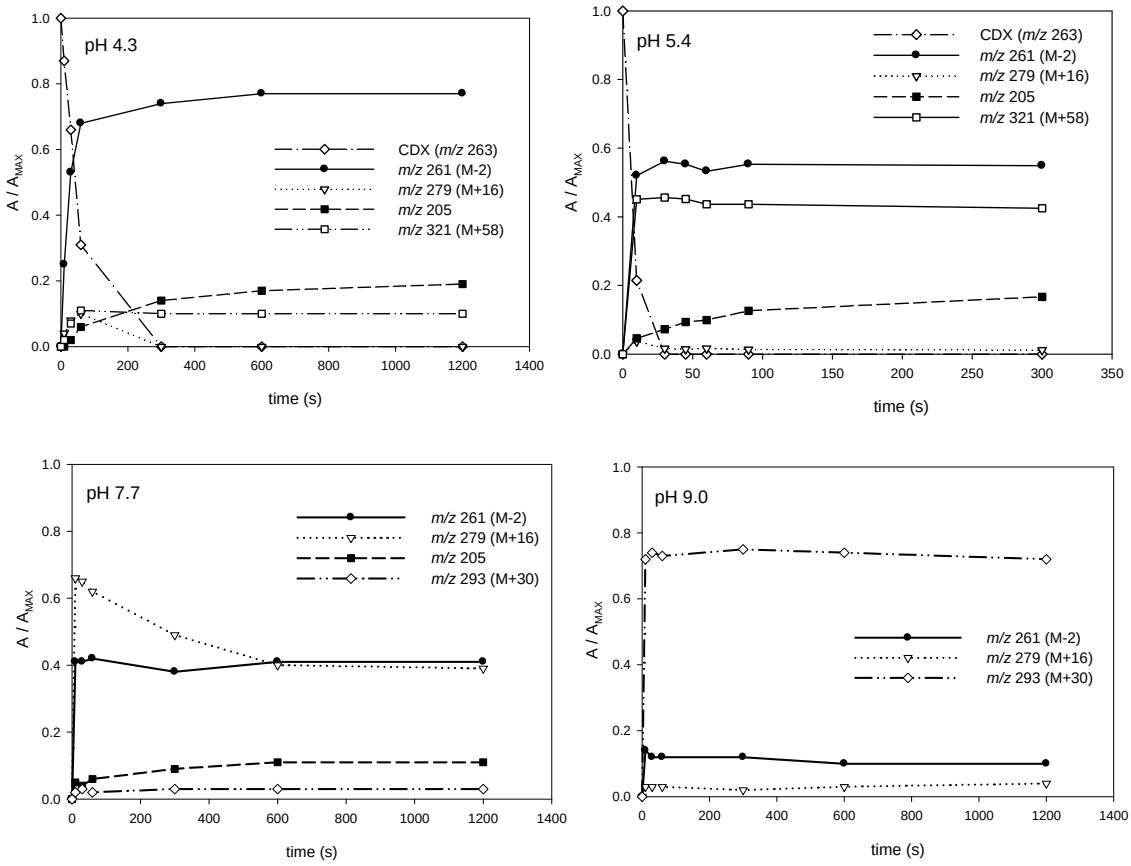

Figure 3. CDX product evolution under excess free chlorine conditions at pH 4.3, 5.4, 7.7, and 9.0 at 23˚C. CDX rapidly decayed in < 10 s for pH 7.7 and 9.0. A/A_{MAX} represents the total MS ion counts of each species (CDX and products) (A) divided by the total ion counts of CDX at t = 0 s (A_{MAX}).

The *m/z* 279 from CDX and *m/z* 247 from DCDX (i.e., M+16 products) were negligible at acidic pH, but significant at neutral pH conditions (Figures 3 and S5). H_2O fragmentation (-18) was observed in *m/z* 279 (Figure S3b). Both products are identified as hydroxylated compounds formed by nucleophilic attack by OH^- or H_2O at the side-chain imine C, which are likely to be in the keto form in water than the enol form due to

greater stability (*33,34*) (Scheme 1). The *m/z* 261 from CDX and *m/z* 229 from DCDX (i.e., M-2 products) are identified as a result of intramolecular nucleophilic attack by the carbonyl group at the imine C leading to side-chain ring closure (Scheme 1). Such ring closure has been reported in oxidation of semicarbazones with similar hydrazone moieties (3*5,36*). The ring closure apparently altered the fragmentation pattern of the side chain, where the common methoxy fragment was no longer present (spectra in Figures S3c and S4c).

At pH 8.9-9.0, the *m/z* 293 from CDX and 261 from DCDX (i.e., M+30 products) were dominant (Figures 3 and S5). The change in mass suggests addition of two O to the parent compound, which may be resulted from attacks by two OH^- to the parent compound at this higher pH. To probe this possibility, chlorination of CDX was conducted in $H_2{}^{18}O$. Experiments found complete degradation of CDX, but little formation of the *m/z* 293 product. Instead, *m/z* 261 and 205 were formed with abundances of 80% and 20%, respectively, of the total product concentration. Formation of *m/z* 261 in this case was unusually high in comparison to experiments conducted in regular water where *m/z* 261 was only ~12% of the total product concentration. This shift in product formation is believed to be caused by the isotope effect of O atom. Isotope effects are a difference in rate or equilibrium position due to a difference in the isotope present in the reaction system. If a particular atom is less tightly bound in the transition state of a reaction than in the reactant, the reaction involving the heavier isotope of that atom will go more slowly (*37*). In this case, because reaction rate with the heavier $^{18}OH^-$ nucleophile is slower, the intramolecular carbonyl nucleophile becomes sufficiently competitive.

Formation of an azoxy compound (R-C(O)-N=N(O)-R') may explain the M+30 product (Scheme 1). Conversion of aldehyde alkyl- and phenylhydrazones to their azoxy compounds by oxidation with peracids was reported (*38,39*). Similarity between oxidation by HOCl and by peracids in kinetics and reactivity was also reported (*30,40,41*). The fragmentation pattern of *m/z* 293 indicates 3 *N*-oxide groups on the molecule (Figure S3d), consistent with the proposed structure.

Structures of product *m/z* 205 from CDX and *m/z* 189 and 175 from DCDX are also proposed (Scheme 1) based on molecular mass and fragmentation patterns (Figures S3e and S4e,f). The product evolution suggests that these products may be generated from slow decay of the M+16 products (Figures 3 and S5).

The same types of by-products were found in the reactions of CDX and DCDX with CC at near neutral pH. It is expected that similar transformation pathways exist during reaction with CC and with free chlorine given identical product formation. Product formation in surface waters was also found to be similar to the products found using synthetic water under excess free chlorine conditions.

Scheme 1. Proposed reaction pathways for CDX and DCDX with free and combined chlorine.

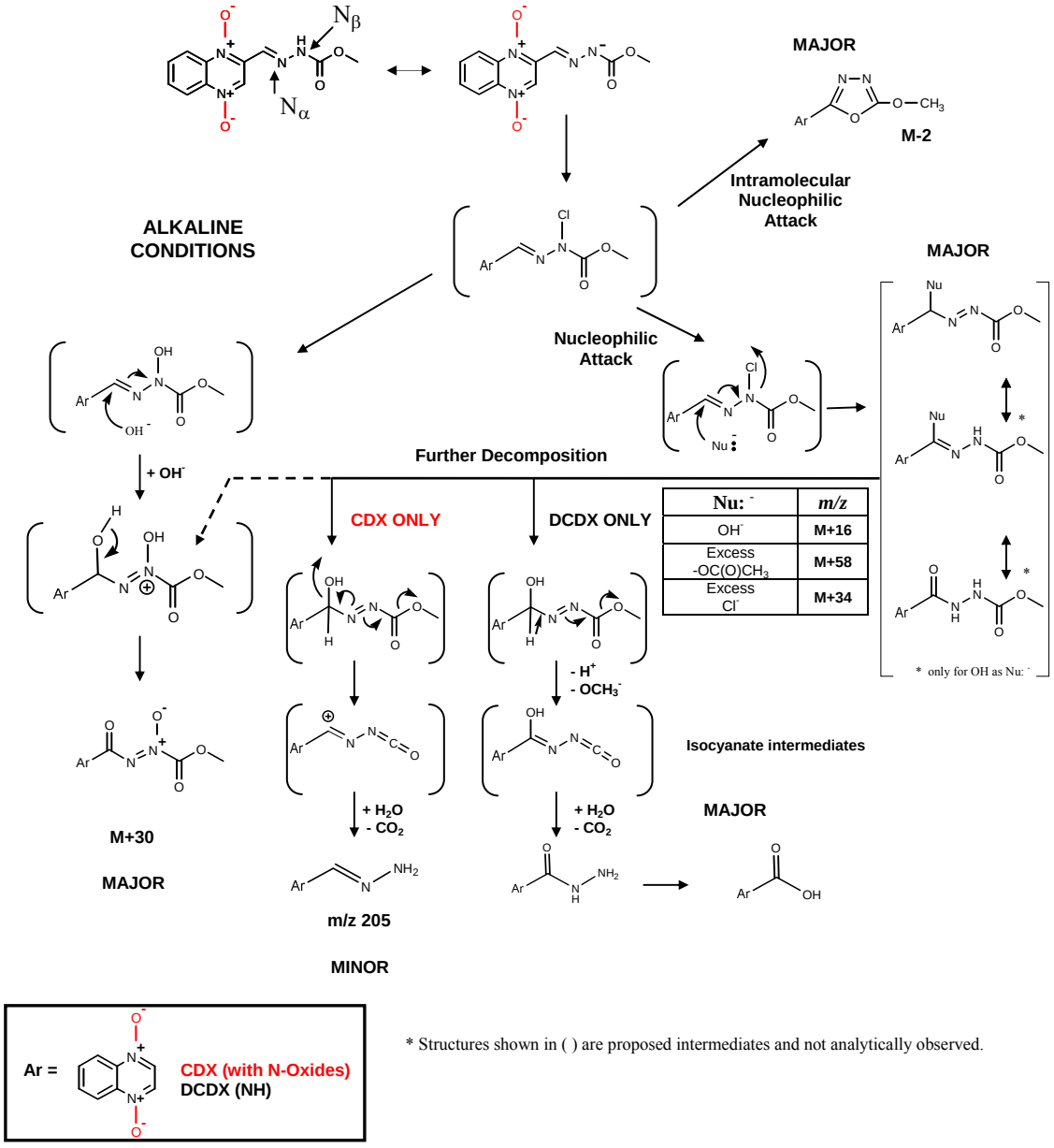

* Structures shown in ( ) are proposed intermediates and not analytically observed.

2.3.5 Proposed CDX and DCDX Reaction Pathways. The above results clearly show that CDX and DCDX share similar mechanisms in reaction with chlorine via their hydrazone side chain (-CH=N_α-N_βH-). The kinetic modeling indicates that deprotonation of hydrazone N-H results in a negative charge that substantially enhances reactivity toward electrophilic chlorine, implying that the hydrazone N_β is a critical site for initial chlorine attack. It is, however, well recognized that amide N is less reactive to chlorine due to electron-withdrawing effect of the neighboring carbonyl group. Earlier studies have reported second-order rate constants in the order of 10^{-1} $M^{-1}s^{-1}$ for amides, compared to $10^{7\text{-}8}$ $M^{-1}s^{-1}$ for primary and secondary amines and 10^{4} $M^{-1}s^{-1}$ for tertiary amines (*42*). Despite that the hydrazone N_β does have a neighboring carbonyl group, the hydrazone linkage apparently gives a uniquely high reactivity to chlorine. No reports are available on reaction of chlorine with hydrazone structures closely resemble that of CDX and DCDX. However, we found that the magnitude and pH profile of CDX's rate constants in reaction with chlorine strikingly similar to those of arylazonaphthol dyes that adopt hydrazone tautomeric form as below (*30*).

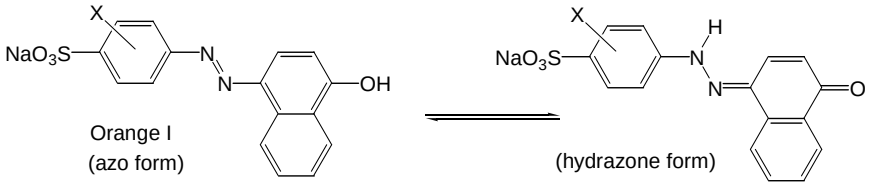

In aqueous media, the hydrazone tautomer dominates for the dyes (*30,40*), and mostly likely for CDX and DCDX as well. These azo dyes are known to be much more reactive to aqueous chlorine than those that do not tautomerize to hydrazone forms (*30,40*). Similar to CDX, Orange I has a pK_a value (10.8) corresponding to deprotonation of hydrazone N-H. Previous work by Oaks and Gratton (*30,40*) also concluded that the

neutral HOCl and anionic dye species as the key reactant species through examination of a series of substituted Orange I compounds on the aryl ring (shown above) that would lead to different pK_a for the dyes (see more details in the original papers). Using the same approach and others (e.g., the N_β-methylated analog was found to react much slower with chlorine), the authors identified the hydrazone N_β as the initial reaction site with chlorine.

Furthermore, atomic charges of CDX and DCDX in aqueous phase were calculated by the Charge Model 2 (CM2) program (*43*). The calculated charges for the hydrazone atoms (in the order of C, N_α and N_β) were +0.115, -0.225 and -0.505 for CDX, and +0.116, -0.235 and -0.506 for DCDX. Since N_β has the highest electron density, it should naturally be the first site of attack by the chlorine electrophile. The very similar electron density within the hydrazone linkage for CDX and DCDX also indicates that the difference in their reactivities mostly stems from the difference in intramolecular H-bonding as discussed earlier.

Based on the information presented thus far, reaction pathways for CDX/DCDX with chlorine are proposed in Scheme 1. In general, the reaction begins with an initial HOCl attack at the hydrazone N_β of CDX^- or $DCDX^-$, leading to an N-chloro intermediate. The N-chloro intermediate is then subject to attack by a nucleophile available intramolecularly (i.e., the carbonyl group) or in water (e.g., OH^-, CH_3COO^- and Cl^-) at the imine C to release HCl or Cl^- to yield various nucleophile-added products. The product evolution indicates that the hydroxylated products (i.e., M+16) may gradually decay, probably via formation of an isocyanate intermediate that quickly decomposes in water (*44*), to yield the *m/z* 205 product for CDX and the *m/z* 189 and 175 products for

DCDX. All the above pathways were observed in acidic to slightly basic conditions. The product distribution at different pH clearly shows that, as pH increases, the much stronger OH^- nucleophile becomes more abundant and plays an increasingly greater role in product formation.

At alkaline pH (8.9-9.0), attack by two OH^- ions becomes possible due to their higher concentration, one at the imine C and the other at N_β. In the presence of excess chlorine, the hydroxylated intermediate is finally oxidized to an azoxy compound (i.e., M+30). As discussed earlier, if the same alkaline reaction occurs in $H_2{}^{18}O$ water, the isotope effect shifts the reaction to the intramolecular nucleophilic attack pathway that would not occur normally because of out-competition by the more reactive OH^- nucleophile. This observation supports the proposed mechanism that nucleophilic attack occurs after the chlorine attack.

2.4 Environmental Significance

It is clear that CDX and DCDX are highly reactive antibacterial agents with free and combined chlorine, that will not readily mineralize, but will form multiple non-chlorinated, high molecular weight by-products. While this is evident in synthetic waters, further experimental evidence using surface waters verifies that both the kinetics and product formation assessed in this study are comparable to the true observations that would be found given a complex water matrix. This study also determined that the structurally related compounds, ODX, QDX, QXO, QX, and QNO are nonreactive towards free chlorine attack. Therefore, moieties such as quinoxaline with or without the presence of the *N*-oxide moiety can be considered highly unreactive species in regard to free chlorine oxidation.

Antibacterial activity of agents such as CDX rests on the presence of the *N*-oxide groups which impair DNA synthesis by forming a radical upon *N*-oxide reduction (*45,46*). In this study, the CDX *N*-oxide moiety was not transformed during reaction with free chlorine, and all by-products formed continued to possess this functional group. Such by-product formation is opposite to findings where the *N*-oxide moiety is readily cleaved via oxidation by MnO_2 in soils and sediments (*6*). This suggests that, upon free chlorine addition in wastewater and water treatment facilities, the activity of CDX by-products formed will not be comprised and can act as potent biological agents further downstream.

2.5 Acknowledgements

We thank Georgia Water Resources Institute for financial supports for this study. A.D. Shah thanks partial financial supports from Saehan Industries, Inc. in Korea and NSF IGERT Fellowship. We gratefully thank Dr. Paul Winget at the US EPA National Exposure Research Laboratory, Athens, Georgia, for performing atomic charge calculations.

2.6 Supporting Information

Additional text and figures address (1) chemical reagents, stock solutions, and surface water samples; (2) experimental setup for CDX reaction with free chlorine in $H_2{}^{18}O$ at pH 9; (3) DAD detection wavelengths, HPLC mobile phase conditions, and MS parameters; (4) results for CDX hydrolysis without oxidant addition; (5) $Na_2S_2O_3$ quenching effects on observed CDX kinetics; (6) competition kinetic results; (7) CDX and DCDX reaction kinetics with combined chlorine; (8) spectra of CDX and DCDX chlorination by-products; (9) DCDX product evolution under excess free chlorine conditions; (10) CDX products formed with and without acetate addition; (11) CDX-Cl product formed upon NaCl addition.

2.7 References

(1) FAO/WHO. Joint expert committee on food additives. Evaluation of certain veterinary drug residues in food. *Tech. Ser.* **1990**, 799, 45.

(2) WHO. Toxicological evaluation of certain veterinary drug residues in food. *WHO Food Additives Ser.* **1991,** 27.

(3) JECFA 60th meeting of the joint FAO/WHO Expert Committee on Food Additives. Toxicological evaluation of certain veterinary drug residues in food. *WHO Food Additives Ser.* **2003**, 51, 50-59.

(4) Commission Regulation No. 2788/98. *Off. J. Eur. Commun.* **1998.**

(5) Strock, T. J.; Sassman, S. A.; Lee, L. S. Sorption and related properties of the swine antibiotic carbadox and associated N-oxide reduced metabolites. *Environ. Sci. Technol.* **2005,** 39, 3134-3142.

(6) Zhang, H.; Huang, C.-H. Reactivity and transformation of antibacterial N-oxides in the presence of manganese oxide. *Environ. Sci. Technol.* **2005,** 39, 593-601.

(7) Kawata, H.; Kikuchi, K.; Kokubun, H. Studies of the photoreactions of heterocyclic *N*-dioxides - identification of the oxaziridine intermediate of quinoxaline-1,4-dioxide. *J. Photochem*. **1983**, 21, 343-350.

(8) Cheeseman, G. W. H., Torzs, E. S. G. Quinoxalines and related compounds. Part VII. Some reactions of quinoxaline *N*-oxides. *J. Chem. Soc. C.* **1966**, 157-160.

(9) Haddadin, M. J.; Agopian, G.; Issidorides, C.H. Synthesis and photolysis of some substituted quinoxaline di-*N*-oxides. *J. Org. Chem.* **1971,** 36, 514-518.

(10) Jarrar, A. A.; Fataftah, Z. A. Photolysis of some quinoxaline-1,4-dioxides. *Tetrahedron* **1977,** 33, 2127-2129.

(11) Kochevar, I. E. Photoallergic responses to chemicals. *Photochem. Photobiol.* **1979**, 30, 437-442.

(12) Devries, H.; Bojarski, J.; Donker, A. A.; Bakri, A.; Vanhenegouwen, G. Photochemical-reactions of quindoxin, olaquindox, carbadox and cyadox with protein, indicating photoallergic properties. *Toxicology* **1990,** 63, 85-95.

(13) Kolpin, D. W.; Furlong, E. T.; Meyer, M. T.; Thurman, E. M.; Zaugg, S. D.; Barber, L. B.; Buxton, H. T. Pharmaceuticals, hormones, and other organic wastewater contaminants in U.S. streams, 1999-2000: A national reconnaissance. *Environ. Sci. Technol.* **2002,** 36, 1202-1211.

(14) Miao, X. S.; Bishay, F.; Chen, M.; Metcalfe, C. D. Occurrence of antimicrobials in the final effluents of wastewater treatment plants in Canada. *Environ. Sci. Technol.* **2004,** 38, 3533-3541.

(15) Adams, C.; Wang, Y.; Loftin, K.; Meyer, M. Removal of antibiotics from surface and distilled water in conventional water treatment processes. *J. Environ. Eng. - Asce* **2002,** 128, 253-260.

(16) Dodd, M. C.; Huang, C.-H. Transformation of the antibacterial agent sulfamethoxazole in reactions with chlorine: Kinetics, mechanisms, and pathways. *Environ. Sci. Technol.* **2004,** 38, 5607-5615.

(17) Dodd, M. C.; Shah, A. D.; Von Gunten, U.; Huang, C.-H. Interactions of fluoroquinolone antibacterial agents with aqueous chlorine: Reaction kinetics, mechanisms, and transformation pathways. *Environ. Sci. Technol.* **2005,** 39, 7065-7076.

(18) Renew, J. E.; Huang, C.-H. Simultaneous determination of fluoroquinolone, sulfonamide, and trimethoprim antibiotics in wastewater using tandem solid phase extraction and liquid chromatography-electrospray mass spectrometry. *J. Chromatogr. A* **2004,** 1042, 113-121.

(19) Rebenne, L. M.; Gonzalez, A. C.; Olson, T. M. Aqueous chlorination kinetics and mechanism of substituted dihydroxybenzenes. *Environ. Sci. Technol.* **1996,** 30, 2235-2242.

(20) Bruylants, A.; Feytmants-de Medicis, E. In *The Chemistry of the Carbon-Nitrogen Double Bond*; Patai, S., Ed.; John Wiley & Sons: London, 1970; pp 468-492.

(21) Safraoui, A.; Calmon, M.; Calmon, J. P. Kinetics of the alkaline-hydrolysis of several alkyl phenylcarbazates. *J. Chem. Soc.- Perk. Trans. 2* **1991**, 1349-1352.

(22) Vlasak, P.; Mindl, J. Kinetics and mechanism of alkaline hydrolysis of aryl carbazates. *J. Chem. Soc.- Perk. Trans. 2* **1997**, 1401-1403.

(23) Gurol, M. D.; Nekouinaini, S. Kinetic behavior of ozone in aqueous solutions of substituted phenols. *Ind. Eng. Chem. Fund.* **1984,** 23, 54-60.

(24) Haag, W. R.; Yao, C. C. D. Rate constants for reaction of hydroxyl radicals with several drinking water contaminants. *Environ. Sci. Technol.* **1992,** 26, 1005-1013.

(25) Einschlag, F. S. G.; Carlos, L.; Capparelli, A. L. Competition kinetics using the UV/H_2O_2 process: a structure reactivity correlation for the rate constants of hydroxyl radicals toward nitroaromatic compounds. *Chemosphere* **2003,** 53, 1-7.

(26) Huber, M. M.; Canonica, S.; Park, G. Y.; Von Gunten, U. Oxidation of pharmaceuticals during ozonation and advanced oxidation processes. *Environ. Sci. Technol.* **2003,** 37, 1016-1024.

(27) Deborde, M.; Rabouan, S.; Duguet, J. P.; Legube, B. Kinetics of aqueous ozone-induced oxidation of some endocrine disruptors. *Environ. Sci. Technol.* **2005,** 39, 6086-6092.

(28) *CRC Handbook of Chemistry and Physics*, 82nd ed.; Lide, D.R., Ed.; CRC Press: Boca Raton, FL, 2001.

(29) Gallard, H.; Von Gunten, U. Chlorination of phenols: Kinetics and formation of chloroform. *Environ. Sci. Technol.* **2002,** 36, 884-890.

(30) Oakes, J.; Gratton, P. Kinetic investigations of azo dye oxidation in aqueous media. *J. Chem. Soc.-Perkin. Trans. 2* **1998**, 1857-1864.

(31) Stumm, W.; Morgan, J.J. *Aquatic Chemistry: Chemical Equilibria and Rates in Natural Waters*, 3rd ed.; John Wiley & Sons: New York, 1996.

(32) Hine, J. *Physical Organic Chemistry*, 2nd ed.; McGraw-Hill Book Company: New York, NY, 1962.

(33) Katritzky, A., R. *Advances in Heterocyclic Chemistry*; Academic: New York, NY, 1963.

(34) Elguero, J.; Marzin, C.; Katritzky, A. R.; Linda, P. *Advances in Heterocyclic Chemistry. Supplement 1: the Tautomerism of Heterocycles*; Academic: New York, NY, 1976.

(35) Warkentin, J. Oxidative cyclization of derivatives of carbonyl compounds. *Synthesis* **1970**, 2, 279-286.

(36) Scott, F.L.; Lambe, T.M.; Butler, R.N. Ambient oxidative ring closure of semicarbazones. *J. Chem. Soc.- Perk. Trans. 1* **1972**, 1918-1923.

(37) Boyd, M. *Organic Chemistry*. 5th edition, Allyn and Bacon, Inc., Newton, MA, 1987.

(38) Witkop, B.; Kissman, H. On the mechanism of oxidation. IX. Oxidation and autoxidation of hydrazones. *J. Am. Chem. Soc.*, **1953**, 75, 1975-1980.

(39) Gillis, B. T.; Schimmel, K. F. Peracetic acid oxidation of hydrazones. I. Aromatic aldehyde alkylhydrazones. *J. Org. Chem.*, **1962**, 27, 413-417.

(40) Oakes, J.; Gratton, P. Kinetic investigations of the oxidation of arylazonaphthol dyes in hypochlorite solutions as a function of pH. *J. Chem. Soc.-Perkin. Trans. 2* **1998**, 2201-2206.

(41) Oakes, J.; Gratton, P. Kinetic investigations of the oxidation of methyl orange and substituted arylazonaphthol dyes by peracids in aqueous solution. *J. Chem. Soc.-Perkin Trans. 2* **1998**, 2563-2568.

(42) Armesto, X. L.; Canle, L. M.; Garcia, M. V.; Santaballa, J. A. Aqueous chemistry of N-halo-compounds. *Chem. Soc. Rev.,* **1998**, 27, 453-460.

(43) Li, J.; Zhu, T.; Cramer, C. J.; Truhlar, D. G. New class IV charge model for extracting accurate partial charges from wave functions. *J. Phys. Chem. A* **1998,** 102, 1820-1831.

(44) Loudon, G. M. *Organic Chemistry*; Benjamin/Cummings Publishing Company, Inc.: Menlo Park, California, 1988.

(45) Kim, H. K.; Miller, L. F.; Bambury, R. E.; Ritter, H. W. Nitrones. 7. Alpha-quinoxalinyl-N-substituted nitrone 1,4-dioxides. *J. Med. Chem.* **1977,** 20, 557-560.

(46) Suter, W.; Rosselet, A.; Knusel, F. Mode of action of quindoxin and substituted quinoxaline-di-N-oxides on escherichia-coli. *Antimicrob. Agents Ch.* **1978,** 13, 770-783.

2.8 Supporting Information

Text S1. Chemical reagents, stock solutions, and surface water samples.

Text S2. Experimental setup for CDX reaction with free chlorine in $H_2{}^{18}O$ at pH 9.

Text S3. DAD detection wavelengths, HPLC mobile phase conditions, and MS parameters.

Text S4. Results for CDX loss at low and neutral/high pH without oxidant addition.

Text S5. $Na_2S_2O_3$ quenching effects on observed CDX kinetics.

Text S6. CDX and DCDX reaction kinetics with combined chlorine.

Figure S1. CDX/DCR competition kinetics.

Figure S2. DCDX/CDX competition kinetics.

Figure S3. Spectra of CDX chlorination by-products.

Text S1. Chemical Reagents: CDX, QX, QNO, and 4,6-dichlororesorcinol (DCR) from Sigma-Aldrich, and ODX from MP Biomedicals were at ≥ 97% purity. DCDX, QDX, and QXO were synthesized from methods described previously (*1*). $H_2{}^{18}O$ was obtained from Cambridge Isotope Laboratories at > 97% purity. NaOCl was obtained from Fisher Scientific at ~5% solution concentration. All other chemicals were of reagent grade or higher and used directly without further purification. Reagent water (18.2 MΩ-cm at 25°C) was prepared from a Millipore water purification system.

Stock Solutions: Stock solutions for CDX, DCDX, ODX, QDX, QXO and QNO were prepared at 25-50 mg/L in 50/50% (v/v) methanol/water. Stock solutions for QX and DCR were prepared at 100 mg/L in 10/90% (v/v) methanol/water and pure methanol, respectively. Stock solutions were stored at ~4°C and used for up to two months. Free chlorine concentrations were prepared at 100 mg/L (kinetic experiments) and 500 mg/L (by-product assessment experiments) as Cl_2 and were monitored using the standard iodometric titrimetric method (*2*). Combined chlorine (CC) was prepared similarly to methods described earlier (*3*) in which pre-buffered solutions (phosphate buffer, pH ~7) of free chlorine (200 mg/L as Cl_2) and NH_4Cl (302 mg/L) were mixed at an 1:2 molar ratio, forming CC stock solutions between 80-100 mg/L as Cl_2. Concentrations of NH_2Cl and $NHCl_2$ were measured using the standard DPD/FAS titrimetric method (*2*). CC stock solutions were stored at ~4°C and used within 9 hours.

Surface Water Samples: Source water was first collected from the Chattahoochee river (Cochran Shoals/ Power Island, Chattahoochee River National Recreation Area) in the greater Atlanta, GA, USA region. Source water was stored at ~ 4°C upon arrival, filtered

through a 0.45 μm glass fiber filter, and used within 24 hours from time of collection. Non-purgeable organic carbon was measured using a Shimadzu TOC-Vws analyzer.

Residual free chlorine was measured for these source water samples using the standard DPD/FAS titrimetric method (*2*) and found to not persist at > 18.0 μg/L as Cl_2 (method detection limit). Levels of residual free chlorine and combined chlorine were also measured using the standard DPD/FAS titrimetric method (*2*) upon addition of free chlorine to surface water samples in order to measure potential formation of NH_2Cl and $NHCl_2$. Given an initial free chlorine dose of 14.2 mg/L as Cl_2 (0.2mM) spiked into pure surface water (dose is equivalent to CDX reaction conditions), 11.9 mg/L as Cl_2 residual total chlorine was found, of which 92.1%, 3.8%, and 4.6% (mg/L as Cl_2) were free chlorine, NH_2Cl, and $NHCl_2$, respectively.

Text S2. Batch experiments were also conducted for CDX reaction with free chlorine in $H_2{}^{18}O$ at pH 9. CDX was added at 26 μM from a 25 mg/L pure methanol stock solution, and 10 mM sodium borate was added directly to $H_2{}^{18}O$ to achieve pH ~9. Final $H_2{}^{16}O$ interference was < 3.5%. Excess free chlorine (260 μM) was added to initiate the reaction but was not quenched. After 10-12 min, the reaction mixture was injected into the HPLC/DAD/MS for analysis.

Text S3. DAD Detection Wavelengths: Detection wavelengths for CDX, DCDX, QX, QDX and DCR were 308, 280, 235, 250, and 295 nm, respectively. Detection wavelengths for QXO and QNO were 230 nm.

Analysis of CDX and Structurally Related Compounds (Batch Experiments): The mobile phase for all compounds studied consisted of a 20 mM acetic acid solution with

5% acetonitrile (eluent A) and acetonitrile (eluent B). The mobile phase started at 5% B (95% A), increased to 15% B in 5 min, 23% B in 20 min, and 95% B from 21-25 min. An additional period of 100% B from 27-30 min was used in DCDX analysis.

Analysis of CDX, DCDX, and DCR (Competition Kinetic Experiments): The mobile phase for simultaneous CDX and DCR analysis consisted of a 20 mM acetic acid solution with 5% acetonitrile (eluent A) and methanol (eluent B) in which the gradient started and remained at 40% B (60% A) for 5 min, increased to 75% B at 10 min, 95% at 12 min, and 100% B from 17-20 min. Simultaneous detection of DCDX and CDX used the same mobile phase for DCDX in batch experiments.

MS Parameters: MS analysis was conducted by electrospray ionization in positive mode at both low and high fragmentation voltages (80 and 220 eV) to yield optimal low and high fragmentation patterns with a mass scan range of *m/z* 100-1000. The drying gas was at 10 L/min at 350°C, the nebulizer pressure 25 psig, and the capillary voltage 4000 V.

Text S4. Batch experiments were conducted without oxidant for CDX at low pH (50 mM phosphate buffer at pH 2.5-3 or acetate buffer at pH 4) and neutral/high pH (50 mM phosphate buffer at pH 7 or borate buffer at pH 9-11) conditions to assess potential hydrolysis. At pH 7.21, only ~5.3% pf CDX loss was observed over a reaction time of 336 hrs (14 days). At pH 8.83, 31.1 % loss was observed over a reaction time of 288 hrs (12 days) with k_{obs} (s^{-1}) ~ 2.8×10^{-7} s^{-1}. At pH 10.38, k_{obs} was 1.64×10^{-6} s^{-1}. All high pH experiments described here were conducted in duplicate. At low pH from 2.81 to 4.04, no reaction achieved half-life after 287 hrs (11 days and 23 hrs). The k_{obs} for pH 2.81, 3.02, and 4.04 were about 5.65×10^{-7}, 3.92×10^{-7} s^{-1}, 1.22×10^{-7} s^{-1}, respectively.

Text S5. To determine the effect of the quenching agent, $Na_2S_2O_3$, on the observed kinetic rates for CDX, excess free chlorine (100 mM) was added to CDX (10 mM) that was previously buffered to ~ pH 4. One sample was aliquoted and directly injected into the HPLC at 2 min 53 s without addition of $Na_2S_2O_3$. A second sample was aliquoted and quenched at the same rxn time (2 min 53 s) and placed on the HPLC for analysis. CDX peak area was compared between the quenched and unquenched sample. Results indicate that > 50% of CDX in both samples had reacted, and the difference in peak area between the unquenched and quenched sample was < 5.5%, suggesting that any back reaction caused by $Na_2S_2O_3$ addition was negligible.

Text S6. Two or more replicates were conducted for combined chlorine experiments. For CDX, the average k_{app}^{CDX} was 1.50 $M^{-1}s^{-1}$ at pH 7.17 where an excess amount of pre-buffered CC (at pH 7, x_{NH2Cl}:x_{NHCl2} = 0.8:0.2) was added. The average k_{app}^{DCDX} for DCDX was 0.285 $M^{-1}s^{-1}$ at pH 7.15 under similar conditions. In comparison to free chlorine, both CDX and DCDX react at an ~ four orders of magnitude slower rate with CC. However, similar difference between CDX and DCDX reactivity was found, as CDX reacts 5.3 (CC) or 6.5 (free chlorine) times faster than DCDX at near neutral pH. Half-lives at pH 7.2 of CDX and DCDX with CC are 78 and 406 min, respectively.

Figure S1. Competitional loss of CDX/DCR with varying substoichiometric amounts of free chlorine to determine k_{app}^{DCR}/ k_{app}^{CDX} at pH 6.18-10.65 and 25°C.

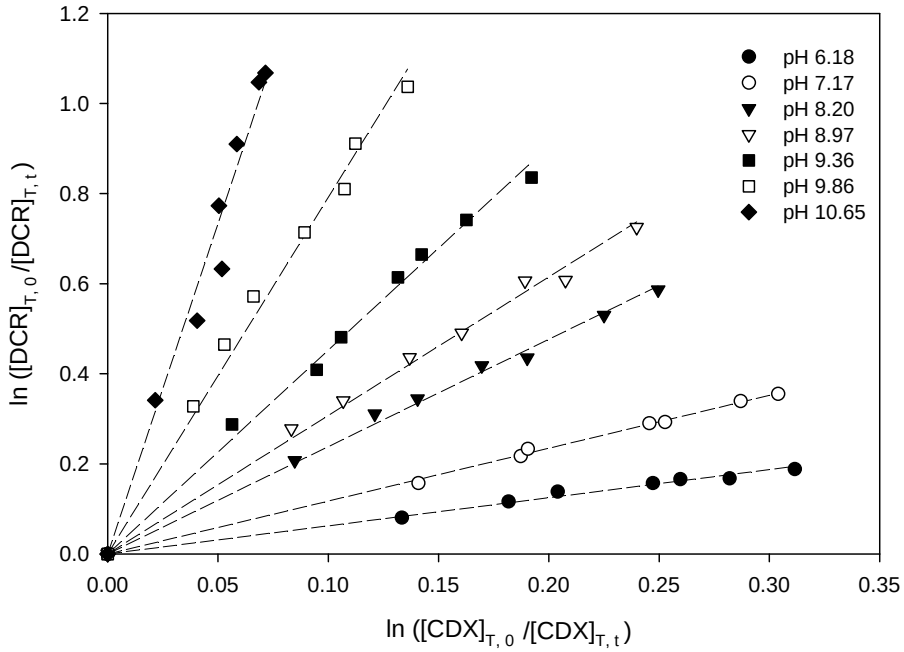

Figure S2. Competitional loss of DCDX/CDX with varying substoichiometric amounts of free chlorine to determine k_{app}^{CDX} / k_{app}^{DCDX} at pH 6.25-10.65 and 25ºC.

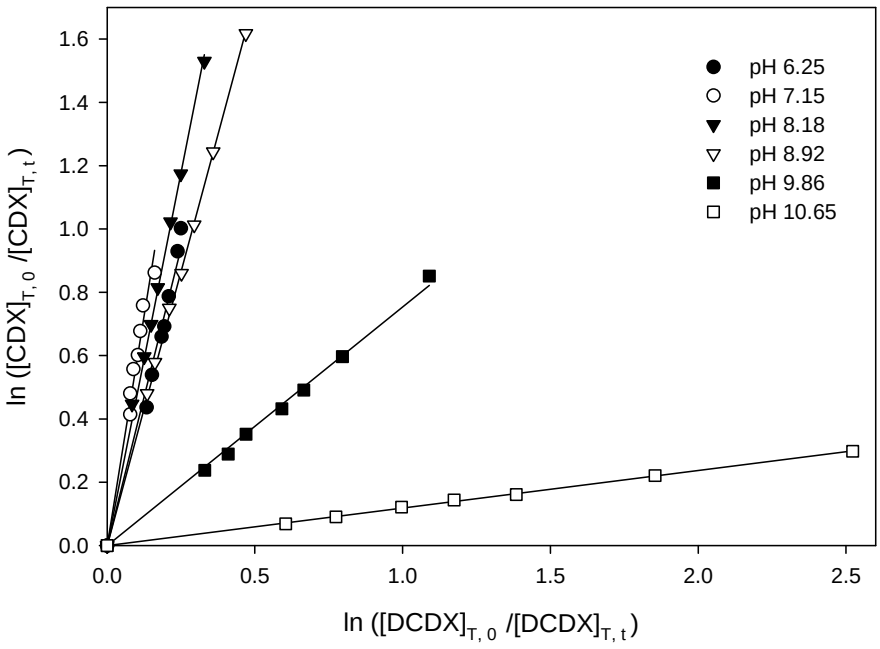

Figure S3. Mass spectra and structures of CDX chlorination by-products (ESI+, 220 eV), (a) *m/z* 321 (M+58) (M, (b) *m/z* 279 (M+16), (c) *m/z* 261 (M-2), (d) *m/z* 293 (M+30), (e) *m/z* 205.

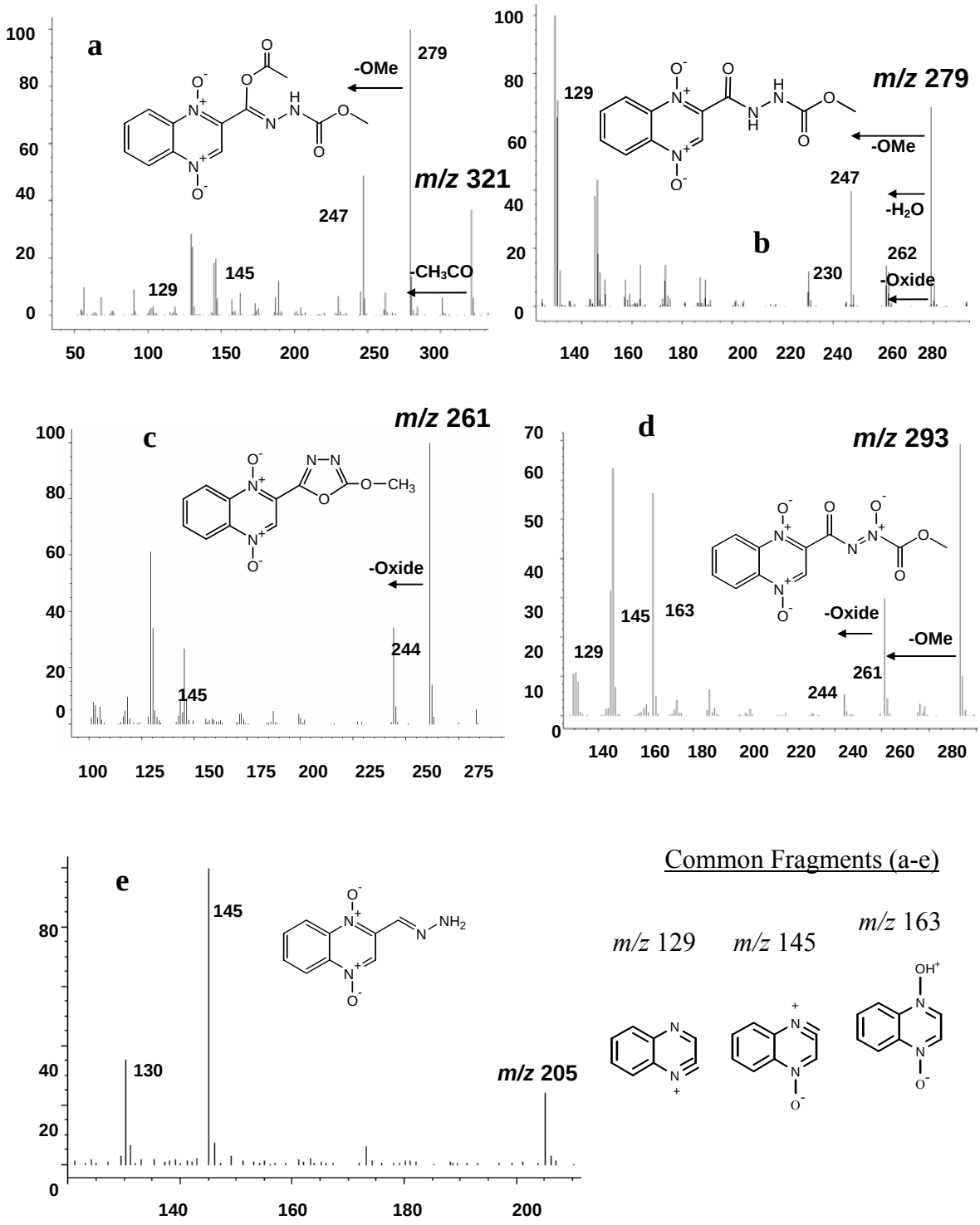

Figure S4. Mass spectra and structures of DCDX chlorination by-products (ESI+, 220 eV), (a) *m/z* 289 (M+58), (b) *m/z* 247 (M+16), (c) *m/z* 229 (M-2), (d) *m/z* 261 (M+30), (e) *m/z* 189, (f) *m/z* 175 (80 eV).

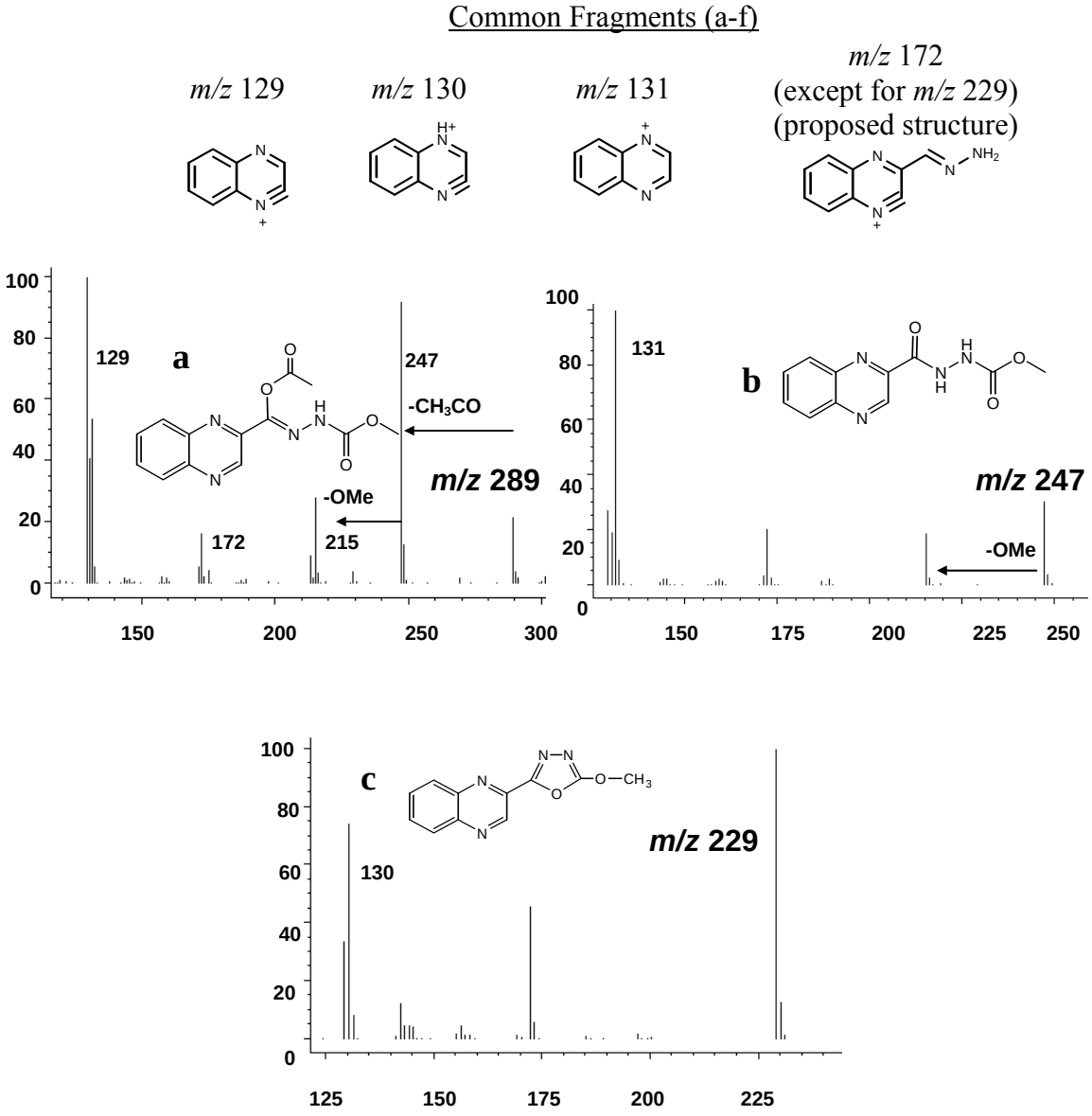

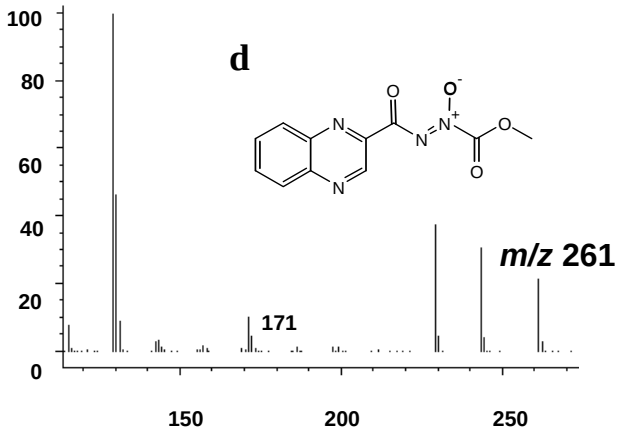
d
100
80
60
40
20
0
171
m/z 261
150
200
250

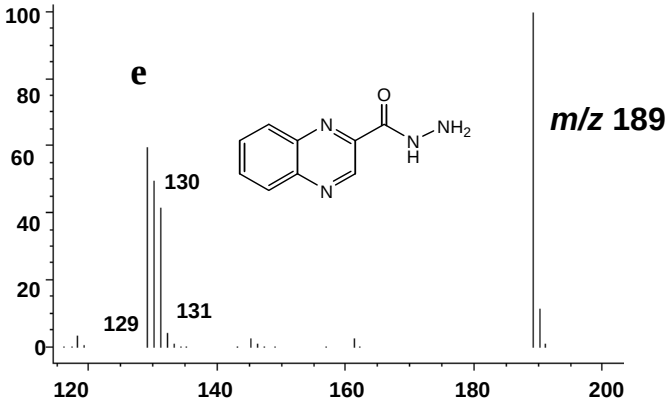
e
100
80
60
40
20
0
130
129
131
m/z 189
120
140
160
180
200

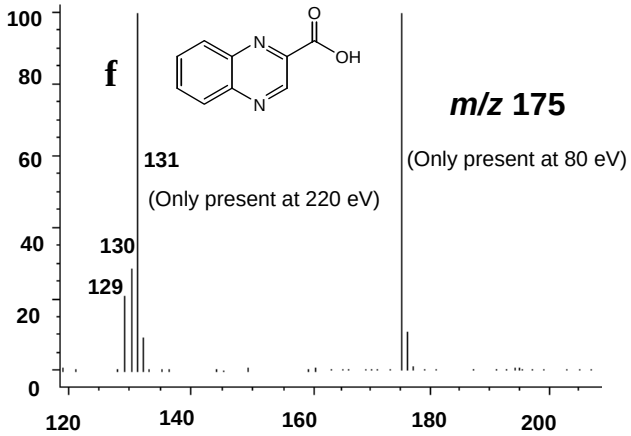
f
100
80
60
40
20
0
131
(Only present at 220 eV)
130
129
m/z 175
(Only present at 80 eV)
120
140
160
180
200

Figure S5. DCDX product evolution under excess free chlorine conditions at pH 5.2, 7.5, and 8.9 at 25˚C. DCDX rapidly decayed in < 10 s for pH 7.5 and 8.9.

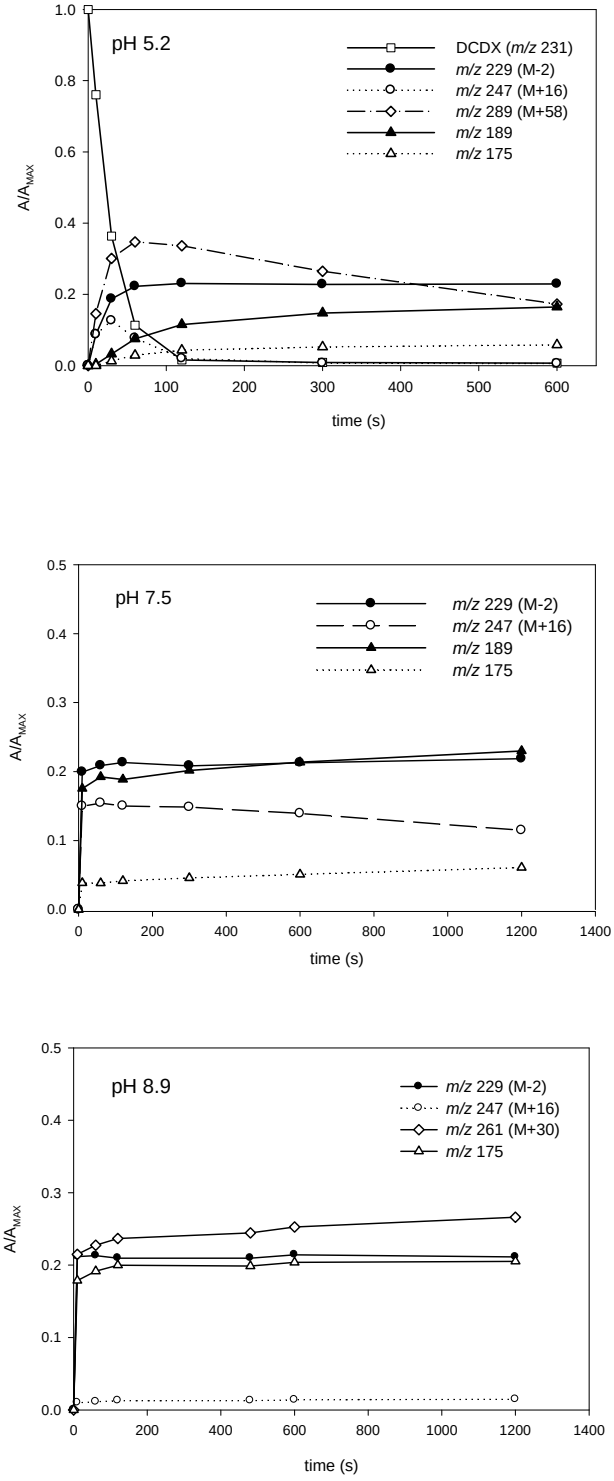

Figure S6. Results below indicate by-products formed after addition of acetate buffer into reaction matrix. Experimental conditions are as follows: $[CDX]_i$ = 20 μM, [free chlorine]$_i$ =20 μM, reaction time= 4-5 min, 25˚C, acetate buffer (pH 5) = 50 mM, pH= 5.04.

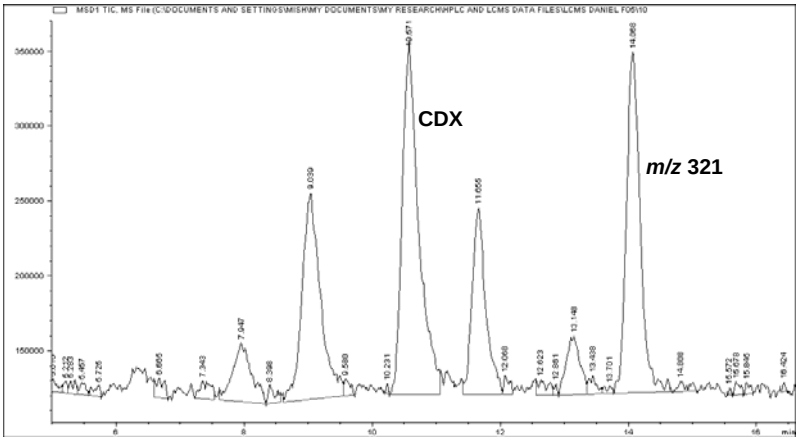

Results below indicate by-products formed with no addition of acetate buffer into reaction matrix. Experimental conditions are as follows: $[CDX]_i$ = 20 μM, [free chlorine]$_i$ = 20 μM, reaction time= 4-5 min, 25˚C, acetate buffer (pH 5) = 50 mM, pH= 4.98.

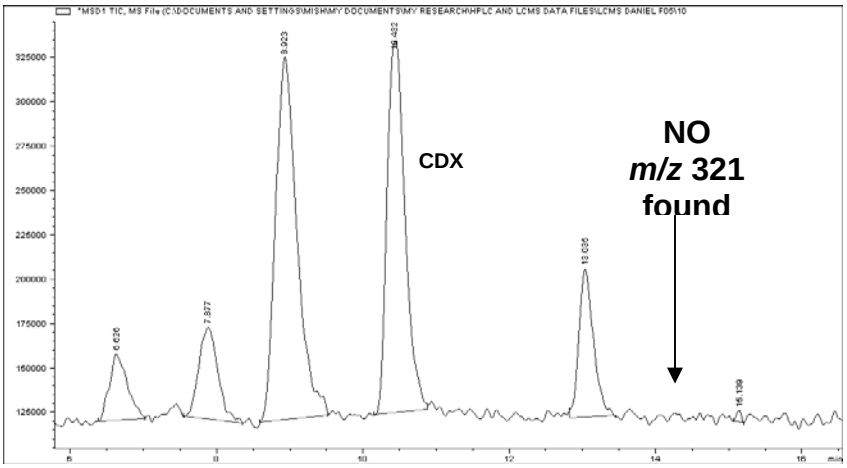

Figure S7. Results below show chlorinated by-product formed upon addition of NaCl (50 mM) at pH 4.92. Experimental conditions are as follows: $[CDX]_i$ = 20 μM, [free chlorine]$_i$ = 20 μM, reaction time = ~10 min, 25˚C, no buffer added, pH adjusted with HCl and NaOH, pH= 4.92.

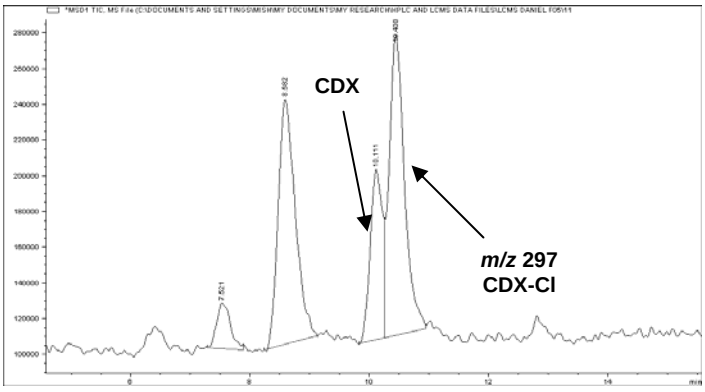

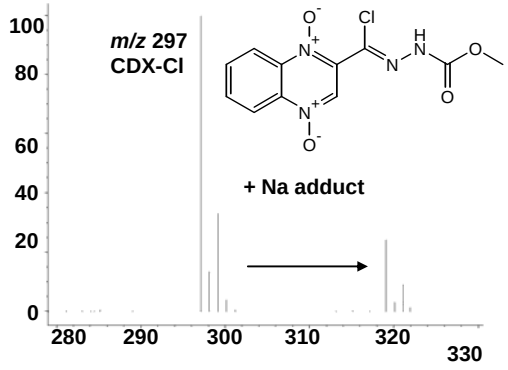

References

(1) Zhang, H.; Huang, C.-H. Reactivity and transformation of antibacterial N-oxides in the presence of manganese oxide. *Environ. Sci. Technol.* **2005,** 39, 593-601.

(2) Standard Methods for the Examination of Water and Wastewater, 20th ed.; APHA, AWWA, WPCF: Washington, DC, 1998.

(3) Dodd, M. C.; Huang, C.-H. Transformation of the antibacterial agent sulfamethoxazole in reactions with chlorine: Kinetics, mechanisms, and pathways. *Environ. Sci. Technol.* 2004, 38, 5607-5615.

CHAPTER 3

Tertiary Amines Enhance Reactivity of Organic Contaminants with Aqueous Chlorine.

3.1 Introduction

Tertiary amines along with other aliphatic amines (e.g., ammonia and primary and secondary amines) are well known to react quickly with aqueous chlorine to form chloramines. However, previous studies suggest that the reactivity of tertiary amines with aqueous chlorine is notably different. First, the elementary reaction rate constants (k_{HOCl} (hypochlorous acid / neutral amine)) of tertiary amines at 10^3-10^4 $M^{-1}s^{-1}$ (Antelo et al., 1985; Abia et al., 1998) are typically orders of magnitude lower than those of ammonia or primary/secondary amines which range at 2.9×10^6- 4.2×10^6 $M^{-1}s^{-1}$ (Margerum et al., 1978; Morris and Isaac, 1983; Qiang and Adams, 2004b) and 10^7-10^8 $M^{-1}s^{-1}$ (Abia et al., 1998; Antelo et al., 1992, 1995; Margerum et al., 1978; Morris, 1967), respectively. Second, substituents are found to have an opposite effect on the chlorination of tertiary amines compared to primary/secondary amines. This was assessed using a Taft's plot developed by Abia et al., 1998 and further modified by Deborde and von Gunten, 2008 to correlate the logarithm of the chlorination rate constants of various basic aliphatic amines to their Taft's constants (σ^*). Primary/secondary amines exhibit a similar plot in the Taft correlation where the slope of the straight line is positive ($\rho = 1.14 \pm 0.26$), whereas tertiary amines exhibit a Taft linear correlation with a negative slope ($\rho = -2.24 \pm 0.82$) (Abia et al., 1998; Deborde and von Gunten, 2008). This difference suggests that primary/secondary amines adopt a negative charge at the transition state ($\rho > 0$) whereas tertiary amines adopt a positive charge at the

nitrogen atom ($\rho < 0$) (Abia et al., 1998). Thus, the mechanisms behind the initial chlorination step are expected to differ. Because of the higher reactivity and positive ρ value, primary/secondary amines are hypothesized to form a highly ordered negatively charged transition state where water molecules are hydrogen-bonded to both HOCl and nitrogen to form a ten-membered ring. This transition state is followed by proton and chlorine transfer. On the other hand, tertiary amines undergo an elementary step where chlorine transfer develops into a chlorammonium ion, a nitrogen atom bearing a positive charge ($(R)_3$-N^+-Cl) (Abia et al., 1998).

Once these aliphatic chloramine species are formed, they can continue to serve as oxidants. Monochloramine (NH_2Cl) generally reacts about four orders of magnitude slower in comparison to HOCl (Larson and Weber, 1994; Morris, 1967). Chlorinated primary amines are also known to be slow oxidants towards certain biological substrates such as NADH and ascorbate, where reaction rate constants ranged from 2.8 to 76 $M^{-1}s^{-1}$, approximately 4-5 orders of magnitude less than with HOCl (Peskin and Winterbourn, 2001; Prutz et al., 2001).

In contrast, chlorinated tertiary amines (chlorammonium ions) appear to have substantially greater chlorination potential. A number of studies indicate that chlorinated tertiary amines either generated in-situ (e.g., formed upon addition of tertiary amines and HOCl) or pre-formed as a chlorinated salt may greatly enhance chlorination rates in comparison to HOCl (Dodd et al., 2005; Masuda et al., 2001; Prutz, 1998; 2001) and also affect product distribution (Smith and McKeer, 1983; Smith et al., 1987). If excess chlorine is present, even very low dosages of tertiary amine can significantly enhance

reaction rates (Prutz, 1998), possibly due to the regeneration of the chlorinated amine over time. The overall scheme of these reaction pathways is shown below:

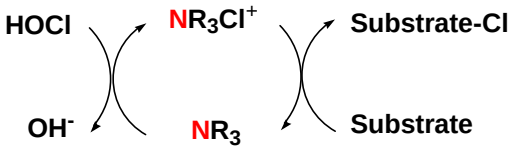

The objective of this study was to systematically evaluate the impact that tertiary amines and their chlorinated counterparts (chlorammonium species) have on the chemical reactivity, reaction kinetics, and product formation of various organic contaminants with aqueous chlorine. While studies have previously assessed the effect of tertiary amines and their chlorammonium species in biological matrices, no known studies to date have addressed their importance during wastewater and water treatment. We monitored reaction kinetics with varying amine dosages and compared the effect of each chlorinated amine/organic contaminant interaction with each other. By-product identification and distribution over time were used to facilitate identification of reactive functional groups and reaction mechanisms and pathways and see if they differ from aqueous chlorine reactions alone. In addition, the impact of chlorinated tertiary amines on the overall chlorine demand was assessed in terms of organic contaminant degradation.

Model compounds for natural organic matter and contaminants of varying structural characteristics were selected and included salicylic acid (SA), flumequine (FLU) and trimethoprim (TMP) (Figure 1). SA is found in aquatic humic material (Larson and Rockwell, 1979), FLU is from the group of popular fluoroquinolone antibacterial agents (Walsh, 2003), and TMP is an antibacterial agent commonly prescribed in tandem with sulfamethoxazole and found in wastewater effluent and surface

waters (Kolpin et al., 2002). The model tertiary amines investigated were trimethylamine (TMA) (found in urine (Zhang et al., 1992)), 4-morpholineethanesulfonic acid (MES) (common organic buffer), nitrilotriacetic acid Abia et al., (common chelating agent), creatinine (CRE) (found in urine (Murray et al., 2000)), and acetylcholine (ACC) (biological neurotransmitter (Sletten et al., 2005) and quarternary amine which may transform into a tertiary amine, see later discussions).

Figure 1. Structures and speciation of the organic contaminants and tertiary/quarternary amines investigated in this study.

Organic Contaminants:

Salicylic acid (SA)

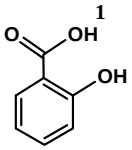

pK_{a1} = 2.9[a]

Flumequine (FLU)

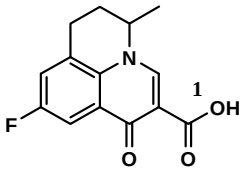

pK_{a1} = 6.5[b]

Trimethoprim (TMP)

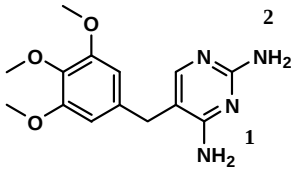

pK_{a1} = 3.2[c], pK_{a2} = 7.1[d]

Tertiary/Quarternary Amines:

Trimethylamine (TMA)

pK_{a1} = 9.8[e]

4-Morpholineethanesulfonic acid (MES)

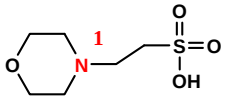

pK_{a1}= 6.1[f]

Nitrilotriacetic acid

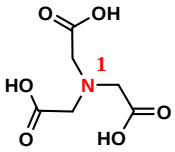

pK_{a1}= 0.7-1.3[g-i]

Creatinine (CRE)

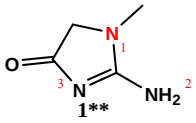

pK_{a1} = 4.8 [j,k]

Acetylcholine (ACC)

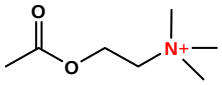

* Number associated with ionization site is equal to pK_a number (e.g. site corresponding to pK_{a1} is labeled "1").

** Positive charge is delocalized:

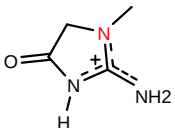

[a]Geiser et al., 2005, [b] Barbosa et al., 2001, [c]Qiang and Adams, 2004a, [d]Roth and Strelitz, 1969, [e]Jones, 1997, [f]Good et al., 1966, [g]Martell and Smith, 1974, [h]Mederos et al., 1987, [i]Sanchiz et al., 1999, [j]Grzybowski and Datta, 1964, [k]Kotsyubynskyy et al., 2004

3.2 Experimental Section

3.2.1 Chemicals and Reagent Preparation

SA, TMP, MES, CRE, and ACC were purchased from Sigma-Aldrich. FLU, TMA, and NTA were purchased from MP Biomedicals, Acros Organics, and Fisher Scientific, respectively. 3,4,5-Trimethoxytoluene (TMT) and 2,4-Diamino-5-methyl pyrimidine (DAMP) were purchased from Sigma-Aldrich and Daniel Fine Chemicals (Edmonton, Canada), respectively. 3-chlorosalicylic acid (3-Cl SA), 5-chlorosalicylic (5-Cl SA), and 3,5-dichlorosalicylic acid (3,5-diCl SA) were purchased from Sigma-Aldrich. All chemicals were at > 97% purity. NaOCl was obtained from Fisher Scientific at ~5% solution concentration. All other chemicals were of reagent grade or higher and used directly without further purification. Reagent water (18.2 MΩ-cm at 25°C) was prepared from a Millipore water purification system.

Stock solutions for SA and FLU were prepared at 1.0 g/L and 200 mg/L, respectively, in pure methanol. Stock solutions for TMP, 3-Cl SA, 5-Cl SA, and 3,5-diCl SA were prepared at 100 mg/L in 10/90% (v/v) methanol/water. Stock solutions of MES, CRE, and ACC were prepared at 100 mg/L, and NTA was prepared at 1.0 g/L, all in pure water. Stock solutions were stored at ~4°C and used for up to two months. Stock solutions for TMA were prepared at 1.0 g/L in pure water and stored for up to 48 hrs at ~ 4°C in sealed air-tight vials with minimal headspace before use. Free chlorine stock solutions were prepared at 50-500 mg/L as Cl_2 and were monitored using the standard iodometric titrimetric method (APHA et al., 1998).

3.2.2 Reaction Setup

To assess kinetic rates and reaction byproducts, batch reactions were conducted in capped 25-mL amber glass vials at circumneutral pH conditions (pH 7.0-7.3) under continuous stirring at 23°C. The initial concentrations of organic contaminants (Figure 1) were 5.0 μM, except for TMP byproduct analysis, where the initial concentration was 10.0 μM. Reactions were buffered using 10 mM phosphate (NaH_2PO_4/Na_2HPO_4). Next, experiments with free chlorine only were spiked with 10× or 40× molar amounts of free chlorine compared to the organic contaminant in order to initiate the reaction (40× used with SA and FLU in order to measure k_{app} ($M^{-1}s^{-1}$)). For reactions with amine, varying concentrations of tertiary amine/quarternary amine in either sub-stoichiometric or excess molar amounts compared to the organic contaminant concentration ([tertiary amine/quarternary amine]$_i$ = 0.25-25 μM (0.05-5× [organic contaminant]$_i$)) were first added into the reactor, and then 10x free chlorine was added. Sample aliquots were periodically taken and instantaneously quenched with ascorbic acid or $NH_4Cl/THAM/CH_3COOH$. Ascorbic acid was used for all experiments except TMP byproduct analysis as it was verified to have negligible effect on changing either the organic contaminant (SA, FLU, and TMP) concentrations or SA and FLU byproduct concentrations over time. For TMP byproduct analysis, ascorbic acid was found to significantly alter the byproducts formed, a result similarly observed when previous experiments were conducted using $Na_2S_2O_3$ as a quenching agent (Dodd and Huang, 2007). Therefore, a "softer" quenching technique using $NH_4Cl/THAM/CH_3COOH$ was modified from Dodd and Huang, 2007 and adopted for this analysis.

3.2.3 Analysis of Organic Contaminants

Loss of the organic contaminant over time was monitored using an Agilent 1100 HPLC system with a Zorbax RX-C18 column (4.6 × 250 mm, 5 μm) at a flow rate of 1.0 mL/min. SA and FLU were detected using a fluorescence detector (FLD) with excitation and emission wavelengths (λ_{EX} and λ_{EM}) of λ_{EX} = 235 nm, λ_{EM} = 410 nm and λ_{EX} = 312 nm, λ_{EM} = 366 nm, respectively. TMP was detected using a diode-array UV/vis detector (DAD) with a detection wavelength (λ) of 205 nm. The mobile phase for SA consisted of a 0.1 M acetic acid +5%$_{vol}$ MeOH solution (eluent A) and methanol (eluent B) in gradient mode. The mobile phase for FLU and TMP consisted of a 40 mM phosphate buffer (H_3PO_4/NaH_2PO_4) solution (eluent A) and acetonitrile (eluent B) in isocratic (60% A, 40% B) and gradient mode, respectively.

3.2.4 Analysis of Reaction Byproducts

Reaction byproducts were analyzed by an Agilent 1100 HPLC/DAD/MSD system with a Zorbax SB-C18 column (2.1 × 150 mm, 5 μm) at a flow rate of 0.2 mL/min. Mobile phases similar to HPLC analysis were used for SA, FLU, and TMP with exception to eluent A, where a 0.2%$_{vol}$ formic acid solution (SA and TMP) and a 0.1 M acetic acid +5%$_{vol}$ MeOH solution (FLU) were used instead. MS analysis was conducted by electrospray ionization in negative (SA) and positive mode (FLU and TMP) at both low and high fragmentation voltages (80 and 220 eV) to yield optimal low and high fragmentation patterns with a mass scan range of *m/z* 50-1000. The drying gas was at 10 L/min at 350°C, the nebulizer pressure 25 psig, and the capillary voltage 4000 V.

3.3. Results and Discussion

3.3.1 Reactivity of Organic Contaminants with Free Chlorine

Reactions of SA, FLU, and TMP with free chlorine alone were assessed as a control to compare the general reactivity with aqueous chlorine when various amines were added. Their overall reaction with free chlorine could be characterized by a second-order rate expression (eq. 1):

$$\frac{d\,[org.cont.]}{dt} = -k_{app}^{\text{free chlorine}}[org.cont.]_T[free\ chlorine]_T = -k_{obs}^{\text{free chlorine}}[org.\,cont.]_T \qquad (1)$$

Subscript T represents the total concentration of all species for each compound. Under excess chlorine conditions, the loss of SA, FLU, and TMP on a log scale was well correlated with time ($R^2 > 0.97$ for all replicates), verifying first order kinetics with respect to the organic contaminant. First order kinetics with respect to free chlorine was confirmed for SA and FLU by adding varying doses of excess free chlorine (0.2-0.5mM), where a well-correlated linear trend ($R^2 > 0.99$ (SA) and $R^2 > 0.97$ (FLU)) was found between the free chlorine concentration and the pseudo-first order rate constant, k_{obs}. For TMP, first order kinetics with respect to free chlorine was confirmed in a previous study by Dodd and Huang, 2007. The apparent second-order rate constants (k_{app} ($M^{-1}s^{-1}$)), obtained by dividing k_{obs} (s^{-1}) by $[\text{free chlorine}]_T$, for SA, FLU, and TMP were 7.80×10^{-2}, 2.63×10^{-1}, and 2.07×10^{1} $M^{-1}s^{-1}$, respectively. Thus, in terms of reactivity to free chlorine, TMP > FLU > SA.

3.3.2 Overall Amine Influence

Experiments were then conducted with five different amines, MES, TMA, NTA, CRE, and ACC, to individually assess their influence on SA, FLU, and TMP reactivity in the

presence of excess (10×) free chlorine. In all cases, the loss of organic contaminant was compared with and without amine addition. The amine was considered to enhance reactivity when $[\text{organic contaminant}]_{\text{w/ amine}} < [\text{organic contaminant}]_{\text{w/out amine}}$ at any $t > 0$. MES and TMA were found to enhance SA, FLU and TMP degradation when 0.05-25μM of either amine was dosed into the reaction matrix. For NTA, no significant enhancement of SA reactivity was observed ($[NTA]_i$ =10-25μM, pH 7.2), and only a marginal difference was found for TMP ($k_{obs}^{TMP} = 1.46\times10^{-3}$- 2.57×10^{-3} s^{-1} with $[NTA]_i$ =0-25μM, respectively, pH 7.2-7.3). CRE and ACC also did not influence SA, FLU, or TMP degradation ($[CRE]_i$ = 2.5-10 μM or $[ACC]_i$ = 2.5-10 μM, pH 7.2-7.3).

On the basis of literature, we hypothesized that amines affect the reactivity of organic contaminants with free chlorine via the following steps (eqs 2-3):

$$R_3N + \textit{free chlorine} \xrightarrow{k_{app}^{1}} R_3N^+Cl + H_2O/OH^- \qquad (2)$$

$$R_3N^+Cl + org.cont \xrightarrow{k_{app}^{2}} org.cont.product + R_3N \qquad (3)$$

In order for an amine to enhance the transformation of organic contaminants in the presence of free chlorine, the initial reaction of the amine with free chlorine to form the chlorammonium species, $(R)_3$-N^+-Cl, (eq 2) needs to be favorable. One approach was to evaluate the pK_a and Lewis basicity of each amine. This allowed us to compare the overall reactivity of the amine nitrogen's electron pair and relate its protonation potential in forming $(R)_3$-N^+-H (quantitatively assessed using its pK_a) to its chlorination potential in forming $(R)_3$-N^+-Cl. A similar correlation was made by Morris 1967 where the reactivity of various amines to form a N-chloro compound on a log scale increased linearly with basicity (pK_b) (Morris, 1967). As listed in Figure 1, the pK_a values for MES

(pK_a = 6.1) and TMA (pK_a = 9.8) are greater in value than for NTA (pK_a = 0.7-1.3) and CRE (pK_a = 4.8), suggesting that the amine nitrogens for MES and TMA have a stronger desire to form $(R)_3$-N^+-H and thus may have a stronger desire to form $(R)_3$-N^+-Cl. It is important to note that for CRE, the only relevant protonation site is at N_3 and not at N_1 (see Figure 1) which is the tertiary amine N originally hypothesized to form $(R)_3$-N^+-Cl. Thus, the inability to directly protonate N_1 contributes even more so to its low chlorination potential. For the quarternary amine, ACC, it is naturally assumed that it cannot directly react with free chlorine to form $(R)_3$-N^+-Cl due to its lack of reactive nitrogen lone pair electrons. However, previous research related to *N*-nitrosodimethylamine (NDMA) (a disinfection byproduct) formation suggests that certain quarternary amines ($(R)_4$-N^+) may dealkylate to form tertiary amines ($(R)_3$-N), and subsequently react with free chlorine to form $(R)_3$-N^+-Cl (Park, 2008; Walse and Mitch, 2008). In this case though, ACC was not found to enhance the reaction of these specific organic contaminants over time, perhaps due to negligible degradation of ACC to tertiary amine in the presence of chlorine during the reaction time period.

3.3.3 Influence of MES and TMA

Because MES and TMA were found to be the most effective amines in our study, they were the focus of our subsequent analyses to better understand the mechanisms that drive their enhancement effect. These two amines were evaluated for their effect on organic contaminant degradation in the presence of excess (10×) free chlorine as a function of time. First, it should be noted that MES and TMA likely reacted faster than the organic contaminant with free chlorine only ($k_{app}^{MES/TMA+free\ chlorine}$ (k_{app}^{1} (eq 2)) > $k_{app}^{org.cont+free\ chlorine}$($k_{app}^{free\ chlorine}$ (eq 1))) as no lag phase was observed during organic contaminant

degradation. This is also supported by previously reported k_{app} values at pH 7 for TMA and other tertiary amines with free chlorine that range from 5.2×10^{1}-1.6×10^{2} $M^{-1}s^{-1}$ (Abia et al., 1998; Antelo et al., 1985; Deborde and von Gunten, 2008) which are greater than 2.5 times the k_{app} values determined for SA, FLU, or TMP reaction with free chlorine.

In general, as seen in Figure 2 (1a-b and 2a-b), complete loss of parent SA and FLU occurred well within 6 hrs when 2.5-25 μM MES was added, but complete conversion was never achieved with equivalent doses of TMA (only 69% and 51% conversion for SA and FLU, respectively, was reached with $[TMA]_i$ =10 μM). In contrast to the reactions enhanced by MES, reactions enhanced by TMA (Figure 2 (2a-2b)) strongly deviated from pseudo-first order kinetics where the target organic contaminants decayed rapidly up to ~45 min and then decayed at a significantly slower rate up to 360 min. This result is possibly due to auto-decomposition of TMA after its reaction with free chlorine. Previous studies (Ellis and Soper, 1954; Mitch and Sedlak, 2004) indicate that after being formed, the chloroammonium ion ($(R)_3$-N^+-Cl) may alternatively undergoes an elimination reaction to lose HCl and create an iminium ion which is then followed by hydrolysis to form dimethylamine and formaldehyde, as seen below:

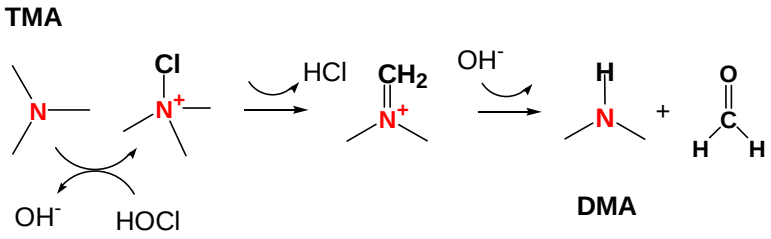

TMA is considered to be more susceptible to the above reaction pathway than MES since MES has a tertiary amine nitrogen tightly bound within the morpholine ring structure that

is assumed to be less available. It should also be noted that for TMP degradation (Figure 2 (1c-2c)), >93% conversion was achieved within 20 min for all MES and TMA doses tested. The reaction of TMP with free chlorine in the presence and absence of tertiary amines is considerably faster than those of SA and FLU. TMP apparently is a faster reactant towards $(R)_3$-N^+-Cl in comparison to SA and FLU and thus the auto-decomposition of chlorinated TMA did not significantly occur during the TMP degradation reaction time.

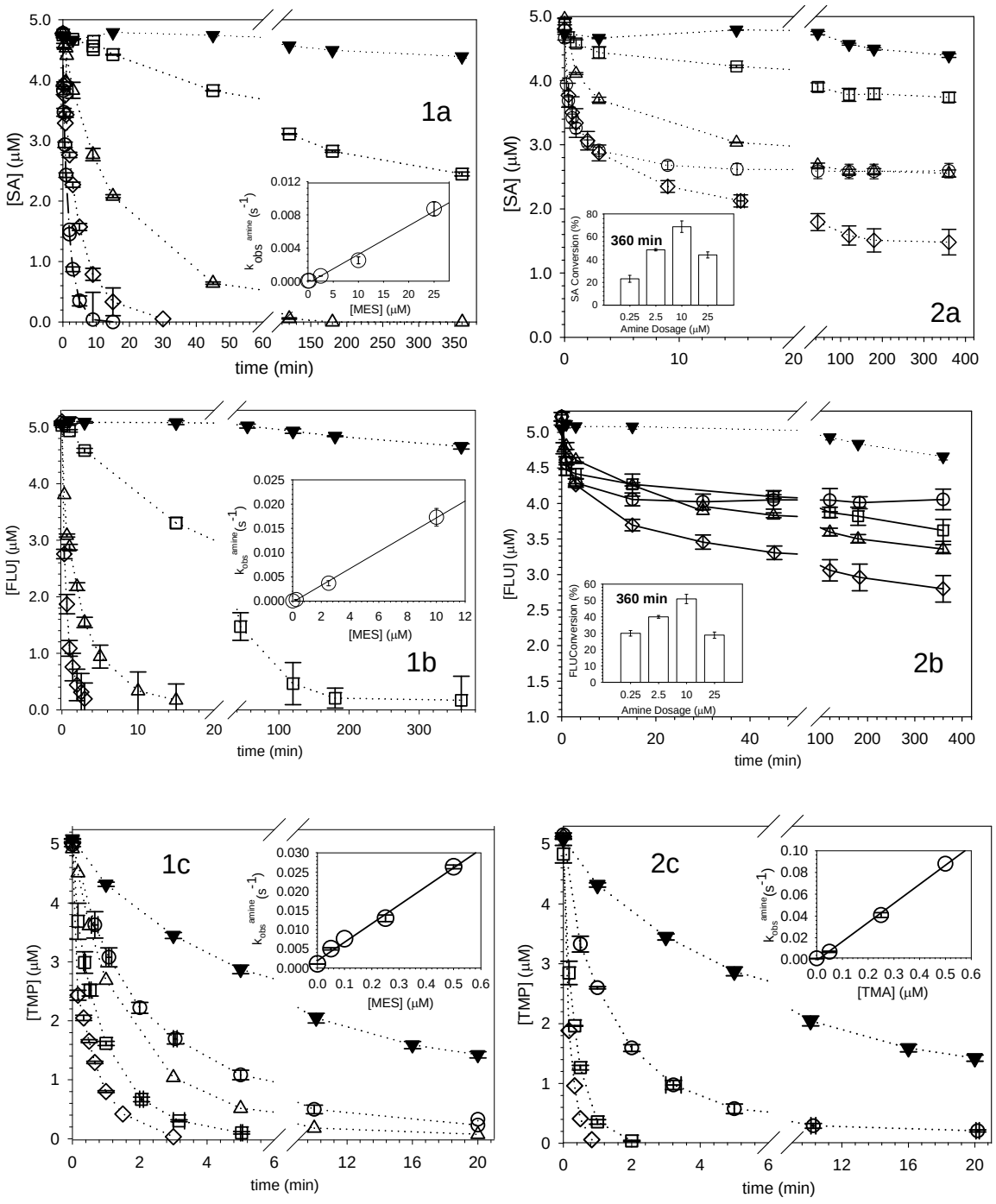

Figure 2. SA (1a-2a), FLU (1b-2b), and TMP (1c-2c) degradation enhanced over time by addition of (a) MES or (b) TMA and excess free chlorine (10×). For SA and FLU, amine dosages range from no amine addition (free chlorine only) (▼), 0.25μM (□),2.5μM (△),10 μM (◇), to 25 μM (○). For TMP, amine dosages range from no amine addition (free chlorine only) (▼), 0.05μM (○), 0.1 μM (△), 0.25 μM (□), to 0.5 μM (◇). Subplots represent the linear correlation of the

observed rate constant (k_{obs}) with respect to amine dose (R^2 = 0.987-0.999) (1a-c and 2c) or % SA or FLU conversion at 360 min with varied amine dosages (2a-2b). Error bars represent the standard error of $\geq$ 3 replicates. (pH 7.0-7.3, 23°C)

The effect of MES dose on organic contaminant (SA, FLU, and TMP) degradation was then examined when dosages ranging from 0.05-25 μM of MES were added, as seen in Figure 2 (1a-1c). MES dosages for TMP experiments were in general lower than those used for SA and FLU experiments due to the faster reaction of TMP with free chlorine alone. If equivalent doses were used, TMP would degrade too rapidly (< 10s) and could not be monitored. In the case of SA, FLU, and TMP, an increase in MES dosage increased the rate of organic contaminant degradation. A modified second-order rate expression was developed to include the amine addition and more specifically, the additional oxidant $(R)_3$-N^+-Cl, present in the reaction matrix. Eq 1 was modified to obtain eq 4 which is described as follows:

$$\frac{d\,[org.cont.]}{dt} = -k_{app}^{\text{free chlorine}}\,[org.cont.]_T\,[free\ chlorine]_T - k_{app}^{\,2}\,[org.cont.]_T\,[(R)_3N^+Cl]_T \qquad (4)$$

Given that $[(R)_3$-N^+-$Cl]_T$ is constant over time, the values $[(R)_3$-N^+-$Cl]_T$ and $k_{app}^{\,2}$ can be combined together along with $[\text{free chlorine}]_T$ and $k_{app}^{\,free\ chlorine}$ to form a new pseudo-first order rate constant, $k_{obs}^{\,amine}$, as seen in eq 5. This constant, $k_{obs}^{\,amine}$, is similarly included in the pseudo-first order rate equation, as seen in eq 6:

$$k_{obs}^{\,\text{amine}} = k_{app}^{\,\text{free chlorine}}\,[free\ chlorine]_T + k_{app}^{\,2}\,[(R)_3N^+ - Cl]_T \qquad (5)$$

$$\frac{d\,[org.cont.]}{dt} = -k_{obs}^{\,\text{amine}}\,[org.cont.]_T \qquad (6)$$

When applying eq 6 to the kinetic data provided in Figure 2 (1a-1c) (not including the control experiments with free chlorine only), each reaction correlated well to this model ($R^2 \geq 0.95$, except for the reaction of SA with 0.25 μM MES where $R^2 = 0.90$), and the k_{obs}^{amine} values were calculated. The ability to calculate these values further supports the rationale that $[(R)_3\text{-}N^+\text{-}Cl]_T$ which is a component of k_{obs}^{amine} (eq 5), must be constant or at a steady-state condition as a function of time. $[(R)_3\text{-}N^+\text{-}Cl]_T$ can thus be defined as $[(R)_3\text{-}N^+\text{-}Cl]_{ss}$.

These k_{obs}^{amine} values were also found to be linearly proportional to the initial MES dose, $[MES]_i$, as shown in the subplots presented in Figure 2 (1a-1c) where $k_{obs}^{free\ chlorine}$ (eq 1) was plotted at $[MES]_i = 0$ μM. Therefore, the $[MES^+\text{-}Cl]_{ss}$ formed in each experiment – while unknown – was considered to be not only constant over time but linearly proportional to the initial amine dose, $[MES]_i$, as well.

Next, the linear correlations with respect to dose were compared to each other, as seen in Figure 3 to evaluate whether certain organic contaminants are more responsive to MES addition than others. Here, the slope of each line is defined as $\triangle[k_{obs}^{amine}] / \triangle [MES]_i$ and was found to be 3.46×10^{-4}, 1.74×10^{-3}, and 4.84×10^{-2} for the reactions with SA, FLU, and TMP, respectively. A greater slope suggests greater reactivity of the target compound with $MES^+\text{-}Cl$, and thus the reactivity order is as follows where TMP > FLU > SA. This order of reactivity is similar in sequence to their reaction with free chlorine alone, suggesting that the reaction mechanisms involved with either oxidant, free chlorine or $MES^+\text{-}Cl$, are identical as well.

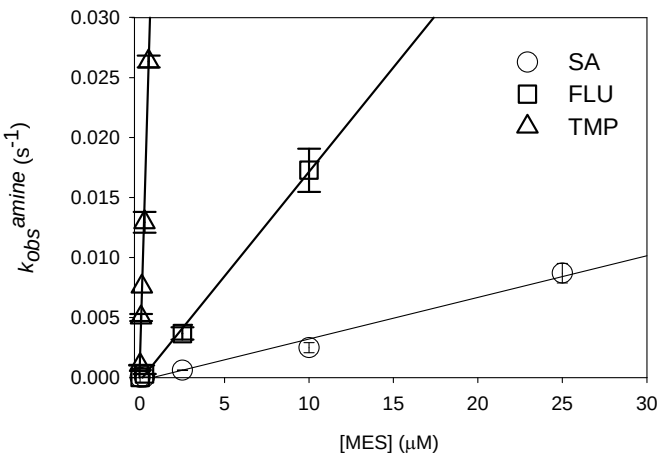

Figure 3. Comparing SA, FLU, and TMP reactivity with each other in the presence MES ([free chlorine]$_i$ = 50μM, pH 7.0-7.3, 23°C)

Upon further examination of the kinetic model described in eq. 5 and 6, one additional value to determine was $k_{app}{}^2$ which is a reaction rate constant that could provide insight towards the reactivity of SA, FLU, and TMP with MES$^+$-Cl alone as well as towards the overall strength of this oxidant in comparison to free chlorine and other environmentally relevant oxidants. $k_{app}{}^2$ can be calculated using eq. 5 since k_{obs}^{amine}, $k_{app}^{freechlorine}$ and [free chlorine]$_T$ are known, but is limited by [$(R)_3$-N$^+$-Cl]$_T$ or [$(R)_3$-N$^+$-Cl]$_{ss}$ since this value is unknown. However, one approach to evaluate [$(R)_3$-N$^+$-Cl]$_{ss}$ is to consider that while its concentration depends on the extent of the amine + free chlorine reaction in eq. 2, it at least must be $\leq$ than the total MES concentration that can form MES$^+$-Cl. It should be further noted that this concentration is not necessarily equivalent to the initial amount of MES added, [MES]$_i$, due to the effect of speciation. Speciation effects play a significant role since tertiary amines can be present in both their unprotonated and protonated forms (e.g., MES/ HMES$^+$ and TMA/ HTMA$^+$ whose pK_a values are listed in Figure 1). However, their reaction with free chlorine is dominated by the unprotonated species alone while the protonated species is considered negligible.

This assumption can be made due to an earlier study that assessed the reaction of various tertiary and secondary amines with free chlorine as a function of pH (Abia et al., 1998). The k_{obs} values for each amine followed a bell-shaped pH profile, with a maximum at $pH_{max} = (pK_{a,HOCl} + pK_{a,substrate}) / 2$, suggesting that the opposite species, HOCl and R_3N / R_2NH, dominate reactivity while R_3NH^+ / $R_2NH_2^+$ and OCl^- did not. Thus, the total amount of MES that can form MES^+-Cl is equal to the unprotonated MES concentration at pH 7.0-7.3 which is 0.89-0.94×$[MES]_i$. So, if $[MES^+\text{-}Cl]_{ss} = 0.89\text{-}0.94\times[MES]_i$, a minimum $k_{app}{}^2$ can be determined, but if $[MES^+\text{-}Cl]_{ss} < 0.89\text{-}0.94\times[MES]_i$, then the $k_{app}{}^2$ value will be greater than this minimum value. In the end, the $k_{app}{}^2$ values for SA, FLU, and TMP reaction with $[MES^+\text{-}Cl]_{ss}$ are calculated to be $\geq 2.6 \pm 0.94\times10^2$, $1.6 \pm 0.29\times10^3$, and $6.7 \pm 1.5\times10^4$ $M^{-1}s^{-1}$, respectively, which were averaged due to the range of dosages tested.

A similar matrix of experiments was also conducted for TMA (Figure 2 (2a-2c)) where dosages ranged from 0.05-25 μM. In this case, SA and FLU degradation did not necessarily increase at a faster rate in accordance to an increased TMA dose. As seen in the subplots provided in Figure 2 (2a and 2b), the % conversion of SA and FLU at 360 min is enhanced when $[TMA]_i$ increases from 0.25 to 10 μM but decreases when 25 μM is added. It is hypothesized that this decrease in % conversion at the high 25 μM amine dose is related to the lower $[TMA]_i$: $[\text{free chlorine}]_i$ ratio and the greater concentration of unreacted TMA present, ultimately leading to a greater auto-decomposition rate of TMA-Cl^+ in solution. An earlier study by Ellis and Soper suggested that the reaction rate of TMA-Cl^+ auto-decomposition to form dimethylamine and formaldehyde is proportional to the concentration of TMA-Cl^+ and the concentration of unreacted TMA as well (Ellis

and Soper, 1954). In this case, unreacted TMA can act as a nucleophile by removing a proton from the α-carbon from TMA-Cl^+ during the initial elimination reaction (Ellis and Soper, 1954).

For TMP, the auto-decomposition of TMA did not have a strong effect as previously discussed, and thus the k_{obs}^{amine} values for this reaction system were determined and found to increase proportionally with dose, as seen in the subplot provided in Figure 2 (2c). The k_{app} [2] value could be determined as well following the method described previously and was found to be $\geq 7.2 \pm 2.9\times10^7$.

Similar to MES, the organic contaminant response to TMA was also compared with each other. This task was challenging as reaction rate constants for SA and FLU could not be assessed. Further attempts to compare reactivity by normalizing the degradation curves for a given TMA dose with respect to their reactivity with free chlorine alone also proved difficult. In this case, the extent of TMP reaction when compared to SA and FLU with free chlorine alone was significantly greater at any time *t*, and thus SA, FLU, and TMP could not be effectively compared with each other. However, a comparison between SA and FLU could be made alone. At 360 min (subplots in Figure 2 (2a-2b)), the % conversion of SA was 8.6-17.9% greater than FLU for all TMA doses tested except when $[TMA]_i = 0.25$ μM. This trend is opposite in sequence to the other reactions with MES/free chlorine or free chlorine alone, although the specific mechanisms leading to this observed phenomenon are not currently understood.

3.3.4 MES and TMA Enhancement Efficiencies

For TMP reactions, the enhancement efficiency with TMA was found to be greater than MES since $k_{obs}^{TMA} = 1.4\text{-}3.3\times k_{obs}^{MES}$ for all equivalent amine doses. For SA and FLU reactions, this comparison proved significantly more challenging again due to the potential auto-decomposition of TMA over longer reaction times. A comparison was attempted though by selecting a shorter reaction time of 3 minutes where negligible auto-decomposition was considered. However, as seen in Figure 4, SA and FLU degradation with either MES or TMA exhibited a varied response, where low amine doses (e.g., 0.25-2.5 μM (SA) and 0.25μM (FLU)) indicated that TMA was slightly more effective than MES but the opposite was true at higher amine doses (e.g., 10-25 μM (SA) and 2.5-10 μM (FLU)) where MES was the more effective amine. One hypothesis suggests that TMA is in fact a stronger enhancing agent when compared to MES with respect to both SA and FLU degradation but is again limited when the $[amine]_i$ dose increases and the $[amine]_i$: $[free\ chlorine]_i$ ratio decreases since TMA auto-decomposition begins to play a more dominant role.

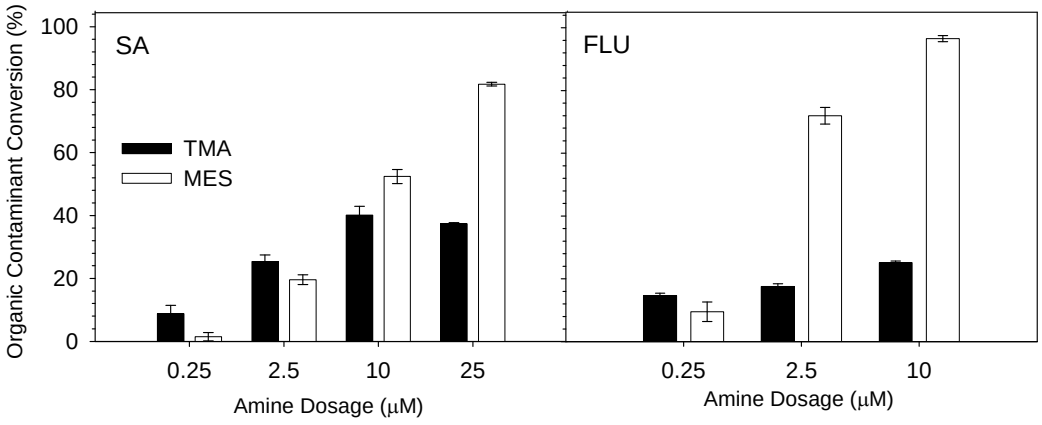

Figure 4. Conversion (%) of SA and FLU when either TMA or MES is added at various doses ranging from 0.05-25μM. ($[free\ chlorine]_i$ = 50μM, pH 7.0-7.3, 23°C)

3.3.5 Byproduct Formation and Distribution

Reaction byproducts were identified and monitored over time after amine addition ([MES or TMA] = 10 μM (SA and FLU reactions) and 0.50 μM (TMP reactions)) and compared to experiments where only free chlorine was added. Product structure identification was based on spectral fragmentation patterns, use of authentic standards (in order to verify proper ring substitution of SA byproducts) and model compounds (TMT and DAMP to assess TMP byproducts), and comparison to previous studies where byproducts were assessed after reaction with free chlorine (Larson and Rockwell, 1977, 1979; Dodd et al., 2005; Dodd and Huang, 2007).

The major byproducts for SA, FLU, and TMA that were identified when only free chlorine was added were identical in retention time and mass/charge ratio (*m/z*) to the major products identified when MES or TMA was added into the reaction matrix. This suggests that the reaction sites susceptible towards attack by all of these oxidants are similar. The major byproducts for SA were 3-Cl SA (*m/z* 171), 5-Cl SA (*m/z* 171), and 3,5-diCl SA (*m/z* 205). The major byproduct for FLU was *m/z* 252 (FLU+1+Cl-COOH). The major byproducts for TMP were *m/z* 325 (TMP+1+1Cl-1H), 359 (TMP+2Cl-2H), 377 (TMP+1+2Cl+1OH-1H), and 411 (TMP+1+3Cl+1OH-2H).

Furthermore, byproduct distribution with and without MES or TMA present was compared to better understand the reaction mechanisms involved. Only SA and TMP reactions were considered since FLU forms only one byproduct with and without amine present in the reaction matrix. Also, byproduct distribution was assessed at the initial stages of organic contaminant degradation primarily to investigate changes towards parent compound reactivity but not necessarily towards the reactivity of byproducts and

intermediates formed down the line. As seen in Figure 5 (a-c), the mole fractions of byproducts formed during SA degradation, 3-Cl SA, 5-Cl SA, and 3,5-diCl SA, were individually compared in the presence of free chlorine alone or with the addition of 10 μM TMA or MES. It should be noted that in Figure 5 (a-c), the mole fractions (y-axis) are plotted against the % loss of SA (x-axis) to better compare distribution between these three systems. While the formation of 5-Cl SA appears to be similar in all cases, a significant difference appears for both 3-Cl SA and 3,5-diCl SA. It appears that the reaction with 10μM TMA is more inclined to transform 3-Cl SA into 3,5-diCl SA, as evidenced by the lower mole fraction of 3-Cl SA observed after ~53% loss of SA in Figure 5a and the increase in 3,5-diCl SA observed after ~ 31% in Figure 5c. Such an effect is most likely not due to the presence of TMA-Cl^+ as this species may auto-decompose at these conditions but is more likely due to the longer reaction times observed allowing for greater transformation of 3-Cl SA to 3,5-diCl SA in the presence of free chlorine alone.

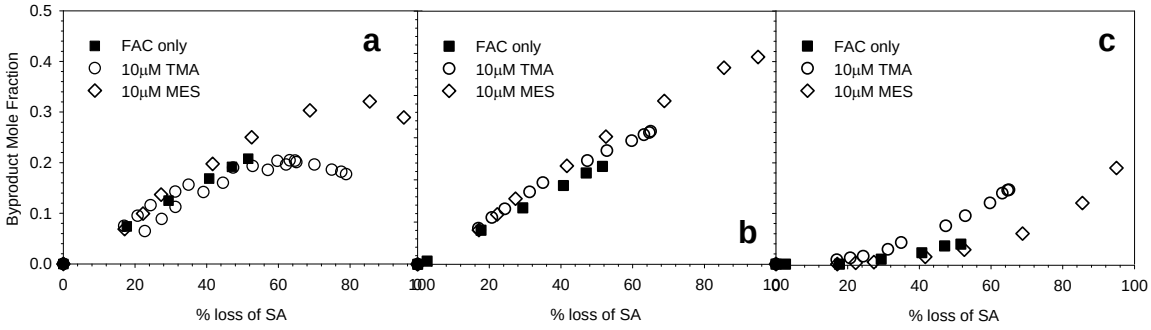

Figure 5. Mole fraction of the SA byproducts which are (a) 3-Cl SA, (b) 5-Cl SA, and (c) 3,5-diCl SA that are formed as a function of % loss of SA with free chlorine only (40×), 10μM TMA/free chlorine (10×), or 10μM MES/ free chlorine (10×) (pH 7.0-7.3, 23°C).

Similarly, the mole fractions of the major byproducts formed during TMP degradation, *m/z* 325, 359, 377, and 411, were individually compared in the presence of free chlorine alone or with the addition of 0.50 μM TMA or MES, as seen in Figure 6 (a-d). Again, the mole fractions (y-axis) are plotted against the % loss of TMP (x-axis) in this Figure 6 (a-d). The greatest difference in terms of byproduct distribution is observed after 50 % loss of TMP. First, as the parent TMP compound degrades, TMA addition appears to generate a slightly increased quantity of the byproducts *m/z* 377 and *m/z* 359 while generating a lower quantity of *m/z* 325 in comparison to the reaction with free chlorine alone. On the other hand, MES addition appears to generate a significantly greater quantity of the byproducts *m/z* 325 and *m/z* 411 while a slightly lower quantity of *m/z* 377 is formed. In general, the byproducts formed in this study were similarly observed in a previous investigation where the chlorination potential of TMP was assessed in detail (Dodd and Huang, 2007). The mass/charge ratios (*m/z*) of these byproducts along with the fragmentation patterns observed indicated that a wide range of chlorinated and OH-substituted compounds are formed where substitution can occur on both the 3,4,5-trimethyloxybenzyl and 2,4-diaminopyrimidinyl moieties of the TMP structure. Further identification of the specific structures of these byproducts will be conducted in future work where substructures of the TMP compound, TMT and DAMP, will be chlorinated with and without the MES and TMA addition, and the byproducts formed will be identified. Once these byproducts are identified, a better understanding regarding the exact influence of MES or TMA addition can then be made.

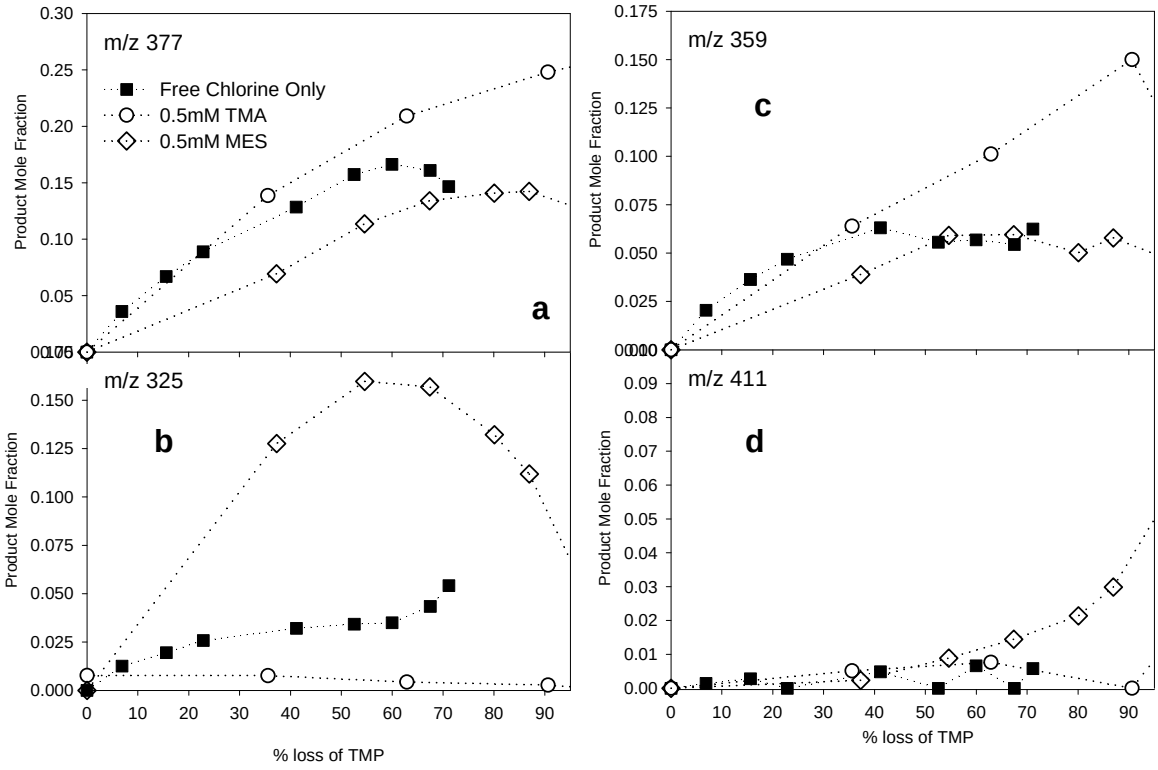

Figure 6. Mole fraction of the TMP byproducts which are (a) *m/z* 377, (b) *m/z* 325, (c) *m/z* 359 and, (d) *m/z* 411 that are formed as a function of % loss of TMP with free chlorine only (10×), 0.5µM TMA/free chlorine (10×), or 0.5µM MES/ free chlorine (10×) (pH 7.0-7.3, 23°C).

3.4 References

Abia, L., Armesto, X.L., Canle, M., Garcia, M.V., Santaballa, J.A. 1998. Oxidation of aliphatic amines by aqueous chlorine. Tetrahedron 54, 521-530.

Antelo, J.M., Arce, F., Armesto, J.L., Garciaverdugo, A., Penedo, F.J., Varela, A. 1985. A kinetic-study of the chlorination of tertiary alcoholamines in alkaline media. International Journal of Chemical Kinetics 17, 1231-1245.

Antelo, J.M., Arce, F., Parajo, M. 1995. Kinetic-study of the formation of n-chloramines. International Journal of Chemical Kinetics 27, 637-647.

Antelo, J.M., Arce, F., Perezmoure, J.C. 1992. Kinetics of the n-chlorination of 2-aminobutyric, 3-aminobutyric, 3-aminoisobutyric and 4-aminobutyric acids in aqueous-solution. International Journal of Chemical Kinetics 24, 1093-1101.

APHA, AWWA, WPCF, 1998. Standard methods for the examination of water and wastewater. 20th ed. Washington, D.C.

Barbosa, J., Barron, D., Cano, J., Jimenez-Lozano, E., Sanz-Nebot, V., Toro, I. 2001. Evaluation of electrophoretic method versus chromatographic, potentiometric and absorptiometric methodologies for determing pka values of quinolones in hydroorganic mixtures. Journal of Pharmaceutical and Biomedical Analysis 24, 1087-1098.

Deborde, M., von Gunten, U. 2008. Reactions of chlorine with inorganic and organic compounds during water treatment - kinetics and mechanisms: A critical review. Water Research 42, 13-51.

Dodd, M.C., Huang, C.H. 2007. Aqueous chlorination of the antibacterial agent trimethoprim: Reaction kinetics and pathways. Water Research 41, 647-655.

Dodd, M.C., Shah, A.D., Von Gunten, U., Huang, C.-H. 2005. Interactions of fluoroquinolone antibacterial agents with aqueous chlorine: Reaction kinetics, mechanisms, and transformation pathways. Environmental Science and Technology 39, 7065-7076.

Ellis, A.J., Soper, F.G. 1954. Studies of n-halogeno-compounds .6. The kinetics of chlorination of tertiary amines. Journal of the Chemical Society 1750-1755.

Geiser, L., Henchoz, Y., Galland, A., Carrupt, P.A., Veuthey, J.L. 2005. Determination of pka values by capillary zone electrophoresis with a dynamic coating procedure. Journal of Separation Science 28, 2374-2380.

Good, N.E., Winget, G.D., Winter, W., Connolly, T.N., Izawa, S., Singh, R.M.M. 1966. Hydrogen ion buffers for biological research. Biochemistry 5, 467-&.

Grzybowski, A.K., Datta, S.P. 1964. Ionisation constant of protonated form creatinine. Journal of the Chemical Society 186-&.

Jones, M., 1997. Organic chemistry. W.W. Norton & Company, New York.

Kolpin, D.W., Furlong, E.T., Meyer, M.T., Thurman, E.M., Zaugg, S.D., Barber, L.B., Buxton, H.T. 2002. Pharmaceuticals, hormones, and other organic wastewater contaminants in us streams, 1999-2000: A national reconnaissance. Environmental Science & Technology 36, 1202-1211.

Kotsyubynskyy, D., Molchanov, S., Gryff-Keller, A. 2004. Creatinine and creatininium cation in water solution. Tautomerism and quantitative interpretation of the solution acidity effect on h-1, c-13 and n-14 nmr chemical shifts. Polish Journal of Chemistry 78, 239-248.

Larson, R.A., Rockwell, A.L. 1977. Gas-chromatographic identification of some chlorinated aromatic-acids, chlorophenols, and their aromatic acid precursors. Journal of Chromatography 139, 186-190.

Larson, R.A., Rockwell, A.L. 1979. Chloroform and chlorophenol production by decarboxylation of natural acids during aqueous chlorination. Environmental Science & Technology 13, 325-329.

Larson, R.A., Weber, E.J., 1994. Reaction mechanisms in environmental organic chemistry. Lewis Publishers, Boca Raton.

Margerum, D.W., Gray, E.T., Huffman, R.P., 1978. In: Brinckman, F.E., Bellama, J.M. (Ed.), Chlorination and the formation of *n*-chloro-compounds in water treatment, Washington, D.C., pp. 279-291.

Martell, A.E., Smith, R.M., 1974. Critical stability constants. Plenum Press, New York.

Masuda, M., Suzuki, T., Friesen, M.D., Ravanat, J.L., Cadet, J., Pignatelli, B., Nishino, H., Ohshima, H. 2001. Chlorination of guanosine and other nucleosides by hypochlorous acid and myeloperoxidase of activated human neutrophils - catalysis by nicotine and trimethylamine. Journal of Biological Chemistry 276, 40486-40496.

Mederos, A., Dominguez, S., Medina, A.M., Brito, F., Chinea, E., Bazdikian, K. 1987. Equilibria in aqueous-solution between be(ii) and nitrilotriacetic, methyl-c-nitrilotriacetic, nitrilodiaceticpropionic, nitriloaceticdipropionic and nitrilotripropionic acids. Polyhedron 6, 1365-1373.

Mitch, W.A., Sedlak, D.L. 2004. Characterization and fate of n-nitrosodimethylamine precursors in municipal wastewater treatment plants. Environmental Science & Technology 38, 1445-1454.

Morris, J.C., 1967. In: Faust, S.D., Hunter, J.V. (Ed.), Kinetics of reactions between aqueous chlorine and nitrogen compounds, New York, pp. 23-53.

Morris, J.C., Isaac, R.A., 1983. In: Jolleys, R.L., Brungs, W.A., Cotruvo, J.A., Cumming, R.B., Mattice, J.S., Jacobs, V.A. (Ed.), A critical review of kinetic and thermodynamic constants for aqueous chlorine-ammonia system, Ann Arbor, Michigan, pp. 49-62.

Murray, R.K., Granner, D.K., Mayes, P.A., Rodwell, V.W., 2000. Harper's biochemistry. 25th ed. Appleton & Lange, Stamford, CT.

Park, S.-H. (2008) Effect of amine-based water treatment polymers on the formation of n-nitrosodimethylamine (ndma) disinfection by-product, Georgia Institute of Technology, Atlanta.

Peskin, A.V., Winterbourn, C.C. 2001. Kinetics of the reactions of hypochlorous acid and amino acid chloramines with thiols, methionine, and ascorbate. Free Radical Biology and Medicine 30, 572-579.

Prutz, W.A. 1998. Reactions of hypochlorous acid with biological substrates are activated catalytically by tertiary amines. Archives of Biochemistry and Biophysics 357, 265-273.

Prutz, W.A., Kissner, R., Koppenol, W.H. 2001. Oxidation of nadh by chloramines and chloramides and its activation by iodide and by tertiary amines. Archives of Biochemistry and Biophysics 393, 297-307.

Qiang, Z., Adams, C. 2004a. Potentiometric determination of acid dissociation constants (pka) for human and veterinary antibiotics. Water Research 38, 2874-2890.

Qiang, Z.M., Adams, C.D. 2004b. Determination of monochloramine formation rate constants with stopped-flow spectrophotometry. Environmental Science & Technology 38, 1435-1444.

Roth, B., Strelitz, J.Z. 1969. Protonation of 2,4-diaminopyrimidines .I. Dissociation constants and substituent effects. Journal of Organic Chemistry 34, 821-&.

Sanchiz, J., Esparza, P., Dominguez, S., Brito, F., Mederos, A. 1999. Solution studies of complexes of iron(iii) with iminodiacetic, alkyl-substituted iminodiacetic and nitrilotriacetic acids by potentiometry and cyclic voltammetry. Inorganica Chimica Acta 291, 158-165.

Sletten, D.M., Nickander, K.K., Low, P.A. 2005. Stability of acetylcholine chloride solution in autonomic testing. Journal of the Neurological Sciences 234, 1-3.

Smith, J.R.L., McKeer, L.C. 1983. High site-selectivity in the chlorination of electron-rich aromatic-compounds by n-chlorammonium salts. Tetrahedron Letters 24, 3117-3120.

Smith, J.R.L., McKeer, L.C., Taylor, J.M. 1987. Highly selective aromatic chlorination .1. The 4-chlorination of anisole and phenol with n-chloroamines in acidic solution. Journal of the Chemical Society-Perkin Transactions 2 1533-1537.

Walse, S.S., Mitch, W.A. 2008. Benzalkonium chloride: An abundant presursor to ndma in chlorinated drinking water. Preprints of Extended Abstracts at the American Chemical Society (ACS) National Meeting, New Orleans.

Walsh, C., 2003. Antibiotics: Actions, origins, resistance. ASM Press, Washington, D.C.

Zhang, A.Q., Mitchell, S.C., Ayesh, R., Smith, R.L. 1992. Determination of trimethylamine and related aliphatic amines in human urine by head-space gas chromatography. Journal of Chromatography: Biomedical Applications 584, 141-145.

CHAPTER 4

Mechanisms of Antibiotic Removal by Nanofiltration Membranes.

4.1 Introduction

Nanofiltration (NF) has been shown in recent years to effectively remove low molecular weight organic compounds such as pesticides [1-3], endocrine-disruptors [4-6], and various pharmaceuticals [4,7,8] during water treatment. Removal of such compounds can occur through multiple mechanisms. Contaminants such as 2-naphthol [9], estrone [10], and non-phenolic pesticides [1], that are hydrophobic or have strong H-bonding characteristics can readily adsorb to membranes at the initial stages of operation, and thus removal is governed by adsorption. In many cases though, removal depends on steady-state rejection where steric effects (i.e., relative compound size to pore size) dominate for uncharged solutes and steric and electrostatic effects dominate for charged solutes. Removal can further be influenced by changes in water quality characteristics such as pH [7,11,12], ionic strength [13], and organic content [14-16].

In our study, we are interested in evaluating the rejection of antibiotics which in recent years have been detected at low levels (up to μg/L) in wastewater effluents and surface waters in the U.S., Canada, and parts of Europe [17-21]. The presence of antibiotic contaminants in the environment is of concern due to their potential to promote bacterial resistance as well as trigger long-term adverse human health effects.

NF membranes may effectively remove antibiotics due to membrane pore size and compound characteristics such as low molecular weight and possible charge effects. It is hypothesized though that water quality characteristics such as pH may significantly affect antibiotic removal primarily due to changes in antibiotic speciation and membrane

charge. Under such varying water quality conditions, only a limited number of studies have assessed their removal [7,8].

Overall, the objectives of our study were to assess the rejection of a number of commonly used human and veterinary antibiotics, such as carbadox (CDX), trimethoprim (TMP), and sulfamethoxazole (SMX) (Table 2) by several loose and tight NF membranes under varying water quality conditions such as pH. These compounds were selected primarily due to their common use in U.S. human and veterinary practices along with the unique compound characteristics (e.g., size and charge) that they possess.

4.2 Materials and Methods

4.2.1 Nanofiltration Membranes

Four polyamide thin film composite NF membranes were used in the filtration experiments, and their detailed specifications are listed in Table 1. Samples were cut from spiral-wound modules and flat sheets received from Saehan and FilmTec, respectively, soaked in reagent water (Millipore, 18.2MΩ-cm at 25°C) for 24 h at room temperature, and then stored in 1% wt $NaHSO_3$ at 4°C.

Table 1. Specifications for NF membranes

Manufacturer	Model	pH range	Salt Rejection (%)			Flux[d] ($L/m^2/h$)
			NaCl[a]	$MgSO_4$[b]	$CaCl_2$[c]	
Saehan	NE 70	3-10	60-70	99.5	-	38.2[a]
Saehan	NE 90	3-10	85-95	99.5	-	38.0[a]
FilmTec	NF 90	3-10	85-90	> 97	-	32.0[a], 40.5[b]
FilmTec	NF 270	3-10	-	> 97	40-60	53.3[b], 62.6[c]

[a] Using 2,000 mg/L NaCl solution. [b] Using 2,000 mg/L $MgSO_4$. [c] Using 500 mg/L $CaCl_2$. All test conditions were conducted at 5.17 bar (Saehan) or 4.83 bar (FilmTec), 15% recovery, and 25°C. [d] Determined using permeate flow rates and membrane module areas provided by the manufacturers.

Zeta-potential (ζ) measurements (ELS-8000, Otsuka Electronics, Japan) were conducted to evaluate the surface charge of the membranes from pH 3.1-10.1 and are shown in Figure 1. The membrane surfaces are negatively charged at circumneutral pH and reach zero point charge (pH_{zpc}) between pH 3.1-3.9 for Saehan NE 70, Saehan NE 90, and FilmTec NF 270 and pH 4.9-6.0 for FilmTec NF 90. The membrane surfaces are positively charged at pH values lower than the pH_{zpc}.

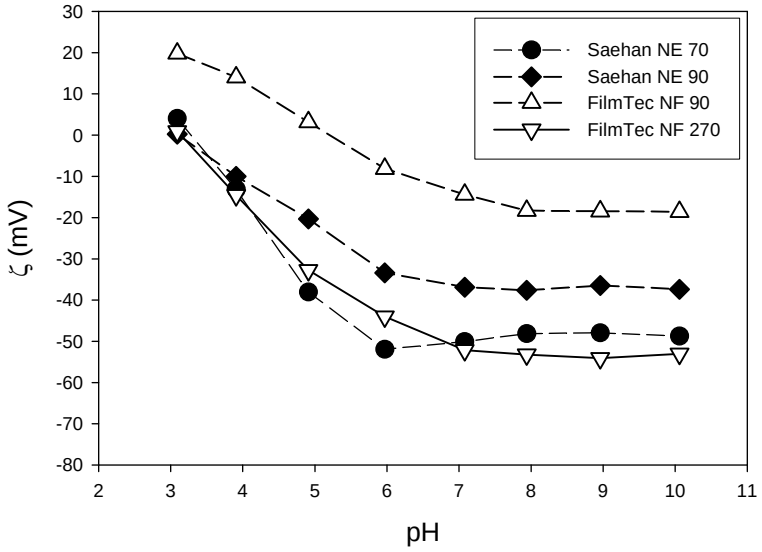

Figure 1. ζ-potential of membranes. ([NaH_2PO_4/Na_2HPO_4] = 1.0 mM (pH 7.0 buffer), pH adjusted from 3.1-10.1 by HCl or NaOH addition)

4.2.2 Chemicals and Reagent Preparation

Trimethoprim (TMP), carbadox (CDX), D-xylose, *meso*-erythritol, and 1,4-dioxane were purchased from Sigma-Aldrich, and sulfamethoxazole (SMX) was purchased from ICN Biomedicals. All these chemicals were at ≥ 97% purity. Other chemicals such as NaH_2PO_4, Na_2HPO_4, HCl, NaOH, and methanol were of reagent grade or higher and used without further purification. The structures and relevant properties of

the antibiotics and other ions in solution are shown in Table 2. Stock solutions for TMP and SMX were prepared at 100 mg/L in 10/90% (v/v) methanol/water. CDX stock solutions were prepared at 25 mg/L in 50/50% (v/v) methanol/water. Stock solutions for D-xylose, *meso*-erythritol, and 1,4-dioxane were prepared at 15.0, 3.0, and 5.0 g/L in pure water, respectively.

Table 2. Structures and relevant properties of the antibiotics and other ions in solution.

Compound	Structure	MW (g/mole)	pK_a values	Diffusion Coefficient *(D)* (10^{-10} m^2/s)	Solute Radius (r_s) (nm)
Carbadox (CDX)	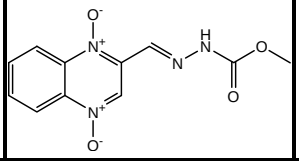	262.2	pK_{a1} =9.6 [22]	8.13[a]	0.354[b]
Sulfamethoxazole (SMX)	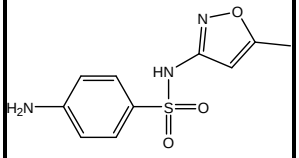	253.3	pK_{a1}= 1.7 [23] pK_{a2} = 5.6 [23]	8.37[a]	0.349[b]
Trimethoprim (TMP)	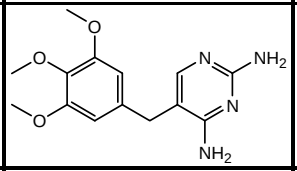	289.5	pK_{a1}= 3.2 [24] pK_{a2}= 7.1 [25]	7.06[a]	0.383[b]
$H_2PO_4^{-1}$				7.44[c]	0.324 [c]
HPO_4^{-2}				6.65[c]	0.363[c]
Na^+				11.7[c]	0.206 [c]
Cl^-				18.0[c]	0.134[c]
H^+				85.1[c]	0.028 [c]
OH^-				46.9[c]	0.051[c]

[a] Calculated using the Wilke-Chang equation [26]. [b] Determined by estimating the Connolly Solvent-Excluded Volume using Chem 3D-Pro (v.5) and calculating the radius assuming the solute is spherical in shape. [c] Ion diffusion constants and hydrodynamic radii are calculated using the Nernst-Einstein equation where the ion drift speed is proportional to the applied field strength [27]. Equivalent ion conductivity values were found at 25°C [15,28], and adjusted to 20°C [29,30].

4.2.3 Experimental Setup

All experiments were performed using a bench-scale cross-flow filtration system designed either to test four membranes simultaneously, where two parallel feed lines accommodated two plate and frame membrane test cells in series, or two membranes simultaneously, where one feed line accommodated two plate and frame membrane test cells in series. The feed channel in each test cell was rectangular, 71 × 34 mm (l × w), to

provide an effective filtration area of 2.43×10^{-3} m^2, and had a feed flow channel height of 5 mm. Feed solution stored in a 35.0 L tank was circulated (3.0 L/min, 0.8 gal/min) and pressurized by a Hydra-Cell diaphragm pump (Hydra-Cell D03, Wanner Engineering, Minneapolis, MN) in which a Sentry pulsation dampener (Blacoh, Riverside, CA) was attached to the outlet port. Both concentrate and permeate lines were returned to the feed tank. Feed temperature was controlled by circulating cooling water through a heat exchange coil immersed inside the feed tank. System pressure was controlled using a needle valve (Swagelok, Solon, OH) and monitored using a pressure gauge (Swagelok, Solon, OH) located downstream of the cells. The feed flow rate was measured using a hydraulic flow meter (King, Atlanta, GA). The permeate flux was measured by collecting and weighing permeate samples periodically over time. All experimental components were made of SS-316 to avoid corrosion or Teflon® or PVDF to avoid adsorption.

4.2.4 Experimental Procedure

Quality Control. Each membrane sample used in this study was initially tested for quality control by assessing $MgSO_4$ rejection. A feed solution of 2,000 mg/L $MgSO_4$ was used at an operating pressure (ΔP) of 5.17 bar (75 psi) for Saehan NE 70 and 90 membranes or 4.83 bar (70 psi) for FilmTec NF 90 and 270 membranes. The experimental $MgSO_4$ rejection was compared to the manufacturer's specifications (99.5% $MgSO_4$ rejection of Saehan membranes and > 97.0% for FilmTec membranes), and only membranes with > 97% $MgSO_4$ rejection were used.

Operating Conditions and Protocol. Membranes were compacted at 140 psi (2 × operating pressure) using reagent water for at least 24 h until the permeate flux was

constant. The feed tank was then replaced with reagent water, and the membrane test unit was initially stabilized for one hour at an operating pressure, cross-flow velocity, and feed tank temperature of 4.83 bar (70 psi), 29.5 cm/s ($Re = 2.94\times10^3$), and 20±0.3°C, respectively. Permeate samples were subsequently collected over ~30 min in 25 mL vials to assess water flux. At $t = 0$ min, stock solutions of the phosphate (NaH_2PO_4/Na_2HPO_4) buffer (pH 7.0, 250 mM) and antibiotic were spiked into the feed tank to achieve final concentrations of 1.0 mM and 500 μg/L, respectively. The solution was mixed for ~ 5 min using a hand-held electric mixer, and the pH was adjusted between 3.0-10.0 by adding HCl or NaOH. The operating time for each experiment lasted up to 12.6 hrs during which the pH was readjusted every 4-6 hrs. Experiments at each phase were provided an appropriate length of time in order to reach steady-state conditions.

Samples from the permeate line (~ 0.5-1.5 mL) and feed tank (1.0 mL) were collected every 40 min and placed into 1.5 mL amber HPLC vials. Permeate samples (~5.0-8.0 mL) were also collected every 80 min into 25 mL amber vials to measure flux. The feed concentration was not greatly affected over time by sampling of the feed and permeate since the total volume collected was ≤ 1.2% of the initial feed tank volume. For pH control, the feed pH was checked and re-stabalized to its target pH following each feed and permeate sampling event (not including sampling events for measuring flux).

Similar experiments were also conducted to measure the rejection of chloride (Cl^-), total phosphate ($PO_{4,TOTAL}$), and H^+ for modeling purposes (see later discussions). In this case, no antibiotic was added, but NaCl (500 mM) was added instead to achieve a final concentration of 1.0 mM. The pH was readjusted every 40 min. Samples from the feed tank (5.0 mL) were collected every 40 min into 25 mL amber vials. Permeate

samples (~5.0-8.0 mL) were also collected into 25 mL amber vials every 40 min for a 4 min duration for analytical analysis and pH and flux measurement. The feed pH was similarly measured and stabilized as above.

4.2.5 Analytical Techniques

CDX, SMP and TMP concentrations were measured using an Agilent 1100 Series HPLC system with a Zorbax RX-C18 column (4.6 × 250 mm, 5μm) at a flow rate of 1.0 mL/min and detected using a diode-array UV/vis detector (DAD). UV detection wavelengths for CDX, SMP, and TMP were 308, 275, and 205, respectively. The mobile phase for CDX consisted of 20 mM acetic acid solution with 5% acetonitrile (eluent A) and acetonitrile (eluent B). The mobile phase started at 5% B (95% A), increased to 15% B in 3 min, 23% B in 6 min, and 95% B from 7-10 min. The mobile phase for SMP and TMP consisted of 1.0 mM trifluoroacetic acid (TFA) (eluent A) and acetonitrile (eluent B). The mobile phase for SMX was held at 40% B (60% A) from 0-3 min, increased to 50% B in 4 min, and 95% B from 5-7 min. The mobile phase for TMP started at 15% B (85% A), increased to 50% B in 10 min, and 95% B from 11-15 min.

Total phosphate ($PO_{4,\,TOTAL}$) and chloride ions (Cl^-) concentrations were measured using a Dionex DX-100 ion chromatography [31] system with a Dionex A64A IonPac guard column and a Dionex AS4A IonPac analytical column and detected using a ED40 conductivity detector. The system operated at a flow rate of 1.0 mL/min using a 1.8 mM sodium carbonate and 1.7 mM sodium bicarbonate solution.

4.2.6 Organic Tracers

Experiments were conducted with D-xylose, *meso*-erythritol, and 1,4-dioxane in order to estimate the membrane pore radius (r_p) for Saehan NE 70 (other membranes were not tested, see details in Results and Discussion section). This membrane was initially compacted at 210 psi using reagent water. Next, the organic tracer was added to achieve a final concentration of 16.0 mg-C/L. Operating pressures were adjusted from 4.83, 6.89, 9.65, 12.4, and 14.48 bar (70, 100, 140, 180, and 210 psi) every 1-3 hrs. Feed and permeate samples were collected every 30 min for analytical analysis and flux measurement.

Concentrations of the organic tracers were measured by evaluating the non-purgeable organic carbon (NPOC) content (mg-C/L) using a Shimadzu TOC-Vws analyzer. The steady-state apparent rejection (R_{app}) was then determined for each organic tracer as a function of permeate flux (J_v) and fit to eqn 6 (R_{app} for uncharged solutes) to solve for the pore radius (r_p) using the Marquardt-Levenberg nonlinear least-squares regression algorithm from SigmaPlot 2004 software (SYSTAT Software, Inc.).

4.3. Results and Discussion

4.3.1 Antibiotic Rejection with Varying pH

For these experiments, both the feed (C_f) and permeate (C_p) concentrations were measured over time. The feed concentration reached steady-state from the first sampling point onward for all CDX, SMX, and TMP experiments conducted from pH 3.0-10.0, indicating that no substantial compound loss was observed by either the membranes or the operating system. The permeate concentration for the majority of experiments

remained constant as well, except in the case of TMP at pH 7.1-10.0 for Saehan NE 70, Saehan NE 90, and Filmtec NF 270 where the permeate concentration at each pH increased (R_{obs} decreased up to 6.9%) due to membrane adsorption until reaching steady-state at ~3-4 hrs.

Steady-state observed rejection (R_{obs}=1-C_p/C_f) was then determined for TMP, SMX, and CDX and plotted as a function of pH, as seen in Figure 2 (a-c).

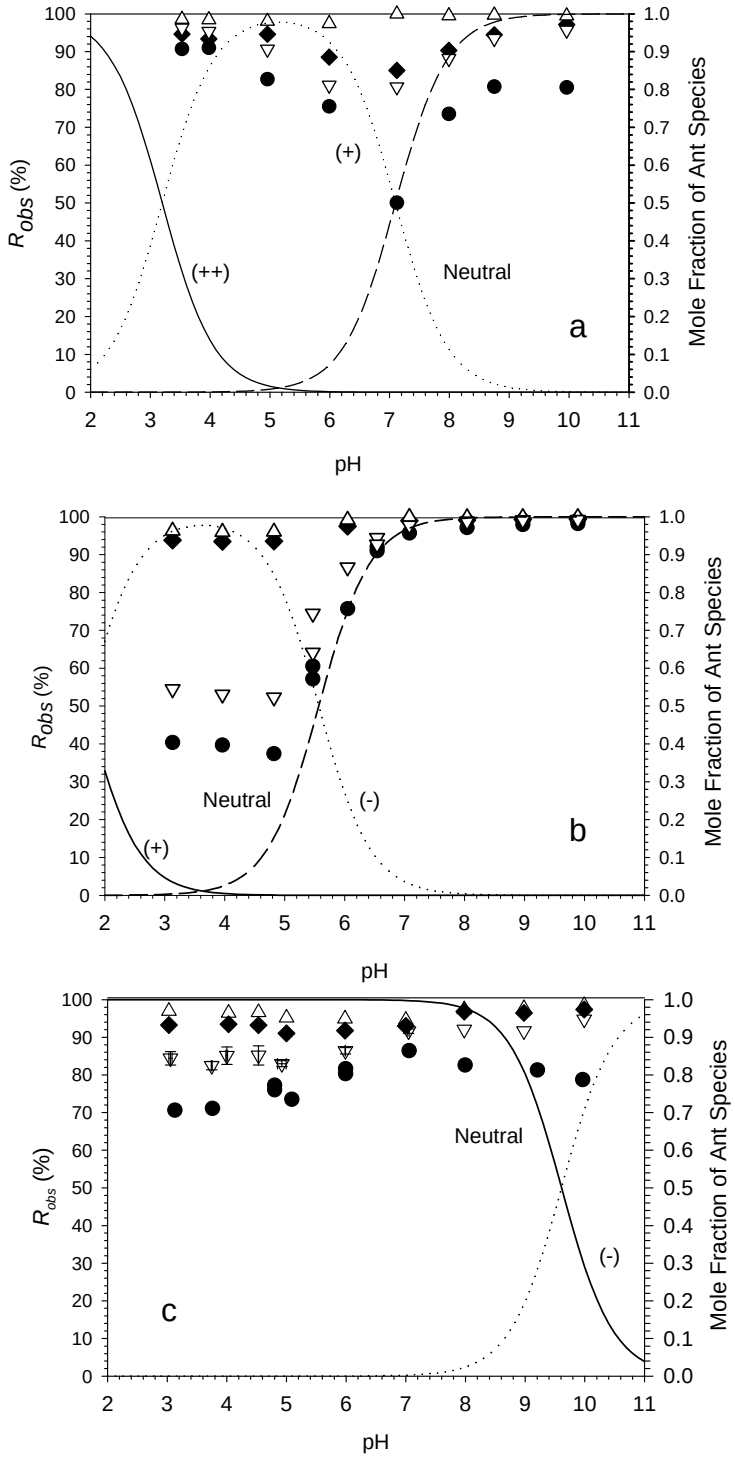

Figure 2. Symbols represent experimentally determined R_{obs} values for (a) TMP, (b) SMX, and (c) CDX from pH 3.0-10.0 using membranes Saehan NE 70 (●), Saehan NE 90 (◆), FilmTec NF 90 (△), and FilmTec NF 270 (▽). Lines represent the mole fractions of each antibiotic species. Error bars represent the standard error of $\geq$ 3 replicates. Average J_v values are 1.15×10^{-5} (Saehan NE 70), 9.73×10^{-6} (Saehan NE 90), 1.03×10^{-5} (FilmTec NF 90), and 1.30×10^{-5} m/s (FilmTec NF 270).

For the each set of experiments for one particular antibiotic (Figure 2), the observed rejection for Saehan NE 70 was lower than for Filmtec NF 270, while the observed rejection of these two membranes was typically lower than for Saehan NE 90 and FilmTec NF 90 when their $R_{obs} \leq 90\%$). One factor contributing to this difference is most likely due to the estimated pore size of these membranes (r_p) which is listed in Table 3 for Saehan NE 70, FilmTec 90, and FilmTec NF 270.

Table 3. Membrane pore size and experimental flux conditions.

Membrane	Organic Tracer	r_p (nm)	J_v (μm/s)
Saehan NE 70	D-xylose	0.35[a]	11.5± 0.3
	meso-Erythritol	0.36[a]	
	1,4-Dioxane	0.34[a]	
Average		0.35[a]	
Saehan NE 90[b]		-	9.7± 0.2
FilmTec NF 90		0.34[c]	10.3± 0.2
FilmTec NF 270		0.42[c]	13.0± 0.2

[a] the raw data and model fit to obtain these r_p values for each organic tracer is documented in Appendix C.
[b] r_p not determined since the majority of experimental R_{obs} values > 90% and was not modeled.
[c] from Nghiem et *al.* 2004

As previously mentioned, r_p for Saehan NE 70 was determined by model fitting the apparent rejection (R_{app}) of the organic tracers, *meso*-Erythritol, d-Xylose, and 1,4-Dioxane, as seen in Figure 3.

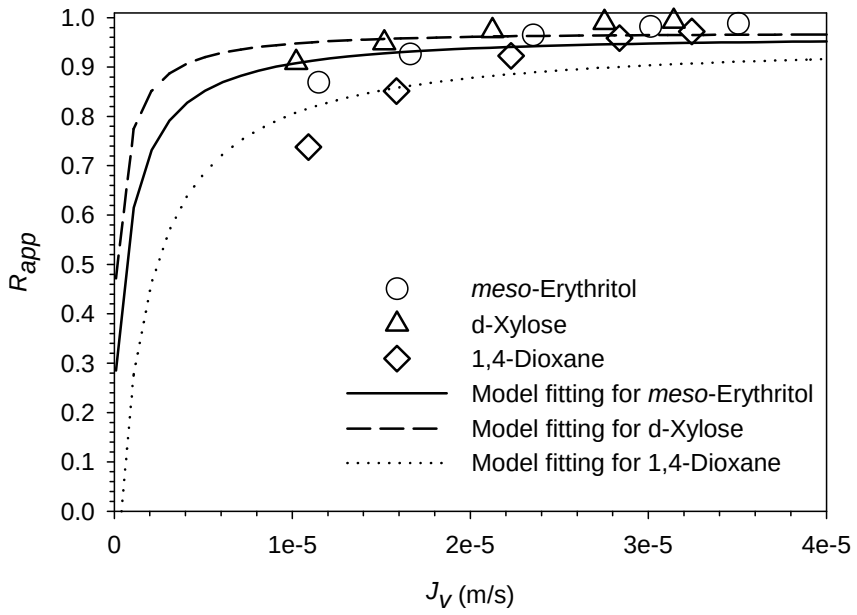

Figure 3. Symbols represent experimentally determined R_{app} values for *meso*-Erythritol, d-Xylose, and 1,4-Dioxane using the Saehan NE 70 membrane. The r_p value was adjusted in order to achieve the best fit to the experimental data. The lines represent the fitted model curves. The optimized r_p value for each model curve that was determined is listed in Table 3.

The r_p values decrease as follows where FilmTec NF 270 > Saehan NE 70 > FilmTec 90. This explains why lower antibiotic rejection is observed for FilmTec NF 270 and Saehan NE 70 in comparison to FilmTec NF 90 where rejection is > 94% for all conditions tested. While the pore size for Saehan NE 90 was not determined, it is considered to be a tighter membrane than Saehan NE 70 and FilmTec NF 270 and more similar to FilmTec NF 90 due to the lower permeate flux observed (Table 3). This is also supported by the SMX and CDX experimental data where antibiotic rejection for Saehan NE 90 differs from FilmTec NF 90 by only $\leq$ 4.1% (Figure 2). It should also be noted that the antibiotic rejection with Saehan NE 70 was observed to be less than FilmTec 270 which contradicts the effect of pore size. In this case, the permeate flux which affects rejection as discussed in the steric-hindrance model and extended Nernst-Planck equation

(see further discussion in Chapter 5), is hypothesized to play a role since the permeate flux for FilmTec NF 270 > Saehan NE 70, as seen in Table 3. Overall, pore size or membrane tightness can be related to antibiotic rejection, which is an expected phenomenon given that steric effects are a dominating removal mechanism of various organic compounds by NF membranes [6,7,32].

In addition, the experimental data presented in Figure 2 (a-c) indicates that antibiotic rejection significantly varies with pH for Saehan NE 70, FilmTec 270, and Saehan NE 90 (TMP only) (rejection of others is too high, $\geq$ 91.0%), due in part to membrane charge as well as to the compound's speciation effects. As discussed in the Materials and Methods section, the membrane surfaces are negatively charged above pH 3.1-3.9 for Saehan NE 70, Saehan NE 90, and FilmTec NF 270 and above pH 4.9-6.0 for FilmTec NF 90. The membranes are positively charged below these pH ranges. This effect is paralleled by the change in speciation of TMP, SMX, and CDX, whose pK_a values are listed in Table 2.

First, as seen in Figure 2a, TMP exhibits unique speciation from pH 3.0-10.0 where it is neutral (TMP) at pH > 7.1 (pK_{a2}), becomes positively charged (TMP^{+1}) below this pK_a, and then holds two positive charges (TMP^{+2}) at pH < 3.2 (pK_{a2}). This seems to result in a characteristic rejection trend where the lowest rejection is found near circumneutral pH conditions. At pH 3.0, TMP^{+2} and TMP^{+1} are present at 61.3% and 38.7% of the total TMP concentration and are likely to be highly rejected due to charge repulsion with the positively charged membrane surface. As the pH increases, the membrane becomes more negatively charged and further draws TMP^{+1} through the

membrane pore due to charge attraction forces. After pK_{a2} = 7.1 is exceeded, TMP losses its positive charge and ultimately leads to lower attraction and greater rejection.

In the case of SMX, this compound becomes negatively charged (SMX^-) at a pH > 5.6 (pK_{a2}). The charge repulsion effects due to a negative membrane are well outlined as the rejection increases from pH 5-7 along a similar trend as the increase in SMX^- concentration, resulting in high rejection of SMX (> 97%) at pH ≥ 8.0. Interestingly enough, rejection is also found to increase slightly at pH ≤ 4.8, as seen in Figure 2. It is suspected to be influenced by the formation of SMX^+ (pK_{a1} = 1.7), albeit with only 5% of the total SMX concentration at pH 3.0, which is repelled by the increasing positive membrane surface charge.

Finally, as seen in Figure 2c, CDX does not appear to exhibit a consistent trend when the pH is varied from 3.0-10.0. For Saehan NE 70, CDX rejection increases from 70.6 to 86.4% from pH 3.1 to 7.1 but decreases to 78.8% at pH 10.0. For FilmTec 270, CDX rejection increases from 84.4% to 94.8% from pH 3.1 to 10. In terms of speciation effects, CDX converts to CDX^- at a pH > 9.6 (pK_{a1}). However, it is considered possible that while CDX is overall a neutral compound, it does contain two *N*-oxide moieties which carry both a negative and positive charge. Such charges may impact the electrostatic interactions between CDX and the charged membrane and affect the overall rejection observed over this pH range.

4.4 Symbols

J_v	solvent flux through the membrane [$L/m^2/s$ or m/s]
ΔP	applied pressure [33]
r_p	pore radius of membrane [m]
r_s	radius of solute (ions or neutral solutes) [m]
R_{app}	apparent rejection of solute [−]
R_{obs}	observed rejection of solute [−]

Greek Letters

λ	ratio of solute radius/pore radius [−]

Subscripts

f	feed
p	permeate or pore
s	neutral solute

4.5 References

1) Y. Kiso, Y. Nishimura, T. Kitao, K. Nishimura, Rejection Properties of Non-Phenylic Pesticides with Nanofiltration Membranes, Journal of Membrane Science 171 (2000) 229-237.

2) B. Van der Bruggen, K. Everaert, D. Wilms, C. Vandecasteele, The Use of Nanofiltration for the Removal of Pesticides from Groundwater: An Evaluation, Water Science and Technology: Water Supply 1 (2001) 99-106.

3) S.S. Chen, J.S. Taylor, L.A. Mulford, C.D. Norris, Influences of Molecular Weight, Molecular Size, Flux, and Recovery for Aromatic Pesticide Removal by Nanofiltration Membranes, Desalination 160 (2004) 103-111.

4) K. Kimura, G. Amy, J.E. Drewes, T. Heberer, T.U. Kim, Y. Watanabe, Rejection of Organic Micropollutants (Disinfection by-Products, Endocrine Disrupting Compounds, and Pharmaceutically Active Compounds) by Nf/Ro Membranes, Journal of Membrane Science 227 (2003) 113-121.

5) A.I. Schafer, L.D. Nghiem, T.D. Waite, Removal of the Natural Hormone Estrone from Aqueous Solutions Using Nanofiltration and Reverse Osmosis, Environmental Science & Technology 37 (2003) 182-188.

6) L.D. Nghiem, A.I. Schafer, M. Elimelech, Removal of Natural Hormones by Nanofiltration Membranes: Measurement, Modeling, and Mechanisms, Environmental Science & Technology 38 (2004) 1888-1896.

7) L.D. Nghiem, A.I. Schafer, M. Elimelech, Pharmaceutical Retention Mechanisms by Nanofiltration Membranes, Environmental Science & Technology 39 (2005) 7698-7705.

8) A.M. Comerton, R.C. Andrews, D.M. Bagley, C.Y. Hao, The Rejection of Endocrine Disrupting and Pharmaceutically Active Compounds by Nf and Ro Membranes as a Function of Compound a Water Matrix Properties, Journal of Membrane Science 313 (2008) 323-335.

9) K. Kimura, G. Amy, J. Drewes, Y. Watanabe, Adsorption of Hydrophobic Compounds onto Nf/Ro Membranes: An Artifact Leading to Overestimation of Rejection, Journal of Membrane Science 221 (2003) 89-101.

10) L.D. Nghiem, A.I. Schafer, T.D. Waite, Adsorption of Estrone on Nanofiltration and Reverse Osmosis Membranes in Water and Wastewater Treatment, Water Science and Technology 46 (2002) 265-272.

11) Y. Yoon, R.M. Lueptow, Removal of Organic Contaminants by Ro and Nf Membranes, Journal of Membrane Science 261 (2005) 76-86.

12) C. Bellona, J.E. Drewes, The Role of Membrane Surface Charge and Solute Physico-Chemical Properties in the Rejection of Organic Acids by Nf Membranes, Journal of Membrane Science 249 (2005) 227-234.

13) L.D. Nghiem, A.I. Schafer, M. Elimelech, Role of Electrostatic Interactions in the Retention of Pharmaceutically Active Contaminants by a Loose Nanofiltration Membrane, Journal of Membrane Science 286 (2006) 52-59.

14) L.D. Nghiem, S. Hawkes, Effects of Membrane Fouling on the Nanofiltration of Pharmaceutically Active Compounds (Phacs): Mechanisms and Role of Membrane Pore Size, Separation and Purification Technology 57 (2007) 176-184.

15) P. Xu, J.E. Drewes, T.U. Kim, C. Bellona, G. Amy, Effect of Membrane Fouling on Transport of Organic Contaminants in Nf/Ro Membrane Applications, Journal of Membrane Science 279 (2006) 165-175.

16) K.V. Plakas, A.J. Karabelas, T. Wintgens, T. Melin, A Study of Selected Herbicides Retention by Nanofiltration Membranes - the Role of Organic Fouling, Journal of Membrane Science 284 (2006) 291-300.

17) X.S. Miao, F. Bishay, M. Chen, C.D. Metcalfe, Occurrence of Antimicrobials in the Final Effluents of Wastewater Treatment Plants in Canada, Environmental Science & Technology 38 (2004) 3533-3541.

18) R. Hirsch, T. Ternes, K. Haberer, K.L. Kratz, Occurrence of Antibiotics in the Aquatic Environment, Science of the Total Environment 225 (1999) 109-118.

19) D.W. Kolpin, E.T. Furlong, M.T. Meyer, E.M. Thurman, S.D. Zaugg, L.B. Barber, H.T. Buxton, Pharmaceuticals, Hormones, and Other Organic Wastewater Contaminants in Us Streams, 1999-2000: A National Reconnaissance, Environmental Science & Technology 36 (2002) 1202-1211.

20) C.S. McArdell, E. Molnar, M.J.F. Suter, W. Giger, Occurrence and Fate of Macrolide Antibiotics in Wastewater Treatment Plants and in the Glatt Valley Watershed, Switzerland, Environmental Science & Technology 37 (2003) 5479-5486.

21) S. Castiglioni, R. Bagnati, R. Fanelli, F. Pomati, D. Calamari, E. Zuccato, Removal of Pharmaceuticals in Sewage Treatment Plants in Italy, Environmental Science & Technology 40 (2006) 357-363.

22) T.J. Strock, S.A. Sassman, L.S. Lee, Sorption and Related Properties of the Swine Antibiotic Carbadox and Associated N-Oxide Reduced Metabolites, Environmental Science & Technology 39 (2005) 3134-3142.

23) H. Lucida, J.E. Parkin, V.B. Sunderland, Kinetic Study of the Reaction of Sulfamethoxazole and Glucose under Acidic Conditions - I. Effect of Ph and Temperature, International Journal of Pharmaceutics 202 (2000) 47-61.

24) Z.M. Qiang, C. Adams, Potentiometric Determination of Acid Dissociation Constants (Pka) for Human and Veterinary Antibiotics, Water Research 38 (2004) 2874-2890.

25) B. Roth, J.Z. Strelitz, Protonation of 2,4-Diaminopyrimidines .I. Dissociation Constants and Substituent Effects, Journal of Organic Chemistry 34 (1969) 821-836.

26) J.R. Welty, C.E. Wicks, R.E. Wilson, G.L. Rorrer, Fundamentals of Momentum, Heat, and Mass Transfer, fourth ed., John Wiley & Sons, New York, 2001.

27) P. Atkins, J. de Paula, Physical Chemistry, seventh ed., Oxford University Press, New York, 2002.

28) A.D. Pethybridge, J.D.R. Talbot, W.A. House, Precise Conductance Measurements on Dilute Aqueous Solutions of Sodium and Potassium Hydrogenphosphate and Dihydrogenphosphate, Journal of Solution Chemistry 35 (2006) 381-393.

29) E.N. Tsurko, R. Neueder, J. Barthel, A. Apelblat, Conductivity of Phosphoric Acid, Sodium, Potassium, and Ammonium Phosphates in Dilute Aqueous Solutions from 278.15 K to 308.15 K, Journal of Solution Chemistry 28 (1999) 973-999.

30) H.S. Harned, B.B. Owen, The Physical Chemistry of Electrolytic Solutions, third ed., Reinhold Publishing, New York, 1958.

31) K. Kosutic, B. Kunst, Removal of Organics from Aqueous Solutions by Commercial Ro and Nf Membranes of Characterized Porosities, Desalination 142 (2002) 47-56.

32) W.R. Bowen, A.W. Mohammad, N. Hilal, Characterisation of Nanofiltration Membranes for Predictive Purposes - Use of Salts, Uncharged Solutes and Atomic Force Microscopy, Journal of Membrane Science 126 (1997) 91-105.

33) J.R. Pappenheimer, E.M. Renkin, L.M. Borrero, Filtration, Diffusion and Molecular Sieving through Peripheral Capillary Membranes a Contribution to the Pore Theory of Capillary Permeability, American Journal of Physiology 167 (1951) 13-46.

CHAPTER 5

Applying Mechanistic Models to Evaluate Antibiotic Removal using Nanofiltration Membranes

5.1 Introduction

For NF membranes, two modeling approaches have been used to predict rejection that involves nonequilibrium thermodynamics and particle dynamics. The nonequilibrium thermodynamics approach defined by Kedem and Katchalsky [1] and Spiegler and Kedem [2] characterizes the membrane as a black box when deriving the related phenomenological equations. It is a model commonly employed for reverse osmosis (RO) membranes but has been applied to NF membranes as well [3-5]. On the other hand, NF membranes are porous membranes that have been widely considered as a bundle of straight cylindrical pores. The particle dynamics approach uses such structural aspects to predict solute transport in the membrane pore by assessing mechanisms such as hindered diffusion, convection, and possibly electromigration [6-8].

For uncharged solutes, one of the earliest influential studies was conducted over a century ago by Ferry [9] who investigated the particular effects of hindered convection in pores. This was followed by additional studies where hindered solute convection as well as diffusion were examined due to its widespread application in biological systems [10-12]. Currently though, the theory behind this approach is well characterized through diffusion and convection hindrance factors which are dimensionless terms relating solute size to pore size and steric-driven boundary conditions at the pore entrance and exit.

For charged solutes, the fundamental relationship governing transport through cylindrical pores is the extended Nernst-Planck equation where diffusion, convection, and electromigration terms are considered [13,14]. This equation can be further incorporated

into other models that characterize membrane electrical properties such as the Teorell-Meyer-Sievers (TMS) and space-charge (SC) models. These two models differ primarily in the spatial distribution of membrane charge, where the TMS model assumes uniform distribution while the SC model assumes a radial distribution of potential across a charged capillary. Several studies have used the TMS or SC models directly [15-17], but an approach originally derived from Goldman, Schlögl, and then Dresner [13,18,19] used a one-dimensional (1-D) version of the extended Nernst-Planck equation that was further adopted to include uniform charge distribution [7,20,21] and hindrance effects [14]. It is this methodology along with equilibrium partitioning at the pore entrance and exit due to both electrical (Donnan) and steric effects [13,14] that can be used to dictate overall solute flux through charged membrane pores. When applying models for uncharged and charged solutes as described above, it is also necessary to assess various solute and membrane parameters. These include parameters such as the solute and membrane pore size (r_s and r_p), membrane thickness to porosity ($\Delta x/A_k$), and membrane charge density (X).

In our study, we were interested in applying such modeling techniques towards the rejection of antibiotics. No known studies to date have attempted to develop such a mechanistic model to predict their rejection when both charged and uncharged antibiotic species are considered involving both steric hindrance and charge effects. Model results were compared to experimental data to elucidate how well antibiotic-membrane interactions could be predicted. Deviations between model prediction and experimentally observed values were found and discussed further.

5.2 Model Development

5.2.1 Hydrodynamic Model for Solute Flux through NF membranes

The predicted transport of solutes through NF membranes is based on the widely accepted understanding that these membranes have pores. These pores are assumed to be cylindrical in shape and hold a uniform pore radius. Within each pore, a hydrodynamic model can be derived in which both the target solute and membrane need to be characterized in order to assess the significance of various membrane transport mechanisms and estimate the solute concentration in the permeate (C_p) and the observed membrane rejection (R_{obs}). For uncharged solutes, the steric-hindrance model is used to predict transport that is dependent on two mechanisms, diffusion and convection, as seen in eq 1 [29], while for charged solutes, an additional mechanism is considered, electromigration, as seen in the modified extended Nernst-Planck equation [13,14] (eq 2) since NF membranes often have charged pores.

$$J_{s,pore} = -K_{s,d} D_s \frac{dc_s}{dx} + K_{s,c} V c_s \qquad (1)$$

$$J_{i,pore} = -K_{i,d} D_i \frac{dc_i}{dx} + K_{i,c} V c_i - \frac{z_i c_i K_{i,d} D_i}{RT} F \frac{d\Psi_m}{dx} \qquad (2)$$

In eq 1, $J_{s,pore}$ is the pore solute flux, D_s is the diffusion coefficient of the solute s, c_s is the concentration in the membrane phase, x is the coordinate in the flow direction through the membrane, V is the solvent velocity, $K_{s,d} \cdot D_s$ is the hindered diffusivity, and K_c is the effective drag factor related to convection. For eq 2, similar variables are defined for ion i but include terms for electromigration transport where z_i is the valency, R is the ideal

gas law constant, T is temperature, F is Faraday's constant, and Ψ_m is the membrane potential.

Numerous studies have used eq 1 or 2 to predict the rejection of various uncharged compounds [8,28,30] or charged compounds and salts [6,20,31,32], respectively, for NF membranes. When assessing the rejection of antibiotics, both approaches will be considered since these compounds can be neutral or charged depending on the pH condition.

5.2.2 Transport of Uncharged Solutes

The hydrodynamic equation (eq 1) used in this study for uncharged solutes can be further integrated over the pore length or membrane thickness (Δx) where the boundary conditions are derived purely by steric interactions between the solute and pore size. The solute size is characterized by defining a solute radius (r_s) which is estimated in various ways (see later discussions), and the pore size is characterized by defining a pore radius (r_p) which is estimated by model-fitting experimental rejection data of other neutral solutes (see later discussions). A ratio between r_s and r_p is defined as λ ($= r_s / r_p$) and used to estimate a distribution coefficient, Φ, which is equal to the equilibrium partition expressions at the entrance or exit of the membrane pore [29,33-35]:

$$\Phi = \frac{c_{x=0}}{C_{wall}} = \frac{c_{x=\Delta x}}{C_p} = (1-\lambda)^2 = \left(1-\frac{r_s}{r_p}\right)^2 \qquad (3)$$

where C_{wall} is the membrane surface concentration, C_p is the solute permeate concentration, and $c_{x=0}$ and $c_{x=\Delta x}$ are the solute concentrations just inside the pore at x=0

and x=Δx, respectively. These boundary conditions from eq 3 are further used to integrate eq 1 over the entire pore length, from x=0 to x=Δx, to yield an analytical solution for the pore solute flux, $J_{s,pore}$ (eq 4). Details regarding the integration of eq 1 to obtain eq 4 are found in Appendix A.

$$J_{s,pore} = 1 - \frac{K_c \Phi V C_{wall}\left[1 - \left(\frac{C_p}{C_{wall}}\right)\cdot \exp(-Pe)\right]}{1 - \exp(-Pe)} \qquad (4)$$

where Pe is the Peclet number defined as:

$$Pe = \frac{K_c V \Delta x}{K_d D_i} = \frac{K_c J_v \Delta x}{K_d D_i A_k} \qquad (5)$$

For these equations, the pore solute flux, $J_{s,pore}$, is also a function of the permeate concentration, C_p, and solvent velocity, V, where $J_{s,pore} = C_p \cdot V$, while the solvent velocity, V, is also a function of the overall solvent flux, J_v, and the effective membrane porosity, A_k, where $V = J_v/A_k$. By substituting these equations into eq 4, a solution for the permeate concentration, C_p, and apparent rejection, R_{app}, can be derived, as seen in eq 6:

$$R_{app} = 1 - \frac{C_p}{C_{wall}} = 1 - \frac{K_c \Phi}{1 - \exp(-Pe)\cdot(1 - \Phi K_c)} \qquad (6)$$

The model parameters, K_c, K_d, and $\Delta x/A_k$, are determined independently using equations described in detail in the Model Parameters section. J_v is measured experimentally, and D_s is solute dependent and estimated using various approaches (see later discussions).

5.2.3 Transport of Charged Solutes

Transport of charged solutes is predicted both by steric interactions and by charge repulsion or attraction between the solute and membrane. The modified extended Nernst-Planck equation (eq 2) which describes the ion flux through the pore can be rewritten in the form of a concentration gradient where the ion flux, J_i, is substituted by $C_p \cdot V$ or $C_p \cdot J_v / A_k$, as seen in eq 7:

$$\frac{dc_i}{dx} = \frac{J_v}{K_{i,d} D_i A_k}\left(K_{i,c} c_i - C_{i,p}\right) - \frac{z_i c_i}{RT} F \frac{d\Psi_m}{dx} \qquad (7)$$

For this equation, the values, $K_{i,c}$, $K_{i,d}$, J_v, and D_i are determined similarly to the methods described above for neutral solutes. The potential gradient ($d\Psi_m/dx$) is determined by first taking the summation of both sides of eq 7, which results in eq 8:

$$\sum_{i=1}^{n} \frac{dc_i}{dx} = \sum_{i=1}^{n}\left[\frac{J_v}{K_{i,d} D_i A_k}\left(K_{i,c} c_i - C_{i,p}\right)\right] - \frac{F}{RT} \cdot \frac{d\Psi_m}{dx} \cdot \sum_{i=1}^{n} z_i c_i \qquad (8)$$

The left side of this equation can be separately solved by applying an electroneutrality equation related to the charge balance inside the membrane, as described in eq 9:

$$\sum_{i=1}^{n} z_i c_i + X = 0 \qquad (9)$$

where X is defined as the membrane charge density and determined by model-fitting rejection of specific ions present in the experimental matrix. Further details regarding the approach used to determine membrane charge density (X) will be described in later

sections. The derivative of eq 9 with respect to x (d/dx) is then taken where the membrane charge density (X) does not vary ($dX/dx = 0$), resulting in eq 10:

$$\frac{d}{dx}\left[\sum_{i=1}^{n} z_i c_i\right] = 0 \qquad (10)$$

After both sides of eq 8 are multiplied by z_i, eq 10 can be substituted into the left side of eq 8, where final rearrangement leads to an equation for the potential gradient ($d\Psi_m/dx$) as seen below (eq 11) [7,13,14]:

$$\frac{d\Psi_m}{dx} = \frac{\sum_{i=1}^{n} \frac{z_i J_v}{K_{i,d} D_i A_k}\left(K_{i,c} c_i - C_{i,p}\right)}{\frac{F}{RT}\sum_{i=1}^{n}\left(z_i^2 c_i\right)} \qquad (11)$$

Upon substituting the potential gradient term into eq 7, the ordinary differential equation can be integrated from $x = 0$ to $x = \Delta x/A_k$ using the initial boundary condition defined as $c_{i,x=0}$. $c_{i,x=0}$ can be found using the following Donnan-steric partitioning expression [13,14] (eq 12) which relates the ion concentrations above and below the interface of either the membrane pore entrance ($x = 0$) or exit ($x = \Delta x/A_k$) :

$$\frac{c_i}{C_i} = \Phi_i \exp\left(-\frac{z_i F}{RT}\left(\Delta\Psi_{d,x=0} \text{ or } \Delta\Psi_{d,x=\Delta x/A_k}\right)\right) \qquad (12)$$

at $x = 0$: $c_i = c_{i,x=0}$, $C_i = C_{wall}$ and $\Delta\Psi_{d,x=0}$

at $x = \Delta x/A_k$ $c_i = c_{i,x=\Delta x/Ak}$ and $C_i = C_p$ and $\Delta\Psi_{d,x=\Delta x,Ak}$

where $\Delta\Psi_d$ is the Donnan electrical potential and Φ is similar to the value described above for neutral solutes. To solve for $c_{i,x=0}$, $\Delta\Psi_{d,x=0}$ is determined by inserting c_i for each ion (eq 12) into the membrane electroneutrality equation (eq 9). In addition, other electroneutrality equations that will be used for model prediction are related to the feed (*f*) and permeate (*p*) solution (eq 13):

$$\sum_{i=1}^{n} z_i C_f = 0 \qquad \sum_{i=1}^{n} z_i C_p = 0 \tag{13}$$

5.2.4 Concentration Polarization

Due to solute rejection, the solute concentration at the membrane surface or right outside the pore entrance (C_{wall}) is found to be higher than the bulk feed concentration (C_f) which is measured experimentally. Such concentration polarization is modeled using film theory (eq 14) where C_{wall} is a function of C_f, C_p, J_v, and the solute mass transfer coefficient, k, which is found using equations described in detail in the Model Parameters section.

$$\frac{C_{wall} - C_p}{C_f - C_p} = e^{J_v / k} \tag{14}$$

For the transport of neutral solutes, the equations described previously in the steric-hindrance model for the apparent rejection (R_{app}) (= 1-C_p/C_{wall}) and the observed rejection (R_{obs}) (= 1-C_p/C_f) can be integrated into eq 14, resulting in an overall relationship between R_{app} and R_{obs}, as seen in eq 15. The final model value for R_{obs} can then be evaluated and compared to the experimental R_{obs} value.

$$\ln\frac{1-R_{app}}{R_{app}} = \ln\frac{1-R_{obs}}{R_{obs}} - \frac{J_v}{k} \qquad (15)$$

For ion transport, eq 14 will be used directly to relate C_f to C_{wall} using an initial guessed value for $C_{i,p}$ ($C_{i,p,initial}$). In this case, the specific numerical method used to obtain a model value for R_{obs} will be discussed in the following sections.

5.3. Model Parameters

5.3.1 Hindrance Factors

Both the hindrance factors for diffusion ($K_{s,d}$ and $K_{i,d}$) and convection ($K_{s,c}$ and $K_{i,c}$) for neutral solutes and ions are functions of λ where λ can be $0 < \lambda \leq 0.95$ and $0 < \lambda < 1.0$ for K_d and K_c, respectively . They are determined using the following expressions (eqs 16-19) [8,36]:

$$K_d(\lambda) = H(\lambda)/\Phi\ (\lambda) \qquad (16)$$

$$K_c(\lambda) = W(\lambda)/\Phi\ (\lambda) \qquad (17)$$

where $H(\lambda)$and $W(\lambda)$are defined as:

$$H(\lambda) = 1 + \frac{9}{8}\lambda\ln(\lambda) - 1.56034\lambda + 0.528155\lambda^2 - 1.91521\lambda^3 - 2.81903\lambda^4 + 0.270788\lambda^5 + 1.0115\lambda^6 - 0.435933\lambda^7 \qquad (18)$$

$$W(\lambda) = (1-\lambda)^2\left[\frac{1 + 3.867\lambda - 1.907\lambda^2 - 0.834\lambda^3}{1 + 1.867\lambda - 0.741\lambda^2}\right] \qquad (19)$$

5.3.2 Membrane Thickness Divided by Porosity ($\Delta x/A_k$)

The membrane thickness divided by porosity *($\Delta x/A_k$)* can be evaluated using the Hagen-Poiseulle equation which relates the water flux to the applied pressure across the membrane, as seen in eq 20:

$$J_v = \frac{r_p^2 \cdot \Delta P}{8\mu \cdot (\Delta x / A_k)} \tag{20}$$

where r_p is the pore radius of the membrane, ΔP is the applied pressure, and μ is the solvent viscosity. The water flux (J_v) is determined experimentally at a certain applied pressure for any given membrane, and if the pore radius (r_p) of the membrane is known, $\Delta x/A_k$ can be calculated.

5.3.3 Mass Transfer Coeffiecient (k)

The mass transfer coefficient (k) for each solute was determined by first evaluating the mass transfer coefficient of salt (NaCl) (k_{salt}) using the following relationship provided below [37]:

$$k_{salt} = \frac{J_{v,salt}}{\ln\left\{\frac{\Delta P}{\pi_f - \pi_p} \cdot \left[1 - \frac{J_{v,salt}}{J_{v,H_2O}}\right]\right\}} \tag{21}$$

To determine k_{salt}, a filtration experiment was performed initially using reagent water at an operating pressure, cross-flow velocity, and feed tank temperature of 4.83 bar (482.6 kPa or 70 psi) (ΔP), 29.5 cm/s, and 20$\pm$0.3°C, respectively. Pure water flux, $J_{v,H2O}$ (L/m^2/h), was measured. Salt (NaCl) was then added to obtain a final bulk feed concentration ($C_{f,salt}$) of 96.6 mM. Permeate samples were taken periodically to measure

salt solution flux, $J_{v,salt}$ (L/m^2/h), and salt permeate concentration, $C_{p,salt}$. The osmotic pressures for both the feed (π_f) (bar) and permeate (π_p) (bar) were determined using Van't Hoff equation (=(C_f or C_p)·R·T·(ϕ_f or ϕ_p)) where the osmotic coefficient (ϕ_f or ϕ_p) was determined from Silvester and Pitzer [38]. The k value was then estimated from k_{salt} using the following relationship (eq 22) since the mass transfer boundary layer for each solute was under the same mixing conditions as salt [39,40]:

$$k = \frac{k_{salt}}{\left[\frac{D_{salt}}{D_s \text{ or } D_i}\right]^{2/3}} \qquad (22)$$

where the salt diffusion constant, D_{salt}, was found from literature [41].

5.4 Numerical Solution for Transport of Charged Solutes

A numerical solution for the transport of charged solutes was developed due to the system of first-order ordinary differential equations needed to solve the concentration of each ion (i) inside the membrane pore. The numerical solution was adopted from Schaep et *al.* 1999 and Lee and Lueptow 2001 and programmed using Matlab 7.4.0 (R2007a). Details regarding this code are presented in Appendix B.

The numerical analysis was conducted in two phases, Phase I and II, and the structure of the program including the model input, internal calculations, and output is outlined in Figure 1 and will be briefly described here. To begin, the experimental values for C_f and J_v along with either the experimental value for C_p ($C_{i,p,exp}$) (Phase I) or an initial guessed value for C_p ($C_{i,p,initial}$) (Phase II) were used to calculate the solute concentration at the membrane surface ($C_{i,wall}$) using the concentration polarization model

(eqs 14). This $C_{i,wall}$ value was then substituted into the boundary condition at $x = 0$ (eq 12) to derive an expression for c_i for each ion in solution (c_i where i = 1,2,…n total ions) as a function of the Donnan electrical potential ($\Delta\Psi_{d,x=0}$). To calculate $\Delta\Psi_{d,x=0}$, these n equations were used along with the electroneutrality equation (eq 9), setting up a total of n+1 equations and n+2 unknowns, where the unknowns were c_1, c_2,…c_n, $\Delta\Psi_{d,x=0}$, and the effective membrane charge density (X). For X, an initial guessed value (Phase I) or a previously calculated value (Phase II) was used in order to solve this system of equations. $\Delta\Psi_{d,x=0}$ was then solved numerically and used to calculate $c_{i,x=0}$ (eq 12). In the next step, $c_{i,x=0}$ could be applied as an initial boundary condition for the first-order differential equation (eq 7 and 11) which was solved numerically by using a fourth/fifth-order Runge-Kutta method to output c_i at x = $\Delta x/A_k$ ($c_{i,\Delta x/Ak}$). From $c_{i,\Delta x/Ak}$, eq 12 was again used as a boundary condition where $c_{i,\Delta x/Ak}$ and C_p were substituted in for c_i and C_i, respectively, for n total ions. Here the equation for C_p (eq 12) was incorporated into the electroneutrality equation for the permeate (eq 13), and $\Delta\Psi_{d,x=\Delta x/Ak}$ was determined numerically. Finally, the predicted C_p value ($C_{i,p,output}$) for each ion could be calculated from eq 12.

This numerical model was operated in a two phase mode, Phase I and II, due to the different output values desired. First, Phase I was conducted in which the Cl^- permeate concentration was fit to its experimentally determined permeate concentration ($C_{i,p,exp}$) from pH 3.1-9.9. An initial guessed value for X ($X_{initial}$) was used for the first iteration and then changed step-wise in proceeding iterations until $C_{i,p,exp}$ and $C_{i,p,ouput}$ were equal. This X value was then substituted directly into Phase II. For Phase II, an initial guess value for C_p ($C_{i,p,initial}$) for each ion was used for the first iteration and then

changed step-wise in proceeding iterations until $C_{i,p,input}$ equaled the $C_{ip,output}$ value, for all n ions.

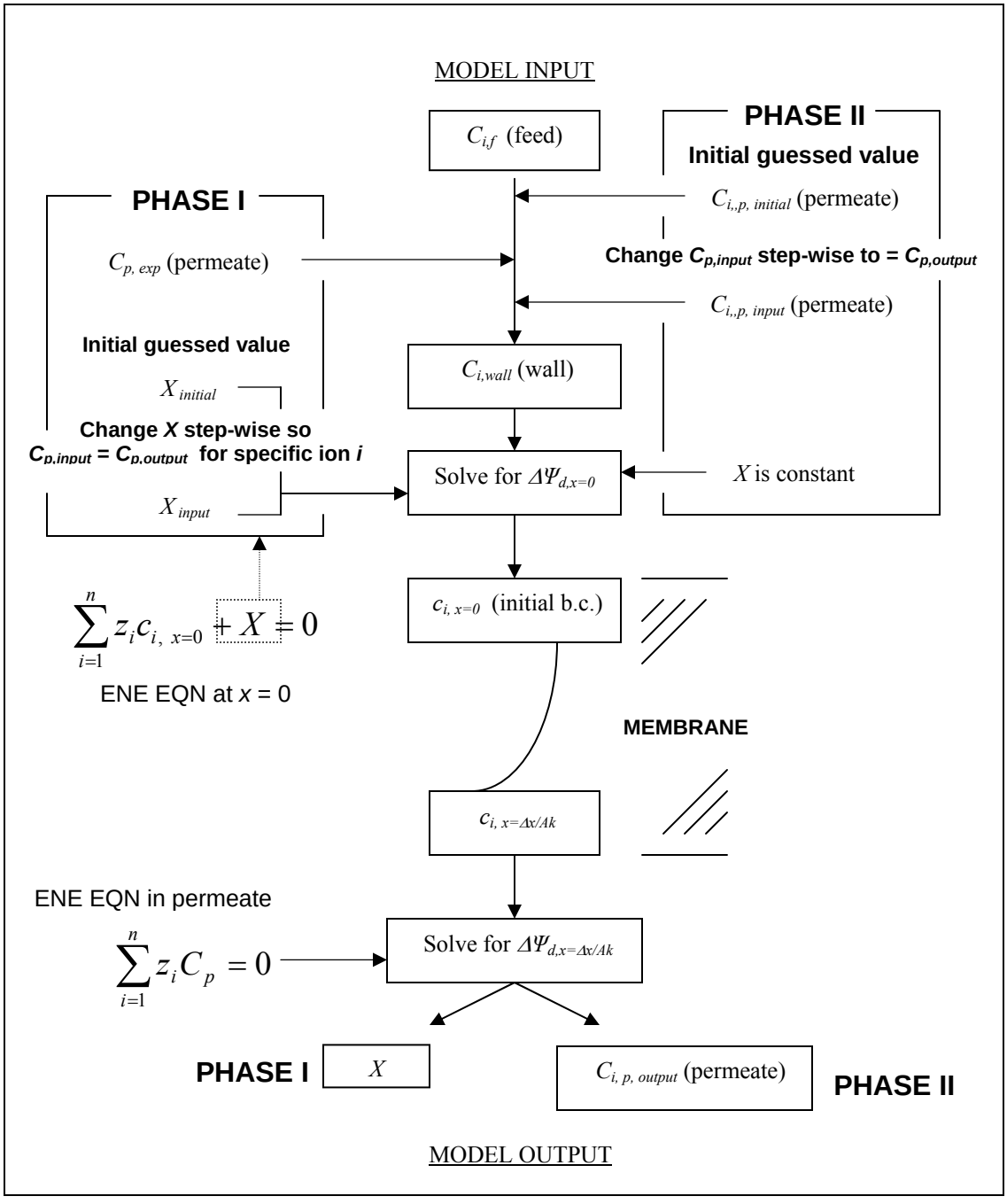

Figure 1. Diagram of the computer model used to obetain the numerical solution for charge balances and ion transport through the membrane.

5.5. Results and Discussion

5.5.1 Modeling of Uncharged Antibiotics

The steric-hindrance model, as described in previous sections, was used to assess the rejection of the uncharged antibiotics. It should be noted that the modeling procedure described henceforth was only done for Saehan NE 70 and FilmTec NF 270 membranes. The experimental rejection for Saehan NE 90 and FilmTec NF 90 did not typically show a significant trend with varying pH due to the overall high rejection observed, and thus these membranes were not modeled.

For Saehan NE 70 and FilmTec NF 270, the first step was to use r_s (TMP, SMX, and CDX) (Table 2, Chapter 4) and r_p (Saehan NE 70 and FilmTec 270) (Table 3, Chapter 4) to calculate λ (= r_s / r_p). For FilmTec 270, the λ values for TMP, SMX, and CDX were 0.912, 0.831, and 0.843, respectively. These values along with other operating and experimentally determined parameters such as ΔP, J_v, and k were then integrated into the steric-hindrance model to determine R_{obs}, which was 94.9, 76.7, and 83.3% for the neutral TMP, SMX, and CDX solutes, respectively.

For Saehan NE 70, the λ values for TMP, SMX, and CDX were all $\geq$ 0.997, suggesting that R_{obs} should be ~ 100% due to steric effects alone. However, this contradicts what was experimentally observed in Figure 2 (a-c) (Chapter 4) where R_{obs} ranged from 37.4-98.2%. It is hypothesized that this discrepancy could be due to a number of factors such as (1) inaccurate r_s estimation, (2) membrane pore size (r_p) distribution [52,53], and (3) the contribution of solute diffusion through the membrane polymer matrix itself – a solute transport mechanism not addressed in the steric-hindrance model but considered in the solution diffusion model which has similarly been

applied to NF membranes in previous studies [54,55]. Currently, all three options are considered possible factors, although only option (1) will be discussed here while the effects of options (2) and (3) will need to be addressed in our future work.

In terms of inaccurate r_s estimation (option (1)), the r_s values listed in Table 2 in Chapter 4 were calculated assuming these antibiotic compounds were spherical in shape. This approach though is only one out of many in an attempt to well characterize solute size. Numerous studies have considered the use of molecular weight, molecular length, molecular width, and mean molecular radius [56-60]. In addition, other studies indicate that the orientation of the molecule can be affected by its dipole moment where the molecule's polar functional groups are attracted to the charged membrane surface [28,61,62], possibly altering the effective r_s value. Thus, it is with the understanding that these antibiotic r_s values may vary that the following approach was taken in regards to developing a model to fit the Saehan NE 70 rejection data in Figure 2 (a-c) (Chapter 4). As will be described in later sections, model curves integrating both the effects of uncharged and charged solutes were first developed for FilmTec NF 270 using the r_s values given in Table 2 (Chapter 4). Differences between the model and experimental data were related to possible r_s inaccuracies, and therefore, the r_s values were varied until the model best fit the data. These revised r_s values will then directly used when modeling Saehan NE 70 rejection.

5.5.2 Modeling of Charged Antibiotics

The theory and numerical modeling approach used to predict the transport of charged solutes has been originally described in previous sections. The information

presented here is related to the additional experimental results used during this modeling procedure along with the final results.

One of the major aspects of predicting charged solute transport was related to assessing total charge and establishing electroneutrality at all points in the *x* direction or flow direction within the membrane pore. In order to do this, the feed (C_f) and permeate ($C_{i,p}$) concentrations (i.e., overall R_{obs}) of all the ions in our experimental matrix were assessed. The ions that required monitoring were as follows: $H_2PO_4^{-1}$ and HPO_4^{-2} (phosphate buffer), Cl^- (HCl addition), Na^+ (buffer and NaOH addition), H^+, OH^-, and the charged antibiotics (e.g. TMP^{+1}, TMP^{+2}, SMX^{-1}, SMX^{+1}, or CDX^{-1}). The charged antibiotic species were previously assessed through the experimental data found in Figure 2 (a-c) (Chapter 4), but separate experiments were conducted in order to determine $PO_{4,TOTAL}$ and Cl^- concentrations as well as the pH in both the permeate and feed. Since the pH was assessed, $H_2PO_4^{-1}$, HPO_4^{-2}, and OH^{-1} concentrations could be determined as well. For these experiments, a similar procedure was used in comparison to the antibiotic experiments but with 1.0 mM NaCl added. Phosphate buffer was also added to achieve circumneutral pH conditions, and the pH was either increased or decreased periodically over time with NaOH or HCl, respectively, to reach the target pH. The experimental results for the observed rejection (R_{obs}) for $PO_{4,TOTAL}$ and Cl^- are shown in Figure 2 (a-b) while the experimental results for H^+ and the calculated OH^- values were also determined but are not presented here.

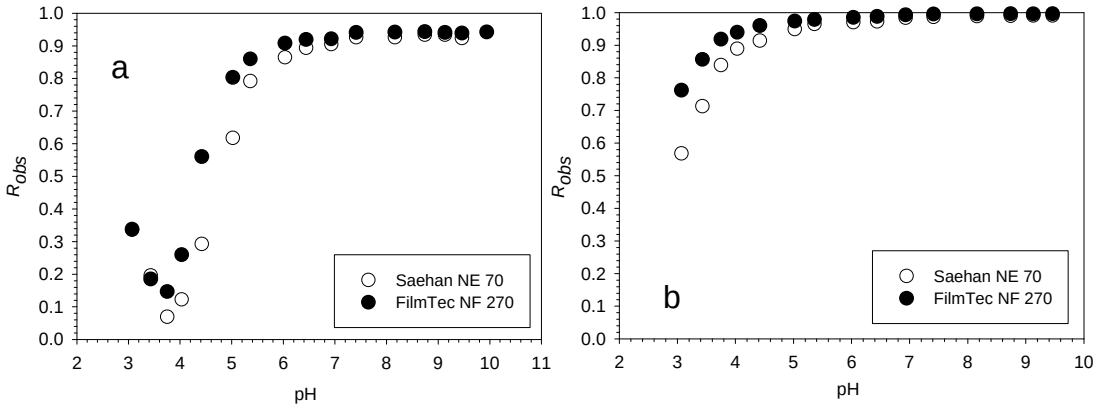

Figure 2. Symbols represent experimentally determined R_{obs} values for (a) Cl^- and (b) $PO_{4,TOTAL}$ from pH 3.1-9.9 using membranes Saehan NE 70 and FilmTec NF 270. Average J_v values are 1.31×10^{-5} (Saehan NE 70) and 1.63×10^{-5} m/s (FilmTec NF 270).

The importance of acquiring this data was two-fold. First, this rejection data could be used in the model as a fitting tool in Phase I to estimate the charge density (X) at each pH condition, as described in Section 4. While theoretically, either Cl^- or $H_2PO_4^{-1}/HPO_4^{-2}$ could be selected, chloride (Cl^-) rejection was used since the rejection of $H_2PO_4^{-1}/HPO_4^{-2}$ was too high (> 91.1%) at pH > 4.4, as seen in Figure 2b. The estimated charge density values for FilmTec NF 270 have been initially determined and are shown in Figure 3.

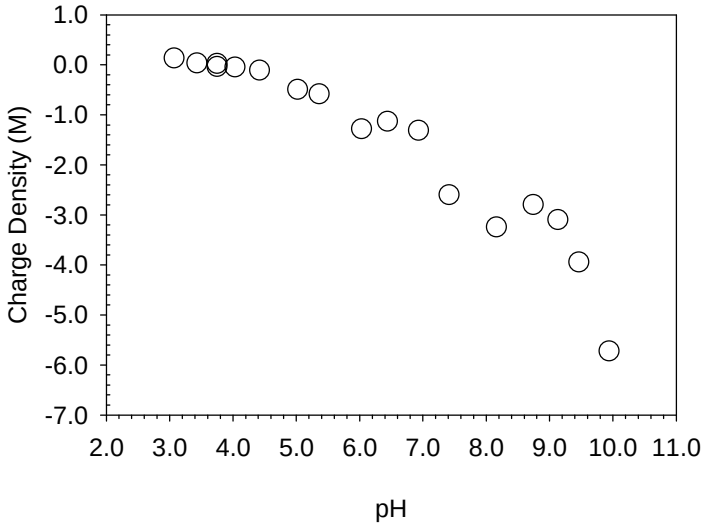

Figure 3. Charge density as a function of pH for FilmTec NF 270 determined by model fitting experimental Cl^- rejection data.

Second, these experimental values were used as input values where the permeate concentrations ($C_{i,p}$) were needed for Phase I while the feed concentrations ($C_{i,f}$) were needed for both Phase I and Phase II. It should be noted that while not determined experimentally, Na^+ concentrations required for the model were calculated by using the electroneutrality equation since all other ion concentrations were known.

Once Phase I was complete, the modeling simulation for Phase II was conducted to obtain $C_{i,p,output}$ and R_{obs} as the output values for all the ions in solution. The model results for TMP^{+1}, TMP^{+2}, SMX^{-1}, SMX^{+1}, or CDX^{-1} rejection specifically were then plotted as a function of pH, as shown in Figure 4.

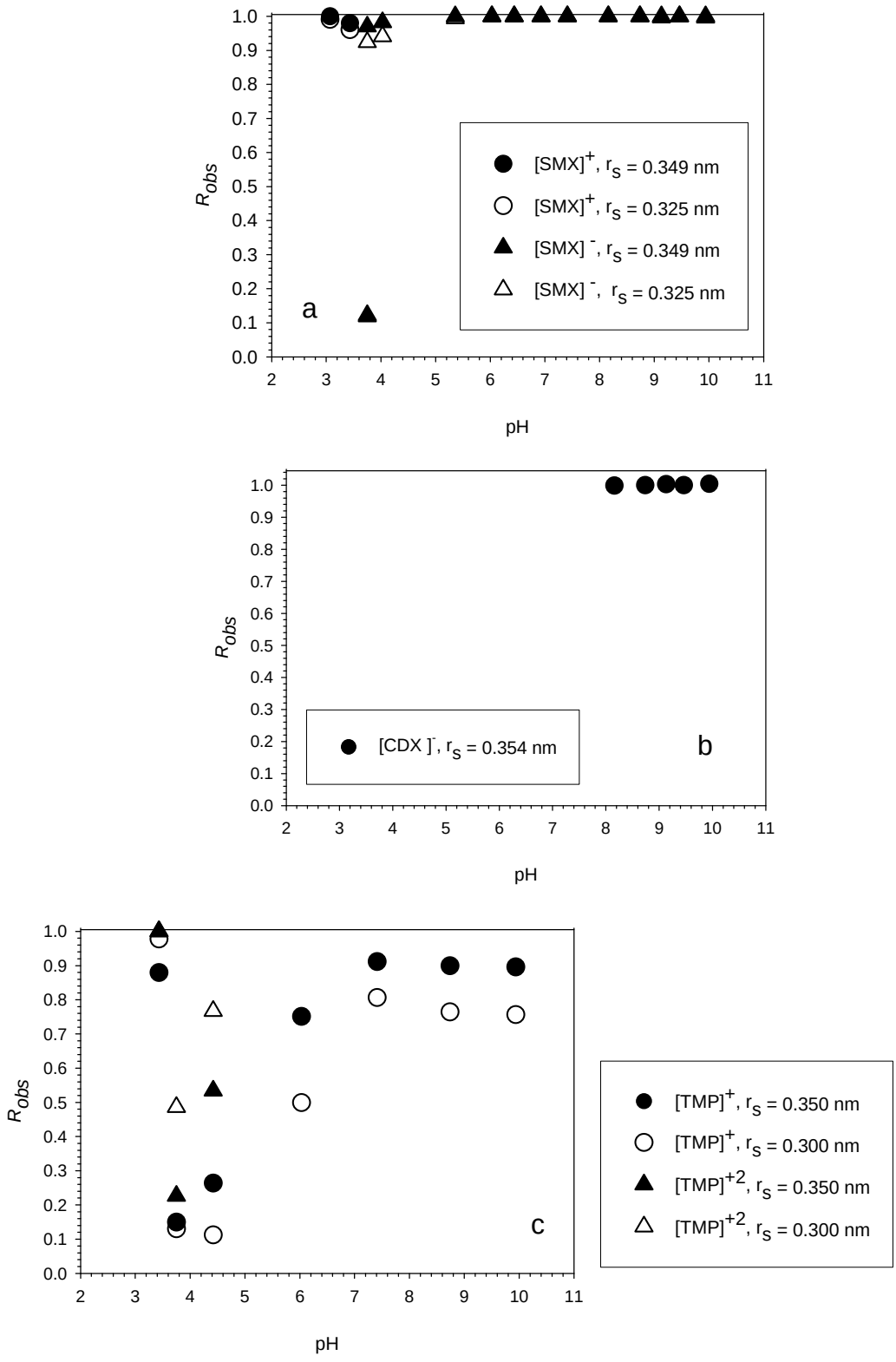

Figure 4. Symbols represent experimentally determined R_{obs} values for (a) SMX^{-1} and SMX^{+1} (b) CDX^{-1} and (c) TMP^{+1} and TMP^{+2}.

5.5.3 Overall Model Rejection for Antibiotics with Varying pH

The overall rejection at each pH condition was then obtained by taking the weighted average of the observed rejection ($R_{obs,i}$) and the mole fraction of each antibiotic species (X_i) for all uncharged and charged species (n total) in the feed, as seen in eq 23:

$$Overall\ R_{obs} = \sum_{i=1}^{n} \left(X_i \cdot R_{obs,i} \right) \qquad (23)$$

Each solute i was only considered in eq 23 if its feed concentration (C_f) was > 1.0% of the total feed concentration (X_i must be > 0.01). Preliminary model results for the overall R_{obs} of TMP, SMX, and CDX using FilmTec NF 270 as a function of pH are shown in Figure 5 and compared to the experimental data from Figure 2 (a-c) (Chapter 4).

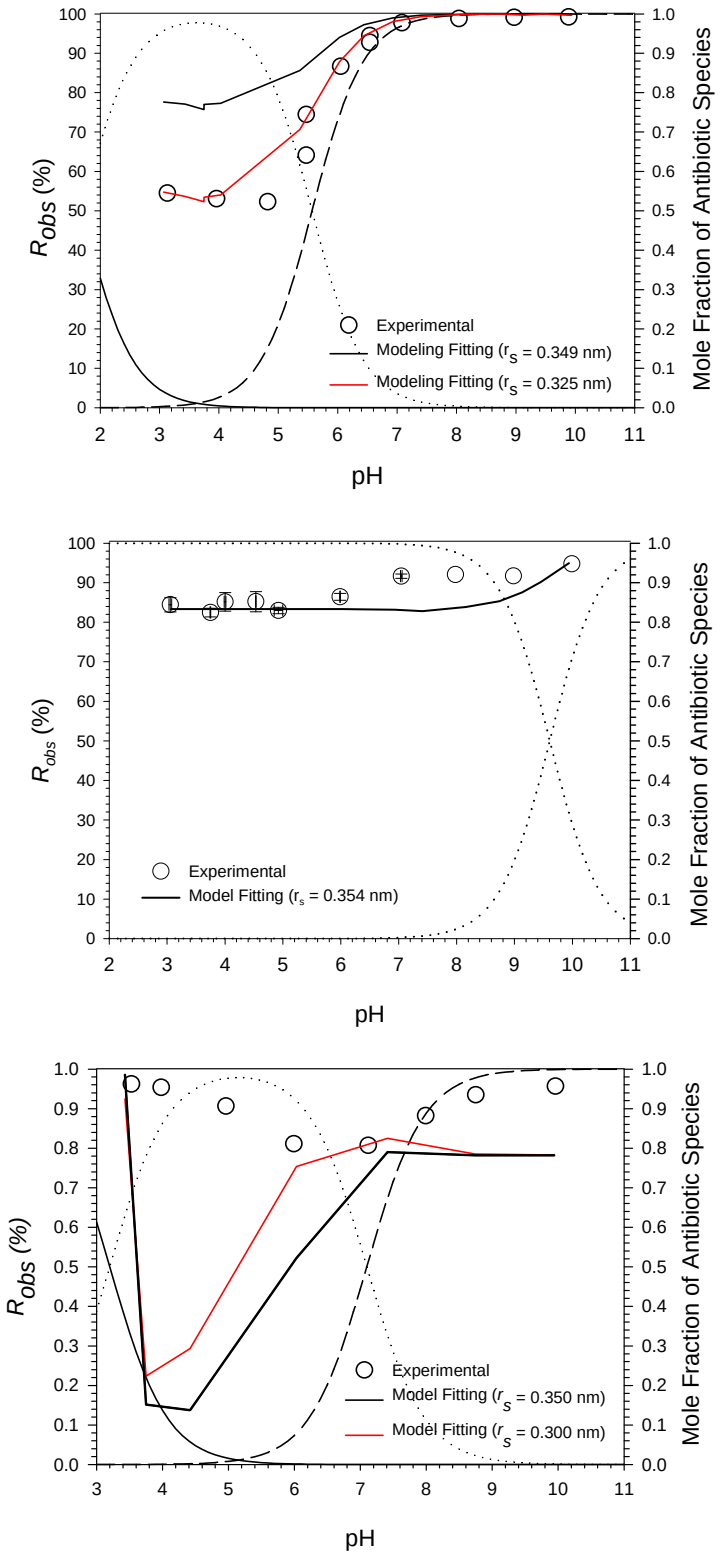

Figure 5. Symbols represent experimentally determined R_{obs} values for (a) SMX, (b) CDX, and (c) TMP using the FilmTec NF 270 membrane. Solid lines represent model results. Dashed and dotted lines represent the mole fractions of each antibiotic species.

For SMX (Figure 5a), the solid black line represents the model results when the input value for SMX solute size (r_s) was initially set at 0.349 nm. Under these conditions, the model correlates well to the data at high pH conditions but significantly deviates from the experimental data at pH < 7.1 where the neutral SMX species begins to dominate. A previous study conducted by Nghiem et *al.* 2005 [28] observed similar results where SMX rejection using the FilmTec NF 270 membrane was 100% at high pH but decreased to 25% at low pH. Nghiem et *al.* hypothesized that at low pH, the low SMX rejection observed was due to molecular polarity, which could orient the molecule to enter the membrane pore along a specific angle, giving it a smaller width, and ultimately decrease the impact of size exclusion on rejection [28]. Therefore, in this study, the solute size (r_s) for SMX was decreased until an optimal value was found at r_s = 0.325 nm where the model best fit the data, as shown by the red solid line in Figure 5a.

CDX (Figure 5b) model results show a similar trend to SMX where the rejection at low pH is dominated by neutral species rejection but increases at higher pH conditions due to electrostatic repulsion effects. The model results match the experimental values at 3.1 < pH $\leq$ 4.9 but underestimates what is observed as pH is increased (4.9 < pH < 10.0). As seen in Figure 4b though, CDX^- rejection is predicted to be ~ 100 %, and thus the model prediction must be underestimated due to the neutral CDX species. It is hypothesized that while CDX is neutral overall, the negative charge on the two *N*-oxide moieties of CDX that is located towards the outside of the molecule may be slightly repelled by the negatively charged membrane, leading to a greater observed rejection at pH > 4.9.

In the case of TMP (Figure 5c), these preliminary results indicate that the model prediction significantly deviates from the experimentally observed rejection in all cases where the solute size (r_s) for TMP was altered from 0.383 (initial estimated value, see Table 2 (Chapter 4)) to 0.300 nm (model curve when r_s = 0.383 nm not shown and model curves for r_s = 0.350 and 0.300 nm are shown in Figure 5c). One factor that may contribute to the discrepancy observed is related to dielectric partitioning which various studies have used in addition to the steric-hindrance model and extended Nernst-Planck equation to assess ion rejection through nanopores [63-65]. Dielectric partitioning is related to change in the dielectric properties (ion solvation/ion flux properties) that occur between the aqueous bulk solution, the membrane material, and the aqueous solution when confined in a nanopore [64]. This phenomenon especially appears to affect divalent cation species (e.g. Mg^{+2} and Ca^{+2}), in which the model values increased significantly to obtain a better fit to the high experimental R_{obs} values observed [64] . For our study, preliminary simulations for both TMP^{+2} and TMP^{+1} indicate that dielectric partitioning significantly alters rejection and possibly aids in acquiring a better model fit to the experimental data, although a complete assessment still needs to be made and will be done so in our future work.

5.6 Symbols

A_k	effective porosity of the membrane [−]
c	solute concentration inside membrane phase [mole/m^3]
C	solute concentration in a liquid phase [mole/m^3]
D	diffusion coefficient of solute [m^2/s]
e	electron charge = 1.6022×10^{-19} [C]
F	Faraday's constant = 96,487 [C/mole]
J_i	ion flux through the membrane [mole/m^2/s]
J_s	neutral solute flux through the membrane [mole/m^2/s]
J_v	solvent flux through the membrane [L/m^2/s or m/s]
k	mass-transfer coefficient [m/s]
$K_{i,d}$	hindrance factor for diffusion for ion i [−]
$K_{i,c}$	hindrance factor for convection for ion i [−]
$K_{s,d}$	hindrance factor for diffusion (for neutral solutes) [−]
$K_{s,c}$	hindrance factor for convection (for neutral solutes) [−]
n	number of ion species in solution [−]
N_A	Avogadro constant = 6.022×10^{23} [molecules/mole]
ΔP	applied pressure [Pa]
r_p	pore radius of membrane [m]
r_s	radius of solute (ions or neutral solutes) [m]
R	gas constant = 8.314 [J/mole/K]
R_{app}	apparent rejection of solute [−]
R_{obs}	observed rejection of solute [−]
T	temperature [K]
V	solvent velocity [m/s]
x	coordinate in the flow direction [m]
Δx	membrane thickness [m]
X	effective membrane charge density [mole/m^3]
z_i	valency of ion i [−]

Greek Letters

$\Delta\Psi_d$	Donnan electrical potential [V]
$\Delta\Psi_m$	electrical potential in the membrane phase [V]
μ	solvent viscosity [kg/m/s]
π	osmotic pressure [Pa]
Φ	steric partitioning term [−]
ϕ	osmotic coefficient [-]
λ	ratio of solute radius/pore radius [−]

Subscripts

f	feed
i	ion
p	permeate
s	neutral solute
wall	membrane surface

5.7 References

1) O. Kedem, A. Katchalsky, Physical Interpretation of Phenomenological Coefficients of Membrane Permeability, Journal of General Physiology 45 (1961) 143-&.

2) K.S. Spiegler, O. Kedem, Thermodynamics of Hyperfiltration (Reverse Osmosis): Criteria for Efficient Membranes, Desalination 1 (1966) 311-326.

3) P. Schirg, F. Widmer, Characterization of Nanofiltration Membranes for the Separation of Aqueous Dye-Salt Solutions, Desalination 89 (1992) 89-107.

4) T.U. Kim, J.E. Drewes, R.S. Summers, G.L. Amy, Solute Transport Model for Trace Organic Neutral and Charged Compounds through Nanofiltration and Reverse Osmosis Membranes, Water Research 41 (2007) 3977-3988.

5) G.T. Ballet, A. Hafiane, M. Dhahbi, Influence of Operating Conditions on the Retention of Phosphate in Water by Nanofiltration, Journal of Membrane Science 290 (2007) 164-172.

6) J. Schaep, C. Vandecasteele, A.W. Mohammad, W.R. Bowen, Analysis of the Salt Retention of Nanofiltration Membranes Using the Donnan-Steric Partitioning Pore Model, Separation Science and Technology 34 (1999) 3009-3030.

7) W.R. Bowen, H. Mukhtar, Characterisation and Prediction of Separation Performance of Nanofiltration Membranes, Journal of Membrane Science 112 (1996) 263-274.

8) L.D. Nghiem, A.I. Schafer, M. Elimelech, Removal of Natural Hormones by Nanofiltration Membranes: Measurement, Modeling, and Mechanisms, Environmental Science & Technology 38 (2004) 1888-1896.

9) J.D. Ferry, Statistical Evaluation of Sieve Constants in Ultrafiltration, Journal of General Physiology 20 (1936) 95-104.

10) J.R. Pappenheimer, E.M. Renkin, L.M. Borrero, Filtration, Diffusion and Molecular Sieving through Peripheral Capillary Membranes a Contribution to the Pore Theory of Capillary Permeability, American Journal of Physiology 167 (1951) 13-46.

11) E.M. Renkin, Filtration, Diffusion, and Molecular Sieving through Porous Cellulose Membranes, J. Gen. Physiol. 38 (1954) 225-243.

12) A.K. Solomon, Characterization of Biological Membranes by Equivalent Pores, Journal of General Physiology 51 (1968) S335-&.

13) L. Dresner, Some Remarks on Integration of Extended Nernst-Planck Equations in Hyperfiltration of Multicomponent Solutions, Desalination 10 (1972) 27-46.

14) W.M. Deen, B. Satvat, J.M. Jamieson, Theoretical-Model for Glomerular-Filtration of Charged Solutes, American Journal of Physiology 238 (1980) F126-F139.

15) X.L. Wang, T. Tsuru, S. Nakao, S. Kimura, Electrolyte Transport through Nanofiltration Membranes by the Space-Charge Model and the Comparison with Teorell-Meyer-Sievers Model, Journal of Membrane Science 103 (1995) 117-133.

16) K.Y. Wang, T.S. Chung, The Characterization of Flat Composite Nanofiltration Membranes and Their Applications in the Separation of Cephalexin, Journal of Membrane Science 247 (2005) 37-50.

17) X.L. Wang, T. Tsuru, M. Togoh, S. Nakao, S. Kimura, Evaluation of Pore Structure and Electrical-Properties of Nanofiltration Membranes, Journal of Chemical Engineering of Japan 28 (1995) 186-192.

18) R. Schlogl, Membrane Permeation in Systems Far from Equilibrium, Berichte Der Bunsen-Gesellschaft Fur Physikalische Chemie 70 (1966) 400-&.

19) D.E. Goldman, Potential, Impedance, and Rectification in Membranes, J. Gen. Physiol. 27 (1943) 37-60.

20) W.R. Bowen, A.W. Mohammad, N. Hilal, Characterisation of Nanofiltration Membranes for Predictive Purposes - Use of Salts, Uncharged Solutes and Atomic Force Microscopy, Journal of Membrane Science 126 (1997) 91-105.

21) X.L. Wang, T. Tsuru, S. Nakao, S. Kimura, The Electrostatic and Steric-Hindrance Model for the Transport of Charged Solutes through Nanofiltration Membranes, Journal of Membrane Science 135 (1997) 19-32.

22) X.S. Miao, F. Bishay, M. Chen, C.D. Metcalfe, Occurrence of Antimicrobials in the Final Effluents of Wastewater Treatment Plants in Canada, Environmental Science & Technology 38 (2004) 3533-3541.

23) R. Hirsch, T. Ternes, K. Haberer, K.L. Kratz, Occurrence of Antibiotics in the Aquatic Environment, Science of the Total Environment 225 (1999) 109-118.

24) D.W. Kolpin, E.T. Furlong, M.T. Meyer, E.M. Thurman, S.D. Zaugg, L.B. Barber, H.T. Buxton, Pharmaceuticals, Hormones, and Other Organic Wastewater Contaminants in Us Streams, 1999-2000: A National Reconnaissance, Environmental Science & Technology 36 (2002) 1202-1211.

25) C.S. McArdell, E. Molnar, M.J.F. Suter, W. Giger, Occurrence and Fate of Macrolide Antibiotics in Wastewater Treatment Plants and in the Glatt Valley Watershed, Switzerland, Environmental Science & Technology 37 (2003) 5479-5486.

26) S. Castiglioni, R. Bagnati, R. Fanelli, F. Pomati, D. Calamari, E. Zuccato, Removal of Pharmaceuticals in Sewage Treatment Plants in Italy, Environmental Science & Technology 40 (2006) 357-363.

27) A.M. Comerton, R.C. Andrews, D.M. Bagley, C.Y. Hao, The Rejection of Endocrine Disrupting and Pharmaceutically Active Compounds by Nf and Ro Membranes as a Function of Compound a Water Matrix Properties, Journal of Membrane Science 313 (2008) 323-335.

28) L.D. Nghiem, A.I. Schafer, M. Elimelech, Pharmaceutical Retention Mechanisms by Nanofiltration Membranes, Environmental Science & Technology 39 (2005) 7698-7705.

29) W.M. Deen, Hindered Transport of Large Molecules in Liquid-Filled Pores, Aiche Journal 33 (1987) 1409-1425.

30) Y. Yoon, R.M. Lueptow, Removal of Organic Contaminants by Ro and Nf Membranes, Journal of Membrane Science 261 (2005) 76-86.

31) S. Lee, R.M. Lueptow, Membrane Rejection of Nitrogen Compounds, Environmental Science & Technology 35 (2001) 3008-3018.

32) W.R. Bowen, A.W. Mohammad, Characterization and Prediction of Nanofiltration Membrane Performance - a General Assessment, Chemical Engineering Research & Design 76 (1998) 885-893.

33) H. Brenner, L.J. Gaydos, Constrained Brownian-Movement of Spherical-Particles in Cylindrical Pores of Comparable Radius - Models of Diffusive and Convective Transport of Solute Molecules in Membranes and Porous-Media, Journal of Colloid and Interface Science 58 (1977) 312-356.

34) J.C. Giddings, E. Kucera, C.P. Russell, M.N. Myers, Statistical Theory for Equilibrium Distribution of Rigid Molecules in Inert Porous Networks . Exclusion Chromatography, Journal of Physical Chemistry 72 (1968) 4397-4408.

35) J.L. Anderson, J.A. Quinn, Restricted Transport in Small Pores - Model for Steric Exclusion and Hindered Particle Motion, Biophysical Journal 14 (1974) 130-150.

36) P. Dechadilok, W.M. Deen, Hindrance Factors for Diffusion and Convection in Pores, Industrial & Engineering Chemistry Research 45 (2006) 6953-6959.

37) I. Sutzkover, D. Hasson, R. Semiat, Simple Technique for Measuring the Concentration Polarization Level in a Reverse Osmosis System, Desalination 131 (2000) 117-127.

38) L.F. Silvester, K.S. Pitzer, Thermodynamics of Electrolytes .8. High-Temperature Properties, Including Enthalpy and Heat-Capacity, with Application to Sodium-Chloride, Journal of Physical Chemistry 81 (1977) 1822-1828.

39) M.S. Isaacson, A.A. Sonin, Sherwood Number and Friction Factor Correlations for Electrodialysis Systems, with Application to Process Optimization, Industrial & Engineering Chemistry Process Design and Development 15 (1976) 313-321.

40) B.X. Mi, C.L. Eaton, J.H. Kim, C.K. Colvin, J.C. Lozier, B.J. Marinas, Removal of Biological and Non-Biological Viral Surrogates by Spiral-Wound Reverse Osmosis Membrane Elements with Intact and Compromised Integrity, Water Research 38 (2004) 3821-3832.

41) V.M.M. Lobo, J.L. Quaresma, Handbook of Electrolyte Solutions: Part B, Elsevier Science, New York, 1989.

42) T.J. Strock, S.A. Sassman, L.S. Lee, Sorption and Related Properties of the Swine Antibiotic Carbadox and Associated N-Oxide Reduced Metabolites, Environmental Science & Technology 39 (2005) 3134-3142.

43) H. Lucida, J.E. Parkin, V.B. Sunderland, Kinetic Study of the Reaction of Sulfamethoxazole and Glucose under Acidic Conditions - I. Effect of Ph and Temperature, International Journal of Pharmaceutics 202 (2000) 47-61.

44) Z.M. Qiang, C. Adams, Potentiometric Determination of Acid Dissociation Constants (Pka) for Human and Veterinary Antibiotics, Water Research 38 (2004) 2874-2890.

45) B. Roth, J.Z. Strelitz, Protonation of 2,4-Diaminopyrimidines .I. Dissociation Constants and Substituent Effects, Journal of Organic Chemistry 34 (1969) 821-836.

46) J.R. Welty, C.E. Wicks, R.E. Wilson, G.L. Rorrer, Fundamentals of Momentum, Heat, and Mass Transfer, fourth ed., John Wiley & Sons, New York, 2001.

47) P. Atkins, J. de Paula, Physical Chemistry, seventh ed., Oxford University Press, New York, 2002.

48) A.D. Pethybridge, J.D.R. Talbot, W.A. House, Precise Conductance Measurements on Dilute Aqueous Solutions of Sodium and Potassium Hydrogenphosphate and Dihydrogenphosphate, Journal of Solution Chemistry 35 (2006) 381-393.

49) P. Xu, J.E. Drewes, T.U. Kim, C. Bellona, G. Amy, Effect of Membrane Fouling on Transport of Organic Contaminants in Nf/Ro Membrane Applications, Journal of Membrane Science 279 (2006) 165-175.

50) E.N. Tsurko, R. Neueder, J. Barthel, A. Apelblat, Conductivity of Phosphoric Acid, Sodium, Potassium, and Ammonium Phosphates in Dilute Aqueous Solutions from 278.15 K to 308.15 K, Journal of Solution Chemistry 28 (1999) 973-999.

51) H.S. Harned, B.B. Owen, The Physical Chemistry of Electrolytic Solutions, third ed., Reinhold Publishing, New York, 1958.

52) W.R. Bowen, J.S. Welfoot, Modelling of Membrane Nanofiltration - Pore Size Distribution Effects, Chemical Engineering Science 57 (2002) 1393-1407.

53) J.A. Otero, O. Mazarrasa, J. Villasante, V. Silva, P. Prádanos, J.I. Calvo, A. Hernández, Three Independent Ways to Obtain Information on Pore Size Distributions of Nanofiltration Membranes, Journal of Membrane Science 309 (2008) 17-27.

54) S. Chellam, J.S. Taylor, Simplified Analysis of Contaminant Rejection During Ground- and Surface Water Nanofiltration under the Information Collection Rule, Water Research 35 (2001) 2460-2474.

55) Y. Zhao, J.S. Taylor, S. Chellam, Predicting Ro/Nf Water Quality by Modified Solution Diffusion Model and Artificial Neural Networks, Journal of Membrane Science 263 (2005) 38-46.

56) B. Van der Bruggen, C. Vandecasteele, Modelling of the Retention of Uncharged Molecules with Nanofiltration, Water Research 36 (2002) 1360-1368.

57) Y. Kiso, T. Kon, T. Kitao, K. Nishimura, Rejection Properties of Alkyl Phthalates with Nanofiltration Membranes, Journal of Membrane Science 182 (2001) 205-214.

58) Y. Kiso, T. Kitao, K. Jinno, M. Miyagi, The Effects of Molecular Width on Permeation of Organic Solute through Cellulose-Acetate Reverse-Osmosis Membranes, Journal of Membrane Science 74 (1992) 95-103.

59) Y. Kiso, Y. Sugiura, T. Kitao, K. Nishimura, Effects of Hydrophobicity and Molecular Size on Rejection of Aromatic Pesticides with Nanofiltration Membranes, Journal of Membrane Science 192 (2001) 1-10.

60) R.R. Sharma, S. Chellam, Temperature Effects on the Morphology of Porous Thin Film Composite Manofiltration Membranes, Environmental Science & Technology 39 (2005) 5022-5030.

61) K. Kosutic, B. Kunst, Removal of Organics from Aqueous Solutions by Commercial Ro and Nf Membranes of Characterized Porosities, Desalination 142 (2002) 47-56.

62) B. Van der Bruggen, J. Schaep, D. Wilms, C. Vandecasteele, Influence of Molecular Size, Polarity and Charge on the Retention of Organic Molecules by Nanofiltration, Journal of Membrane Science 156 (1999) 29-41.

63) W.R. Bowen, J.S. Welfoot, Modelling the Performance of Membrane Nanofiltration - Critical Assessment and Model Development, Chemical Engineering Science 57 (2002) 1121-1137.

64) S. Bandini, D. Vezzani, Nanofiltration Modeling: The Role of Dielectric Exclusion in Membrane Characterization, Chemical Engineering Science 58 (2003) 3303-3326.

65) S. Deon, P. Dutournie, P. Bourseau, Modeling Nanofiltration with Nernst-Planck Approach and Polarization Layer, Aiche Journal 53 (2007) 1952-1969.

5.8 Appendices

Appendix A.

In the steric-hindrance model, eq 1 is integrated over the specified boundary conditions to obtain eq 4. The integration method is described below:

Boundary conditions used over the membrane pore (eq 3):

At $x = 0$ $\quad c = c_{x=0}$ and $c_{x=0} = \Phi * C_{wall}$
At $x=\Delta x$ $\quad c = c_{x=\Delta x}$ and $c_{x=\Delta x} = \Phi * C_p$

Integration method:

$$J_{s,pore} = -K_{s,d} D_s \frac{dc_s}{dx} + K_{s,c} V c_s \quad \text{(eq 1)}$$

after rearrangement:

$$\frac{dc_s}{dx} = -\frac{J_{s,pore}}{K_{s,d} D_s} + \frac{K_{s,c} V c_s}{K_{s,d} D_s} \quad J_{s,pore} = -K_{s,d} D_s \frac{dc_s}{dx} + K_{s,c} V c_s$$

now set: $\alpha = -\frac{J_{s,pore}}{K_{s,d} D_s}$ and $\beta = \frac{K_{s,c} V}{K_{s,d} D_s}$

after substitution:

$$\frac{dc_s}{dx} = \alpha + \beta \cdot c_s$$

and integration by u-substitution:

$$\frac{dc_s}{\alpha + \beta \cdot c_s} = dx \qquad \text{where} \qquad u = \alpha + \beta \cdot c_s$$

$$du = \beta \cdot dc_s$$

then

$$\frac{1}{\beta} \int_{u_0 = \alpha + \beta \cdot c_{x=0}}^{u_{\Delta x} = \alpha + \beta \cdot c_{x=\Delta x}} \frac{du}{u} = \int_0^{\Delta x} dx$$

when integrated:

$$\ln\left[u\right]\Big|_{u_0=\alpha+\beta\cdot c_{x=0}}^{u_{\Delta x}=\alpha+\beta\cdot c_{x=\Delta x}} = \Delta x\cdot\beta$$

and

$$\ln\left[\frac{\alpha+\beta\cdot c_{x=\Delta x}}{\alpha+\beta\cdot c_{x=0}}\right] = \Delta x\cdot\beta \qquad \text{where} \quad Pe = \Delta x\cdot\beta$$

the negative of both sides are taken:

$$-\ln\left[\frac{\alpha+\beta\cdot c_{x=\Delta x}}{\alpha+\beta\cdot c_{x=0}}\right] = -Pe$$

and the exponent of both sides are taken:

$$\left[\frac{\alpha+\beta\cdot c_{x=\Delta x}}{\alpha+\beta\cdot c_{x=0}}\right]^{-1} = \exp\,(-Pe)$$

Final rearrangement and re-substitution of variables:

$$\left[\frac{-J_{s,pore}+K_c\cdot V\cdot c_{x=0}}{-J_{s,pore}+K_c\cdot V\cdot c_{x=\Delta x}}\right] = \exp\,(-Pe)$$

to obtain:

$$J_{s,pore} = \frac{c_{x=0}\cdot K_c\cdot V\cdot\left(1-\frac{c_{x=\Delta x}}{c_{x=0}}\exp\,(-Pe)\right)}{1-\exp\,(-Pe)}$$

insert $c_{x=0} = \Phi^* C_{wall}$ and $c_{x=\Delta x} = \Phi^* C_p$, and finally eq 4 is formed :

$$J_{s,pore} = \frac{\Phi\cdot C_{wall}\cdot K_c\cdot V\cdot\left(1-\frac{C_P}{C_{wall}}\exp\,(-Pe)\right)}{1-\exp\,(-Pe)} \qquad \text{(eq 4)}$$

Appendix B

```
% All Ions are included here

% This is used to fit the ions including the antibiotic species to the
% experimental results by changing the Cp_input value to where both the
% Cp_input and Cp_predicted converge

function CP_predicted

global lamda z FoverRT Kic Kid Jv chargedensity phi
global Cf_Na Cf_H2PO4 Cf_Cl Cf_Ant Cf_H Cf_OH Cf_HPO4
global D_Na D_H2PO4 D_Cl D_Ant D_H D_OH D_HPO4
global Cwall_Na Cwall_H2PO4 Cwall_Cl Cwall_Ant Cwall_H Cwall_OH
Cwall_HPO4
global ci_thk_Na ci_thk_H2PO4 ci_thk_Cl ci_thk_Ant ci_thk_H ci_thk_OH
ci_thk_HPO4
global Cpinput_Na Cpinput_H2PO4 Cpinput_Cl Cpinput_Ant Cpinput_H
Cpinput_OH Cpinput_HPO4

double          chargedensity;
double          temp;
double          F;
double          R;
double          FoverRT;
double          deltaPpsi;
double          deltaP;
double          viscosity;

double          z;
double          Jv;
double          rpore;
double          rion;
double          lamda;
double          phi;
double          dx_porosity;

double          Cf_Na;
double          Cf_H2PO4;
double          Cf_Cl;
double          Cf_Ant;
double          Cf_H;
double          Cf_OH;
double          Cf_HPO4;

double          Cpinput_Na;
double          Cpinput_H2PO4;
double          Cpinput_Cl;
double          Cpinput_Ant;
double          Cpinput_H;
double          Cpinput_OH;
double          Cpinput_HPO4;

double          rejinput_Na;
double          rejinput_H2PO4;
```

```
double          rejinput_Cl;
double          rejinput_Ant;
double          rejinput_H;
double          rejinput_OH;
double          rejinput_HPO4;

double          Cpoutput_Na;
double          Cpoutput_H2PO4;
double          Cpoutput_Cl;
double          Cpoutput_Ant;
double          Cpoutput_H;
double          Cpoutput_OH;
double          Cpoutput_HPO4;

double          rejoutput_Na;
double          rejoutput_H2PO4;
double          rejoutput_Cl;
double          rejoutput_Ant;
double          rejoutput_H;
double          rejoutput_OH;
double          rejoutput_HPO4;

double          k_Na;
double          k_H2PO4;
double          k_Cl;
double          k_Ant;
double          k_H;
double          k_OH;
double          k_HPO4;

double          Cwall_Na;
double          Cwall_H2PO4;
double          Cwall_Cl;
double          Cwall_Ant;
double          Cwall_H;
double          Cwall_OH;
double          Cwall_HPO4;

double          H;
double          W;
double          Kic;
double          Kid;

double          d_x0;
double          d_xthk;

double          ci_x0_Na;
double          ci_x0_H2PO4;
double          ci_x0_Cl;
double          ci_x0_Ant;
double          ci_x0_H;
double          ci_x0_OH;
double          ci_x0_HPO4;

double          D_Na;
```

```
double          D_H2PO4;
double          D_Cl;
double          D_Ant;
double          D_H;
double          D_OH;
double          D_HPO4;

double          x;
double          c;

double          cix_thk;
double          ci_thk_Na;
double          ci_thk_H2PO4;
double          ci_thk_Cl;
double          ci_thk_Ant;
double          ci_thk_H;
double          ci_thk_OH;
double          ci_thk_HPO4;

% Constants

temp =          293; % in Kelvin
F =             96487; %Faraday's constant in C/mole
R =             8.314; %Ideal Gas Constant (J/mole/K)
FoverRT =       F/R/temp; % In V-1 units
deltaPpsi =     70; %Units are in psi
deltaP =        deltaPpsi*6.894757*1000; %Units are in N/m^2 or
kg/s^2/m
viscosity =     1e-3; % At 20 C (kg/m/s)

z=              [1,-1,-1,1,1,-1,-2]; %Unitless
Jv =            1.620e-05; % Units in m/s
rpore=          0.42; % Units are in nm

r_Na =          0.206; % in nm
r_H2PO4 =       0.324;
r_Cl =          0.134;
r_Ant =         0.325;
r_H =           0.028;
r_OH =          0.051;
r_HPO4 =        0.363;

rion =          [r_Na, r_H2PO4, r_Cl, r_Ant, r_H, r_OH, r_HPO4];
lamda =         rion./rpore; % Unitless
phi =           (1-lamda).^2;

dx_porosity =   (rpore/10^9)^2*deltaP/(Jv*8*viscosity);

k_Na =          1e-5; % Units are in m/s
k_H2PO4 =       7.396e-6;
k_Cl =          1.332e-5;
k_Ant =         8.00e-06;
k_H =           3.756e-5;
k_OH =          2.524e-5;
k_HPO4 =        6.863e-6;
```

```
% Charge density needs to be in mole/L

chargedensity = 0.037811516; % in M

% Feed concentration

Cf_H2PO4 =      8.5654e-04; % in M
Cf_Cl =         1.755e-03;
Cf_Ant =        3.50297e-08;
Cf_H =          3.715e-04;
Cf_OH =         (10^-14)/Cf_H;
Cf_HPO4 =       1.421e-07;

Cf_Na = -z(2)*Cf_H2PO4-z(3)*Cf_Cl-z(4)*Cf_Ant-z(5)*Cf_H-z(6)*Cf_OH-
z(7)*Cf_HPO4;

% Permeate Concentration that is the input value

Cpinput_H2PO4 =         Cf_H2PO4*0.001;
Cpinput_Cl =            Cf_Cl*0.001;
Cpinput_Ant =           Cf_Ant*0.001;
Cpinput_H =             Cf_H*0.001;
Cpinput_OH =            Cf_OH*0.001;
Cpinput_HPO4 =          Cf_HPO4*0.00001;

Cpinput_Na =            -z(2)*Cpinput_H2PO4-z(3)*Cpinput_Cl-
z(4)*Cpinput_Ant-z(5)*Cpinput_H-z(6)*Cpinput_OH-z(7)*Cpinput_HPO4;

% Rejection Input Values

rejinput_Na =           (Cf_Na-Cpinput_Na)/Cf_Na;
rejinput_H2PO4 =        (Cf_H2PO4-Cpinput_H2PO4)/Cf_H2PO4;
rejinput_Cl =           (Cf_Cl-Cpinput_Cl)/Cf_Cl;
rejinput_Ant =          (Cf_Ant-Cpinput_Ant)/Cf_Ant;
rejinput_H =            (Cf_H-Cpinput_H)/Cf_H;
rejinput_OH =           (Cf_OH-Cpinput_OH)/Cf_OH;
rejinput_HPO4 =         (Cf_HPO4-Cpinput_HPO4)/Cf_HPO4;

% Initial Cpoutput values to begin the loop

Cpoutput_H2PO4 =         Cf_H2PO4*0.99; % in M
Cpoutput_Cl =            Cf_Cl*0.99;
Cpoutput_Ant =           Cf_Ant*0.99;
Cpoutput_H =             Cf_H*0.99;
Cpoutput_OH =            Cf_OH*0.99;
Cpoutput_Na =            Cf_Na*0.99;
Cpoutput_HPO4 =          Cf_HPO4*0.99;

% Determine Output Rejection for each ion species

rejoutput_Na =           (Cf_Na-Cpoutput_Na)/Cf_Na;
rejoutput_H2PO4 =        (Cf_H2PO4-Cpoutput_H2PO4)/Cf_H2PO4;
rejoutput_Cl =           (Cf_Cl-Cpoutput_Cl)/Cf_Cl;
```

```
rejoutput_Ant =          (Cf_Ant-Cpoutput_Ant)/Cf_Ant;
rejoutput_H =            (Cf_H-Cpoutput_H)/Cf_H;
rejoutput_OH =           (Cf_OH-Cpoutput_OH)/Cf_OH;
rejoutput_HPO4 =         (Cf_HPO4-Cpoutput_HPO4)/Cf_HPO4;
% Step sizes to change Cpinput to obtain convergence

step_size_H2PO4_1 =     1e-4;
step_size_HPO4_1 =      1e-4;
step_size_Cl_1 =        1e-4;
step_size_Ant_1 =       1e-4;
step_size_H_1 =         1e-4;
step_size_OH_1 =        1e-4;

% Beginning of loop

i = 1;
j = 1;

iteration = true;

while iteration

Cpinput_HPO4_1 =         Cpinput_HPO4;
Cpinput_H2PO4_1 =        Cpinput_H2PO4;
Cpinput_H_1 =            Cpinput_H;
Cpinput_OH_1 =           Cpinput_OH;
Cpinput_Ant_1 =          Cpinput_Ant;
Cpinput_Cl_1 =           Cpinput_Cl;
Cpinput_Na_1 =           Cpinput_Na;

rejinput_HPO4_1 =        rejinput_HPO4
rejinput_H2PO4_1 =       rejinput_H2PO4
rejinput_H_1 =           rejinput_H
rejinput_OH_1 =          rejinput_OH
rejinput_Cl_1 =          rejinput_Cl
rejinput_Ant_1 =         rejinput_Ant
rejinput_Na_1 =          rejinput_Na

Cpoutput_HPO4_1 =        Cpoutput_HPO4;
Cpoutput_H2PO4_1 =       Cpoutput_H2PO4;
Cpoutput_H_1 =           Cpoutput_H;
Cpoutput_OH_1 =          Cpoutput_OH;
Cpoutput_Cl_1 =          Cpoutput_Cl;
Cpoutput_Ant_1 =         Cpoutput_Ant;
Cpoutput_Na_1 =          Cpoutput_Na;

rejoutput_HPO4_1 =        rejoutput_HPO4;
rejoutput_H2PO4_1 =       rejoutput_H2PO4
rejoutput_H_1 =           rejoutput_H;
rejoutput_OH_1 =          rejoutput_OH;
rejoutput_Cl_1 =          rejoutput_Cl;
rejoutput_Ant_1 =         rejoutput_Ant;
rejoutput_Na_1 =          rejoutput_Na;

% Convergence criteria
```

```
% For H2PO4

if abs(rejinput_H2PO4 - rejoutput_H2PO4)>= 1.0
    step_H2PO4 = step_size_H2PO4_1;
elseif (abs(rejinput_H2PO4 - rejoutput_H2PO4)>= 0.5) &&
(abs(rejinput_H2PO4 - rejoutput_H2PO4)< 1.0)
    step_size_H2PO4_2 = step_size_H2PO4_1*0.99;
    step_H2PO4 = step_size_H2PO4_2;
elseif (abs(rejinput_H2PO4 - rejoutput_H2PO4)>= 0.1) &&
(abs(rejinput_H2PO4 - rejoutput_H2PO4)< 0.5)
    step_size_H2PO4_3 = step_size_H2PO4_1*0.98;
    step_H2PO4 = step_size_H2PO4_3;
elseif (abs(rejinput_H2PO4 - rejoutput_H2PO4)>= 0.02) &&
(abs(rejinput_H2PO4 - rejoutput_H2PO4)< 0.1)
    step_size_H2PO4_4 = step_size_H2PO4_1*0.97;
    step_H2PO4 = step_size_H2PO4_4;
elseif (abs(rejinput_H2PO4 - rejoutput_H2PO4)>= 0.005) &&
(abs(rejinput_H2PO4 - rejoutput_H2PO4)< 0.02)
    step_size_H2PO4_5 = step_size_H2PO4_1*0.96;
    step_H2PO4 = step_size_H2PO4_5;
else
    step_H2PO4 = 0;
end

if  rejinput_H2PO4 > rejoutput_H2PO4
    Cpinput_H2PO4 = Cpinput_H2PO4+ abs(Cpinput_H2PO4-
Cpoutput_H2PO4)*step_H2PO4;
else
    Cpinput_H2PO4 = Cpinput_H2PO4- abs(Cpinput_H2PO4-
Cpoutput_H2PO4)*step_H2PO4;
end

% For HPO4

if abs(rejinput_HPO4 - rejoutput_HPO4)>= 1.0
    step_HPO4 = step_size_HPO4_1;
elseif (abs(rejinput_HPO4 - rejoutput_HPO4)>= 0.5) &&
(abs(rejinput_HPO4 - rejoutput_HPO4)< 1.0)
    step_size_HPO4_2 = step_size_HPO4_1*0.99;
    step_HPO4 = step_size_HPO4_2;
elseif (abs(rejinput_HPO4 - rejoutput_HPO4)>= 0.1) &&
(abs(rejinput_HPO4 - rejoutput_HPO4)< 0.5)
    step_size_HPO4_3 = step_size_HPO4_1*0.98;
    step_HPO4 = step_size_HPO4_3;
elseif (abs(rejinput_HPO4 - rejoutput_HPO4)>= 0.02) &&
(abs(rejinput_HPO4 - rejoutput_HPO4)< 0.1)
    step_size_HPO4_4 = step_size_HPO4_1*0.97;
    step_HPO4 = step_size_HPO4_4;
elseif (abs(rejinput_HPO4 - rejoutput_HPO4)>= 0.005) &&
(abs(rejinput_HPO4 - rejoutput_HPO4)< 0.02)
    step_size_HPO4_5 = step_size_HPO4_1*0.96;
    step_HPO4 = step_size_HPO4_5;
else
    step_HPO4 = 0;
end
```

```
if  rejinput_HPO4 > rejoutput_HPO4
    Cpinput_HPO4 = Cpinput_HPO4+ abs(Cpinput_HPO4-
Cpoutput_HPO4)*step_HPO4;
else
    Cpinput_HPO4 = Cpinput_HPO4- abs(Cpinput_HPO4-
Cpoutput_HPO4)*step_HPO4;
end

% For H

if abs(rejinput_H - rejoutput_H)>= 1.0
    step_H = step_size_H_1;
elseif (abs(rejinput_H - rejoutput_H)>= 0.5) && (abs(rejinput_H -
rejoutput_H)< 1.0)
    step_size_H_2 = step_size_H_1*0.99;
    step_H = step_size_H_2;
elseif (abs(rejinput_H - rejoutput_H)>= 0.1) && (abs(rejinput_H -
rejoutput_H)< 0.5)
    step_size_H_3 = step_size_H_1*0.98;
    step_H = step_size_H_3;
elseif (abs(rejinput_H - rejoutput_H)>= 0.02) && (abs(rejinput_H -
rejoutput_H)< 0.1)
    step_size_H_4 = step_size_H_1*0.97;
    step_H = step_size_H_4;
elseif (abs(rejinput_H - rejoutput_H)>= 0.005) && (abs(rejinput_H -
rejoutput_H)< 0.02)
    step_size_H_5 = step_size_H_1*0.96;
    step_H = step_size_H_5;
else
    step_H = 0;
end

if  rejinput_H > rejoutput_H
    Cpinput_H = Cpinput_H + abs(Cpinput_H -Cpoutput_H)*step_H;
else
    Cpinput_H = Cpinput_H - abs(Cpinput_H-Cpoutput_H)*step_H;
end

% For OH

if abs(rejinput_OH - rejoutput_OH)>= 1.0
    step_OH = step_size_OH_1;
elseif (abs(rejinput_OH - rejoutput_OH)>= 0.5) && (abs(rejinput_OH -
rejoutput_OH)< 1.0)
    step_size_OH_2 = step_size_OH_1*0.99;
    step_OH = step_size_OH_2;
elseif (abs(rejinput_OH - rejoutput_OH)>= 0.1) && (abs(rejinput_OH -
rejoutput_OH)< 0.5)
    step_size_OH_3 = step_size_OH_1*0.98;
    step_OH = step_size_OH_3;
elseif (abs(rejinput_OH - rejoutput_OH)>= 0.02) && (abs(rejinput_OH -
rejoutput_OH)< 0.1)
    step_size_OH_4 = step_size_OH_1*0.97;
    step_OH = step_size_OH_4;
```

```
elseif (abs(rejinput_OH - rejoutput_OH)>= 0.005) && (abs(rejinput_OH -
rejoutput_OH)< 0.02)
    step_size_OH_5 = step_size_OH_1*0.96;
    step_OH = step_size_OH_5;
else
    step_OH = 0;
end

if  rejinput_OH > rejoutput_OH
    Cpinput_OH = Cpinput_OH + abs(Cpinput_OH -Cpoutput_OH)*step_OH;
else
    Cpinput_OH = Cpinput_OH - abs(Cpinput_OH-Cpoutput_OH)*step_OH;
end

% For Cl

if abs(rejinput_Cl - rejoutput_Cl)>= 1.0
    step_Cl = step_size_Cl_1;
elseif (abs(rejinput_Cl - rejoutput_Cl)>= 0.5) && (abs(rejinput_Cl -
rejoutput_Cl)< 1.0)
    step_size_Cl_2 = step_size_Cl_1*0.99;
    step_Cl = step_size_Cl_2;
elseif (abs(rejinput_Cl - rejoutput_Cl)>= 0.1) && (abs(rejinput_Cl -
rejoutput_Cl)< 0.5)
    step_size_Cl_3 = step_size_Cl_1*0.98;
    step_Cl = step_size_Cl_3;
elseif (abs(rejinput_Cl - rejoutput_Cl)>= 0.02) && (abs(rejinput_Cl -
rejoutput_Cl)< 0.1)
    step_size_Cl_4 = step_size_Cl_1*0.97;
    step_Cl = step_size_Cl_4;
elseif (abs(rejinput_Cl - rejoutput_Cl)>= 0.005) && (abs(rejinput_Cl -
rejoutput_Cl)< 0.02)
    step_size_Cl_5 = step_size_Cl_1*0.96;
    step_Cl = step_size_Cl_5;
else
    step_Cl = 0;
end

if  rejinput_Cl > rejoutput_Cl
    Cpinput_Cl = Cpinput_Cl + abs(Cpinput_Cl -Cpoutput_Cl)*step_Cl;
else
    Cpinput_Cl = Cpinput_Cl - abs(Cpinput_Cl-Cpoutput_Cl)*step_Cl;
end

% For Antibiotic

if abs(rejinput_Ant - rejoutput_Ant)>= 1.0
    step_Ant = step_size_Ant_1;
elseif (abs(rejinput_Ant - rejoutput_Ant)>= 0.5) && (abs(rejinput_Ant -
rejoutput_Ant)< 1.0)
    step_size_Ant_2 = step_size_Ant_1*0.99;
    step_Ant = step_size_Ant_2;
elseif (abs(rejinput_Ant - rejoutput_Ant)>= 0.1) && (abs(rejinput_Ant -
rejoutput_Ant)< 0.5)
    step_size_Ant_3 = step_size_Ant_1*0.98;
    step_Ant = step_size_Ant_3;
```

```
elseif (abs(rejinput_Ant - rejoutput_Ant)>= 0.02) && (abs(rejinput_Ant
- rejoutput_Ant)< 0.1)
    step_size_Ant_4 = step_size_Ant_1*0.97;
    step_Ant = step_size_Ant_4;
elseif (abs(rejinput_Ant - rejoutput_Ant)>= 0.005) && (abs(rejinput_Ant
- rejoutput_Ant)< 0.02)
    step_size_Ant_5 = step_size_Ant_1*0.96;
    step_Ant = step_size_Ant_5;
else
    step_Ant = 0;
end

if  rejinput_Ant > rejoutput_Ant
    Cpinput_Ant = Cpinput_Ant + abs(Cpinput_Ant -Cpoutput_Ant)*step_Ant;
else
    Cpinput_Ant = Cpinput_Ant - abs(Cpinput_Ant-Cpoutput_Ant)*step_Ant;
end

% For Na

Cpinput_Na = -z(2)*Cpinput_H2PO4-z(3)*Cpinput_Cl-z(4)*Cpinput_Ant-
z(5)*Cpinput_H-z(6)*Cpinput_OH-z(7)*Cpinput_HPO4;

Cpinput_H2PO4_2 =       Cpinput_H2PO4;
Cpinput_HPO4_2 =        Cpinput_HPO4;
Cpinput_H_2 =           Cpinput_H;
Cpinput_OH_2 =          Cpinput_OH;
Cpinput_Cl_2 =          Cpinput_Cl;
Cpinput_Ant_2 =         Cpinput_Ant;
Cpinput_Na_2 =          Cpinput_Na;

% New rejection input

rejinput_Na =           (Cf_Na-Cpinput_Na)/Cf_Na;
rejinput_H2PO4 =        (Cf_H2PO4-Cpinput_H2PO4)/Cf_H2PO4;
rejinput_Cl =           (Cf_Cl-Cpinput_Cl)/Cf_Cl;
rejinput_Ant =          (Cf_Ant-Cpinput_Ant)/Cf_Ant;
rejinput_H =            (Cf_H-Cpinput_H)/Cf_H;
rejinput_OH =           (Cf_OH-Cpinput_OH)/Cf_OH;
rejinput_HPO4 =         (Cf_HPO4-Cpinput_HPO4)/Cf_HPO4;

rejinput_HPO4_2 =       rejinput_HPO4
rejinput_H2PO4_2 =      rejinput_H2PO4
rejinput_H_2 =          rejinput_H
rejinput_OH_2 =         rejinput_OH
rejinput_Cl_2 =         rejinput_Cl
rejinput_Ant_2 =        rejinput_Ant
rejinput_Na_2 =         rejinput_Na

% Wall concentration

if Cpinput_H2PO4 < Cf_H2PO4
    Cwall_H2PO4 =   exp(Jv/k_H2PO4)*(Cf_H2PO4-
Cpinput_H2PO4)+Cpinput_H2PO4;
else
```

```
    Cwall_H2PO4 =   Cf_H2PO4;
end

if Cpinput_Cl < Cf_Cl
    Cwall_Cl =   exp(Jv/k_Cl)*(Cf_Cl-Cpinput_Cl)+Cpinput_Cl;
else
    Cwall_Cl =   Cf_Cl;
end

if Cpinput_Ant < Cf_Ant
    Cwall_Ant =  exp(Jv/k_Ant)*(Cf_Ant-Cpinput_Ant)+Cpinput_Ant;
else
    Cwall_Ant = Cf_Ant;
end

if Cpinput_H < Cf_H
    Cwall_H =  exp(Jv/k_H)*(Cf_H-Cpinput_H)+Cpinput_H;
else
    Cwall_H = Cf_H;
end

if Cpinput_OH < Cf_OH
    Cwall_OH =  exp(Jv/k_OH)*(Cf_OH-Cpinput_OH)+Cpinput_OH;
else
    Cwall_OH = Cf_OH;
end

if Cpinput_HPO4 < Cf_HPO4
    Cwall_HPO4 =  exp(Jv/k_HPO4)*(Cf_HPO4-Cpinput_HPO4)+Cpinput_HPO4;
else
    Cwall_HPO4 = Cf_HPO4;
end

Cwall_Na = -z(2)*Cwall_H2PO4-z(3)*Cwall_Cl-z(4)*Cwall_Ant-z(5)*Cwall_H-
z(6)*Cwall_OH-z(7)*Cwall_HPO4;

% Determination of hinderance coefficients

H =    1+9/8*lamda.*log(lamda)-
1.56034*lamda+0.528155*lamda.^2+1.91521*lamda.^3-
2.81903*lamda.^4+0.270788*lamda.^5+1.10115*lamda.^6-0.435933*lamda.^7;
W =    (1-lamda).^2.*(1+3.867*lamda-1.907*lamda.^2-
0.834*lamda.^3)./(1+1.867*lamda-0.741*lamda.^2);

Kid =    H./phi;
Kic =    W./phi;

% Solve for d_x0 (in J/C or Volts)

options=optimset('TolFun',1e-18,'TolX',1e-18,'DiffMinChange',1e-18);
%Using Large Scale Algorithm
[d_x0,resnorm] = lsqnonlin(@myfun,0,[],[],options);

ci_x0_Na =      Cwall_Na*phi(1)*exp(-z(1)*FoverRT*d_x0);
```

```
ci_x0_H2PO4 =   Cwall_H2PO4*phi(2)*exp(-z(2)*FoverRT*d_x0);
ci_x0_Cl =      Cwall_Cl*phi(3)*exp(-z(3)*FoverRT*d_x0);
ci_x0_Ant =     Cwall_Ant*phi(4)*exp(-z(4)*FoverRT*d_x0);
ci_x0_H =       Cwall_H*phi(5)*exp(-z(5)*FoverRT*d_x0);
ci_x0_OH =      Cwall_OH*phi(6)*exp(-z(6)*FoverRT*d_x0);
ci_x0_HPO4 =    Cwall_HPO4*phi(7)*exp(-z(7)*FoverRT*d_x0);

% Setting up the ODE through the membrane

D_Na =      1.170e-9; %Units in m^2/s
D_H2PO4 =   7.439e-10;
D_Cl =      1.798e-9;
D_Ant =     8.37e-10; % Estimated using the Wilke-Chang Equation
D_H =       8.512e-9;
D_OH =      4.689e-9;
D_HPO4 =    6.649e-10;

options = odeset('RelTol',1e-12,'AbsTol',[1e-18 1e-18 1e-18 1e-18 1e-18
1e-18 1e-18]);
[x,c]=ode45(@dfile,[0,dx_porosity],[ci_x0_Na; ci_x0_H2PO4; ci_x0_Cl;
ci_x0_Ant; ci_x0_H; ci_x0_OH; ci_x0_HPO4],options);

c(:,:);
size(c);

[m,n]=size(c);
cix_thk=c(m,:); % in M

ci_thk_Na =     cix_thk(1,1);
ci_thk_H2PO4 =  cix_thk(1,2);
ci_thk_Cl =     cix_thk(1,3);
ci_thk_Ant =    cix_thk(1,4);
ci_thk_H =      cix_thk(1,5);
ci_thk_OH =     cix_thk(1,6);
ci_thk_HPO4 =   cix_thk(1,7);

% Solve for d_xthk (in J/C or Volts)
options=optimset('TolFun',1e-18,'TolX',1e-18,'DiffMinChange',1e-18);
%Using Large Scale Algorithm
[d_xthk,resnorm]=lsqnonlin(@myfun2,0,[],[],options);

% Determine Cp_predicted for each ion species

Cpoutput_Na =          ci_thk_Na /(phi(1).*exp(-z(1)*FoverRT*d_xthk));
% in M
Cpoutput_H2PO4 =       ci_thk_H2PO4 /(phi(2).*exp(-
z(2)*FoverRT*d_xthk));
Cpoutput_Cl =          ci_thk_Cl /(phi(3).*exp(-z(3)*FoverRT*d_xthk));
Cpoutput_Ant =         ci_thk_Ant /(phi(4).*exp(-z(4)*FoverRT*d_xthk));
Cpoutput_H =           ci_thk_H /(phi(5).*exp(-z(5)*FoverRT*d_xthk));
Cpoutput_OH =          ci_thk_OH /(phi(6).*exp(-z(6)*FoverRT*d_xthk));
Cpoutput_HPO4 =         ci_thk_HPO4 /(phi(7).*exp(-z(7)*FoverRT*d_xthk));

Cpoutput_Na_2 =        Cpoutput_Na;
Cpoutput_H2PO4_2 =     Cpoutput_H2PO4;
```

```
Cpoutput_HPO4_2 =      Cpoutput_HPO4;
Cpoutput_H_2 =         Cpoutput_H;
Cpoutput_OH_2 =        Cpoutput_OH;
Cpoutput_Cl_2 =        Cpoutput_Cl;
Cpoutput_Ant_2 =       Cpoutput_Ant;

% Determine Output Rejection for each ion species

rejoutput_Na =           (Cf_Na-Cpoutput_Na)/Cf_Na;
rejoutput_H2PO4 =        (Cf_H2PO4-Cpoutput_H2PO4)/Cf_H2PO4;
rejoutput_Cl=            (Cf_Cl-Cpoutput_Cl)/Cf_Cl;
rejoutput_Ant =          (Cf_Ant-Cpoutput_Ant)/Cf_Ant;
rejoutput_H =            (Cf_H-Cpoutput_H)/Cf_H;
rejoutput_OH =           (Cf_OH-Cpoutput_OH)/Cf_OH;
rejoutput_HPO4 =         (Cf_HPO4-Cpoutput_HPO4)/Cf_HPO4;

rejoutput_HPO4_2 =       rejoutput_HPO4
rejoutput_H2PO4_2 =      rejoutput_H2PO4
rejoutput_H_2 =          rejoutput_H
rejoutput_OH_2 =         rejoutput_OH
rejoutput_Cl_2 =         rejoutput_Cl
rejoutput_Ant_2 =        rejoutput_Ant
rejoutput_Na_2 =         rejoutput_Na

% Step size changes

% Change step size if it is too small

if (abs(rejinput_H2PO4_2-rejoutput_H2PO4_2)> 0.01)
    if (abs(rejoutput_H2PO4_1-rejoutput_H2PO4_2) < 1e-5)
        step_size_H2PO4_1 = step_size_H2PO4_1*1.01;
        Cpinput_H2PO4 = Cpinput_H2PO4_1;
    end
end

if (abs(rejinput_HPO4_2-rejoutput_HPO4_2)> 0.01)
    if (abs(rejoutput_HPO4_1-rejoutput_HPO4_2) < 1e-5)
        step_size_HPO4_1 = step_size_HPO4_1*1.01;
        Cpinput_HPO4 = Cpinput_HPO4_1;
    end
end

if (abs(rejinput_OH_2-rejoutput_OH_2)> 0.01)
    if (abs(rejoutput_OH_1-rejoutput_OH_2) < 1e-5)
        step_size_OH_1 = step_size_OH_1*1.01;
        Cpinput_OH = Cpinput_OH_1;
    end
end

if (abs(rejinput_H_2-rejoutput_H_2)> 0.01)
    if (abs(rejoutput_H_1-rejoutput_H_2) < 1e-5)
        step_size_H_1 = step_size_H_1*1.01;
        Cpinput_H = Cpinput_H_1;
    end
end
```

```
if (abs(rejinput_Cl_2-rejoutput_Cl_2)> 0.01)
    if (abs(rejoutput_Cl_1-rejoutput_Cl_2) < 1e-5)
        step_size_Cl_1 = step_size_Cl_1*1.01;
        Cpinput_Cl = Cpinput_Cl_1;
    end
end

if (abs(rejinput_Ant_2-rejoutput_Ant_2)> 0.01)
    if (abs(rejoutput_Ant_1-rejoutput_Ant_2) < 1e-5)
        step_size_Ant_1 = step_size_Ant_1*1.01;
        Cpinput_Ant = Cpinput_Ant_1;
    end
end

% Change step size if it is too big

if abs(rejoutput_H2PO4_2-rejinput_H2PO4_2)< abs(rejoutput_H2PO4_1-
rejinput_H2PO4_1)

    if (abs(rejoutput_H2PO4_1-rejoutput_H2PO4_2) > 0.1)
        if (abs(rejinput_H2PO4_2-rejoutput_H2PO4_2)> 1)
            drop_H2PO4 = 0.99;
        else
            drop_H2PO4 = 0.98;
        end

        step_size_H2PO4_1 = step_size_H2PO4_1*drop_H2PO4;
        Cpinput_H2PO4 = Cpinput_H2PO4_1;
    end
end

if abs(rejoutput_HPO4_2-rejinput_HPO4_2)< abs(rejoutput_HPO4_1-
rejinput_HPO4_1)

    if (abs(rejoutput_HPO4_1-rejoutput_HPO4_2) > 1)
        if (abs(rejinput_HPO4_2-rejoutput_HPO4_2)> 1)
            drop_HPO4 = 0.99;
        else
            drop_HPO4 = 0.98;
        end

        step_size_HPO4_1 = step_size_HPO4_1*drop_HPO4;
        Cpinput_HPO4 = Cpinput_HPO4_1;
    end
end

if abs(rejoutput_OH_2-rejinput_OH_2)< abs(rejoutput_OH_1-rejinput_OH_1)

    if (abs(rejoutput_OH_1-rejoutput_OH_2) > 0.1)
        if (abs(rejinput_OH_2-rejoutput_OH_2)> 1)
            drop_OH = 0.99;
        else
            drop_OH = 0.98;
        end
```

```
        step_size_OH_1 = step_size_OH_1*drop_OH;
        Cpinput_OH = Cpinput_OH_1;
    end
end

if abs(rejoutput_H_2-rejinput_H_2)< abs(rejoutput_H_1-rejinput_H_1)

    if (abs(rejoutput_H_1-rejoutput_H_2) > 0.1)
        if (abs(rejinput_H_2-rejoutput_H_2)> 1)
            drop_H = 0.99;
        else
            drop_H = 0.98;
        end

        step_size_H_1 = step_size_H_1*drop_H;
        Cpinput_H = Cpinput_H_1;
    end
end

if abs(rejoutput_Cl_2-rejinput_Cl_2)< abs(rejoutput_Cl_1-rejinput_Cl_1)

    if (abs(rejoutput_Cl_1-rejoutput_Cl_2) > 0.1)
        if (abs(rejinput_Cl_2-rejoutput_Cl_2)> 1)
            drop_Cl = 0.99;
        else
            drop_Cl = 0.98;
        end

        step_size_Cl_1 = step_size_Cl_1*drop_Cl;
        Cpinput_Cl = Cpinput_Cl_1;
    end
end

if abs(rejoutput_Ant_2-rejinput_Ant_2)< abs(rejoutput_Ant_1-
rejinput_Ant_1)

    drop_Ant = 1;

    if (abs(rejinput_Ant_2-rejoutput_Ant_2)> 10)
        if (abs(rejoutput_Ant_1-rejoutput_Ant_2) > 1000)
            drop_Ant = 0.999;
        end
    else
        if (abs(rejoutput_Ant_1-rejoutput_Ant_2) > 1)
            drop_Ant = 0.98;
        end
    end

    step_size_Ant_1 = step_size_Ant_1*drop_Ant
    Cpinput_Ant = Cpinput_Ant_1;

end
```

```
% Change step size if it moving in wrong direction

if abs(rejoutput_H2PO4_2-rejinput_H2PO4_2)> abs(rejoutput_H2PO4_1-
rejinput_H2PO4_1)
    if (abs(rejoutput_H2PO4_2-rejinput_H2PO4_2)> 1)
        step_size_H2PO4_1 = step_size_H2PO4_1*1.01;
    end
end

if abs(rejoutput_HPO4_2-rejinput_HPO4_2)> abs(rejoutput_HPO4_1-
rejinput_HPO4_1)
    if (abs(rejoutput_HPO4_2-rejinput_HPO4_2)> 1)
        step_size_HPO4_1 = step_size_HPO4_1*1.01;
    end
end

if abs(rejoutput_OH_2-rejinput_OH_2)> abs(rejoutput_OH_1-rejinput_OH_1)
    if (abs(rejoutput_OH_2-rejinput_OH_2)> 1)
        step_size_OH_1 = step_size_OH_1*1.01;
    end
end

if abs(rejoutput_H_2-rejinput_H_2)> abs(rejoutput_H_1-rejinput_H_1)
    if (abs(rejoutput_H_2-rejinput_H_2)> 1)
        step_size_H_1 = step_size_H_1*1.01;
    end
end

if abs(rejoutput_Cl_2-rejinput_Cl_2)> abs(rejoutput_Cl_1-rejinput_Cl_1)
    if (abs(rejoutput_Cl_2-rejinput_Cl_2)> 1)
        step_size_Cl_1 = step_size_Cl_1*1.01;
    end
end

if abs(rejoutput_Ant_2-rejinput_Ant_2)> abs(rejoutput_Ant_1-
rejinput_Ant_1)
    if (abs(rejoutput_Ant_2-rejinput_Ant_2)> 1)
        step_size_Ant_1 = step_size_Ant_1*1.01;
    end
end

% Plotting data

% Plot every set of iterations

if j == 1000

    figure (1)
    set (gcf,'Name','Convergence Plot')

    subplot(2,4,1), plot(i,abs(rejinput_Na_2-
rejoutput_Na_2),'o','MarkerSize',5,'MarkerFaceColor','g','MarkerEdgeCol
or','k'),legend('Na')
    hold on
```

```
    subplot(2,4,2), plot(i,abs(rejinput_H2PO4_2-
rejoutput_H2PO4_2),'o','MarkerSize',5,'MarkerFaceColor','y','MarkerEdge
Color','k'),legend('H2PO4')
    hold on
    subplot(2,4,3), plot(i,abs(rejinput_Cl_2-
rejoutput_Cl_2),'o','MarkerSize',5,'MarkerFaceColor','m','MarkerEdgeCol
or','k'),legend('Cl')
    hold on
    subplot(2,4,4), plot(i,abs(rejinput_Ant_2-
rejoutput_Ant_2),'o','MarkerSize',5,'MarkerFaceColor','c','MarkerEdgeCo
lor','k'),legend('Ant')
    hold on
    subplot(2,4,5), plot(i,abs(rejinput_H_2-
rejoutput_H_2),'o','MarkerSize',5,'MarkerFaceColor','b','MarkerEdgeColo
r','k'),legend('H')
    hold on
    subplot(2,4,6), plot(i,abs(rejinput_OH_2-
rejoutput_OH_2),'o','MarkerSize',5,'MarkerFaceColor','r','MarkerEdgeCol
or','k'),legend('OH')
    hold on
    subplot(2,4,7), plot(i,abs(rejinput_HPO4_2-
rejoutput_HPO4_2),'o','MarkerSize',5,'MarkerFaceColor','w','MarkerEdgeC
olor','k'),legend('HPO4')
    hold on

    j = 0;

end

% Total number of iterations

total = 100000;

if i > total
    break
end

% Break after final convergence

if (abs(rejinput_H2PO4_2-rejoutput_H2PO4_2)<=0.01) &&
(abs(rejinput_Cl_2-rejoutput_Cl_2)<=0.01) && (abs(rejinput_Ant_2-
rejoutput_Ant_2)<=0.01) && (abs(rejinput_H_2-rejoutput_H_2)<=0.01) &&
(abs(rejinput_OH_2-rejoutput_OH_2)<=0.01) && (abs(rejinput_Na_2-
rejoutput_Na_2)<=0.01) && (abs(rejinput_HPO4_2-rejoutput_HPO4_2)<=0.01)
    iteration = false;
end

i = i+1
j = j+1

end

% List of subfunctions

function S=myfun(d_x0)
```

```
global Cwall_Na Cwall_H2PO4 Cwall_Cl Cwall_Ant Cwall_H Cwall_OH
Cwall_HPO4 phi z FoverRT chargedensity

double          c_x0_1;
double          c_x0_2;
double          c_x0_3;
double          c_x0_4;
double          c_x0_5;
double          c_x0_6;
double          c_x0_7;

double          S;

c_x0_1 =    Cwall_Na.*phi(1).*exp(-z(1).*FoverRT.*d_x0);
c_x0_2 =    Cwall_H2PO4.*phi(2).*exp(-z(2).*FoverRT.*d_x0);
c_x0_3 =    Cwall_Cl.*phi(3).*exp(-z(3).*FoverRT.*d_x0);
c_x0_4 =    Cwall_Ant.*phi(4).*exp(-z(4).*FoverRT.*d_x0);
c_x0_5 =    Cwall_H.*phi(5).*exp(-z(5).*FoverRT.*d_x0);
c_x0_6 =    Cwall_OH.*phi(6).*exp(-z(6).*FoverRT.*d_x0);
c_x0_7 =    Cwall_HPO4.*phi(7).*exp(-z(7).*FoverRT.*d_x0);

S=z(1)*c_x0_1+z(2)*c_x0_2+z(3)*c_x0_3+z(4)*c_x0_4+z(5)*c_x0_5+z(6)*c_x0
_6+z(7)*c_x0_7+chargedensity;

function cprime=dfile(x,c)
global Jv Kid Kic z Cpinput_Na Cpinput_H2PO4 Cpinput_Cl Cpinput_Ant
Cpinput_H Cpinput_OH Cpinput_HPO4 FoverRT D_Na D_H2PO4 D_Cl D_Ant D_H
D_OH D_HPO4

double          B1;
double          B2;
double          B3;
double          B4;
double          B5;
double          B6;
double          B7;

double          B_sum;
double          z_sum;
double          cprime;

cprime=zeros(7,1);

B1 =        z(1)*Jv/Kid(1)/D_Na*(Kic(1)*c(1)-Cpinput_Na);
B2 =        z(2)*Jv/Kid(2)/D_H2PO4*(Kic(2)*c(2)-Cpinput_H2PO4);
B3 =        z(3)*Jv/Kid(3)/D_Cl*(Kic(3)*c(3)-Cpinput_Cl);
B4 =        z(4)*Jv/Kid(4)/D_Ant*(Kic(4)*c(4)-Cpinput_Ant);
B5 =        z(5)*Jv/Kid(5)/D_H*(Kic(5)*c(5)-Cpinput_H);
B6 =        z(6)*Jv/Kid(6)/D_OH*(Kic(6)*c(6)-Cpinput_OH);
B7 =        z(7)*Jv/Kid(7)/D_HPO4*(Kic(7)*c(7)-Cpinput_HPO4);

B_sum =     B1+B2+B3+B4+B5+B6+B7;
z_sum =
z(1)^2*c(1)+z(2)^2*c(2)+z(3)^2*c(3)+z(4)^2*c(4)+z(5)^2*c(5)+z(6)^2*c(6)
+z(7)^2*c(7);
```

```
cprime(1)=  Jv/Kid(1)/D_Na*(Kic(1)*c(1)-Cpinput_Na)-
z(1)*FoverRT*c(1)*(B_sum)/FoverRT/z_sum;
cprime(2)=  Jv/Kid(2)/D_H2PO4*(Kic(2)*c(2)-Cpinput_H2PO4)-
z(2)*FoverRT*c(2)*(B_sum)/FoverRT/z_sum;
cprime(3)=  Jv/Kid(3)/D_Cl*(Kic(3)*c(3)-Cpinput_Cl)-
z(3)*FoverRT*c(3)*(B_sum)/FoverRT/z_sum;
cprime(4)=  Jv/Kid(4)/D_Ant*(Kic(4)*c(4)-Cpinput_Ant)-
z(4)*FoverRT*c(4)*(B_sum)/FoverRT/z_sum;
cprime(5)=  Jv/Kid(5)/D_H*(Kic(5)*c(5)-Cpinput_H)-
z(5)*FoverRT*c(5)*(B_sum)/FoverRT/z_sum;
cprime(6)=  Jv/Kid(6)/D_OH*(Kic(6)*c(6)-Cpinput_OH)-
z(6)*FoverRT*c(6)*(B_sum)/FoverRT/z_sum;
cprime(7)=  Jv/Kid(7)/D_HPO4*(Kic(7)*c(7)-Cpinput_HPO4)-
z(7)*FoverRT*c(7)*(B_sum)/FoverRT/z_sum;

function T=myfun2(d_xthk)
global ci_thk_Na ci_thk_H2PO4 ci_thk_Cl ci_thk_Ant ci_thk_H ci_thk_OH
ci_thk_HPO4 phi z FoverRT

double          Cp_1;
double          Cp_2;
double          Cp_3;
double          Cp_4;
double          Cp_5;
double          Cp_6;
double          Cp_7;

double          T;

Cp_1 =      ci_thk_Na /(phi(1).*exp(-z(1).*FoverRT.*d_xthk));
Cp_2 =      ci_thk_H2PO4 /(phi(2).*exp(-z(2).*FoverRT.*d_xthk));
Cp_3 =      ci_thk_Cl /(phi(3).*exp(-z(3).*FoverRT.*d_xthk));
Cp_4 =      ci_thk_Ant /(phi(4).*exp(-z(4).*FoverRT.*d_xthk));
Cp_5 =      ci_thk_H /(phi(5).*exp(-z(5).*FoverRT.*d_xthk));
Cp_6 =      ci_thk_OH /(phi(6).*exp(-z(6).*FoverRT.*d_xthk));
Cp_7 =      ci_thk_HPO4 /(phi(7).*exp(-z(7).*FoverRT.*d_xthk));

T=
z(1)*Cp_1+z(2)*Cp_2+z(3)*Cp_3+z(4)*Cp_4+z(5)*Cp_5+z(6)*Cp_6+z(7)*Cp_7;
```

CHAPTER 6
Conclusions and Future Work

6.1 Conclusions

The removal of antibiotics in water systems may serve as a unique challenge for water treatment facilities due to their low concentrations and varying physicochemical properties. However, a number of treatment processes have been shown to effectively remove select antibiotics, as discussed in Chapter 1. In particular, chlorination and nanofiltation are two treatment processes that may aid in the removal of these compounds.

As previously discussed, the objectives for this study were to evaluate how different water quality characteristics affected the fate and removal of several target antibiotics during these specific treatments. Water quality characteristics such as pH and the presence of additional contaminants in the reaction matrix including tertiary amines were varied. In our study, while only a select number of antibiotics were investigated, they can further serve as model compounds in regards to better understanding the specific mechanisms that drive their fate and removal due to their varying physical and chemical properties. These mechanisms can then be applied to various other organic contaminants in the water matrix for better predicting their elimination as well.

6.1.1 Effect of pH

Changes in pH can significantly alter antibiotic removal due to its effect on both antibiotic chemical properties (e.g. speciation) and its effect on various chemical properties of other constituents in the treatment process (e.g. oxidant speciation and variations in membrane charge). First, in regards to chlorination, pH can alter reaction rates as well as effect the byproducts formed. For example, a significant pH effect was

observed in our study in relation to the chlorination of the veterinary antibiotic, carbadox (CDX), where the apparent second-order rate constant, k_{app}, ranged from 51.8 to 3.15×10^4 $M^{-1}s^{-1}$ and followed a bell-shaped profile from pH 4-11. In this case, the apparent rate constants were dependent on speciation effects since the reaction was dominated by CDX^- and HOCl while CDX and OCl^- were considered negligible.

Byproducts were also found to be significantly affected as individual studies were conducted to identify and monitor their formation over time at varying pH conditions. It was found that the strength of various nucleophiles were pH dependent, leading to byproducts with OH- addition dominating at pH $\geq$ 7.7 while byproducts without OH^- addition, such as one formed during intramolecular nucleophilic attack, were more dominant at lower pH conditions.

In the case of nanofiltration (NF) membranes, pH along with the membrane pore size were varied to estimate their influence on the steady-state rejection of the antibiotics, trimethoprim (TMP), sulfamethoxazole (SMX), and carbadox (CDX). While the effect of membrane pore size was relatively similar for all three antibiotics tested, the effect of pH was strikingly different. For CDX, pH presented an inconsistent affect. Rejection increased from 70.6 to 86.4% from pH 3.1 to 7.1 but decreased to 78.8% at pH 10.0 for Saehan NE 70 while rejection increased steadily from pH 3.1 to 10 for the FilmTec NF 270 membrane. TMP, on the other hand, exhibited a characteristic trend from pH 3-10 where the lowest rejection, 50.1 and 80.7%, was observed near circumneutral pH conditions but increased above and below this pH to reach close to 91% and 96.2% for Saehan NE 70 and FilmTec NF 270, respectively. In contrast, the SMX removal increased substantially from pH 4.8 to $\geq$ 8.0 as rejection increased from 37.4 and 52.3%

to > 97% for Saehan NE 70 and FilmTec NF 270, respectively. Modeling efforts were then made in order to characterize such rejection trends observed from pH 3-10. Both steric and charge effects were integrated into the model output through the steric-hindrance pore model as well as the extended Nernst-Planck equation. Initial modeling results for the Filmtec NF 270 membrane indicated that for charged antibiotics, repulsion between negatively charged compounds (e.g. SMX^-) and a negatively charged membrane could be well characterized, while attraction between a positively charged compound (TMP^+) and a negatively charged membrane is currently not characterized well and requires further assessment.

6.1.2 Effect of Additional Contaminants in Water Matrix

When competing agents are present in the water matrix, the reactivity of an individual organic contaminant to aqueous chlorine is expected to decrease due to the increase in overall chlorine demand. However, when tertiary amines are added and the chlorine demand is still considered to increase, it appears that the reactivity of an individual organic contaminant in the presence of aqueous chlorine has an opposite effect and increases. This is due to the formation of $(R)_3\text{-}N^+\text{-}Cl$, which is a chlorinating agent more reactive than aqueous chlorine alone. The effectiveness of $(R)_3\text{-}N^+\text{-}Cl$, however, can be limited by certain factors. In our study, certain tertiary amines such as trimethylamine (TMA) and 4-morpholineethanesulfonic acid (MES) were found to enhance the transformation of antibiotics, TMP and flumequine (FLU), as well as the organic contaminant, salicylic acid (SA) while other tertiary amine such as creatinine, nitrilotriacetic acid, and the quarternary amine, acetylcholine were found to be ineffective. It is suspected that these later amines were limited in their ability to form $(R)_3\text{-}N^+\text{-}Cl$

initially. In addition, the enhancement effect can also be limited by the stability of $(R)_3$-N^+-Cl over time. This was found to be particularly true for reactions with TMA where addition of varying TMA dosages led FLU and SA to decay rapidly up to ~45 min but then decay at a slower rate up to 360 min. where complete degradation is never achieved. In the end though, certain amines can exhibit a strong enhancement effect, as observed for MES where pseudo-first order (observed) rate constants, k_{obs}^{amine} (s^{-1}), for TMP, FLU, and SA degradation increased from 1×10^{-3} to 2.6×10^{-2} s^{-1}, 1.3×10^{-5} to 1.7×10^{-2} s^{-1}, and 3.9×10^{-6} to 8.7×10^{-3} s^{-1}, respectively, when MES dosages up to 5× the initial antibiotic/organic contaminant concentration are added.

6.2 Future Work

Chlorination practices in water treatment may form undesired reaction byproducts. For our future work, it is desired to quantitatively assess the biological risk these reaction byproducts possess in comparison to the parent compound. It is considered that toxicological studies may be desired while various models can also be applied such as ECOSAR (US. EPA) that can evaluate ecological structure activity relationships.

Reaction byproduct formation can also be enhanced due to the presence of tertiary amines in the reaction matrix. While our study has investigated their role in synthetic waters, it is desired to apply this analysis to real water matrices. The primary question is related to whether environmentally relevant concentrations of tertiary amines can be quantified especially in wastewater systems where significant concentrations are can potentially are found. Can significantly influence on organic contaminant degradation along with enhancing byproduct formation be achieved? One limitation associated with

this future work is related to accurately isolating tertiary amine concentrations while excluding other primary and secondary organic amines.

In regard to antibiotic removal during nanofiltration (NF) processes, several questions still remain to be answered especially in regard to developing an accurate model fit to the experimental data that has been presented in previous chapters. First, what is leading to the discrepancy in the TMP model results in comparison to the experimental data? Future work will first explore the effect that dielectric effects may have on obtaining a better model fit. Second, what is the impact of other parameters such as pore distribution and the effect of diffusion through the polymer matrix (solution diffusion model) on the model rejection of uncharged antibiotics in particular. Numerous studies have investigated these effects in the past. However, several challenges exist especially in regard to accurately determining pore distribution in these NF membranes. Some potential tools that could be useful include atomic force microscopy with a nanoscale tip and BET analysis.

For all of our NF membrane experiments, antibiotic rejection was evaluated and modeled based on a cross-flow filtration system with a flat plate membrane module. In water treatment facilities, NF membranes are typically configured using spiral wound elements where the change in retentate concentration as a function of module length needs to be considered in addition to various other parameters. In our future work, it is desired to account for this change of module configuration into our current model.

Additional work for the future is to better understand what drives CDX and DCDX to form some products that are different where *m/z* 205 is a byproduct found only in CDX reactions with free chlorine while *m/z* 175 is a byproduct found only in DCDX

reactions with free chlorine. The only structural difference between CDX and DCDX is related to the *N*-oxide moeties present on the quinoxaline ring structure of CDX but which are absent for DCDX. This structural difference is hypothesized to lead to a discrepancy in the electron density within the side chain functional group of CDX and DCDX and more specifically within the hydrazone moeity. This could then lead to changes in electron transfer after initial chlorine and hydroxide (OH^-) attack, thus leading to different reaction pathways and byproduct formation. Currently though, the effect of such *N*-oxide moeties on electron density and transfer is not currently understood and requires further investigation.